

1967

# The general behavior and strength of unbraced multi-story frames under gravity loading, June 1967, a chapter of this Ph.D. was published 72-22

B. M. McNamee

Follow this and additional works at: <http://preserve.lehigh.edu/engr-civil-environmental-fritz-lab-reports>

---

## Recommended Citation

McNamee, B. M., "The general behavior and strength of unbraced multi-story frames under gravity loading, June 1967, a chapter of this Ph.D. was published 72-22" (1967). *Fritz Laboratory Reports*. Paper 1761.  
<http://preserve.lehigh.edu/engr-civil-environmental-fritz-lab-reports/1761>

This Technical Report is brought to you for free and open access by the Civil and Environmental Engineering at Lehigh Preserve. It has been accepted for inclusion in Fritz Laboratory Reports by an authorized administrator of Lehigh Preserve. For more information, please contact [preserve@lehigh.edu](mailto:preserve@lehigh.edu).

396.2

THE GENERAL BEHAVIOR AND STRENGTH OF UNBRACED  
MULTI-STORY FRAMES UNDER GRAVITY LOADING

By

Bernard Michael McNamee

FRITZ ENGINEERING  
LABORATORY LIBRARY

A Dissertation  
Presented to the Graduate Faculty  
of Lehigh University  
in Candidacy for the Degree of  
Doctor of Philosophy  
in  
Civil Engineering

Lehigh University

1967

Approved and recommended for acceptance as a dissertation  
in partial fulfillment of the requirements for the degree of Doctor  
of Philosophy.

March 30, 1967  
(date)

Le-wu Lu, Professor in Charge

Accepted April 17, 1967  
(date)

Special committee directing the  
doctoral work of Mr. Bernard McNamee

Professor David A. VanHorn, Chairman

Professor Le-Wu Lu

Professor George C. Driscoll, Jr.

Professor Alan W. Pense

Professor L. S. Beedle, Ex-Officio

ACKNOWLEDGMENTS

This study is a part of the project on "Frame Stability", which is sponsored jointly by the Welding Research Council and the Department of the Navy. The funds are furnished by the American Iron and Steel Institute, the Office of Naval Research, the Naval Ship Systems Command, and the Naval Facilities Engineering Command under an agreement with the Institute of Research of Lehigh University. The Column Research Council acts in an advisory capacity. The work was carried out at the Fritz Engineering Laboratory, Department of Civil Engineering, Lehigh University. Professor Lynn S. Beedle is Director of the Laboratory and Acting Chairman of the Department.

The author wishes to acknowledge the guidance of the members of the committee, who directed his doctoral work, and in particular Professor Le-Wu Lu, who supervised the work leading to this dissertation.

Appreciation is extended to the author's associates at Fritz Laboratory for their help in the experimental phases of the study and to Dr. William C. Hansel and Mr. Lauren D. Carpenter for their assistance in directing the tests. The basic configuration of the test setup was suggested by Dr. Erol Yarimci. The work of Mr. Kenneth Harpel and the technicians in setting up the tests is gratefully acknowledged.

The author also wishes to acknowledge the help rendered by the staff members of the Lehigh University Computer Laboratory and the Computer Center of the Bethlehem Steel Corporation.

The drawings were done by Miss Sharon Gubich and the manuscript was typed by Misses Grace Mann and Linda Nuss. Their cooperation is appreciated.

TABLE OF CONTENTS

	<u>Page</u>
ABSTRACT	1
1. INTRODUCTION	3
2. THEORETICAL SOLUTIONS	8
2.1 Frame Response	8
2.2 Inelastic Behavior	11
2.3 Equilibrium	12
2.4 Previous Studies	13
2.5 Inelastic Frame Buckling	15
2.6 Proposed Analysis	19
2.7 Small Lateral Loads	20
2.8 Discussion of Proposed Analysis	25
3. FORMULATION OF THE COMPUTER SOLUTION	26
3.1 Load-Response Curves	26
3.2 Loading and Frame Geometry	27
3.3 Basic Assumptions	27
3.4 Equilibrium of Incremental Loads	28
3.5 Matrix Formulation	31
3.6 Plastic Hinges	34
3.7 Reduction in $M_{pc}$	36
3.8 Stability Criterion	38
3.9 Comparisons with an Iteration Solution	39
4. DESCRIPTION OF TESTS	41
4.1 Frame Design	41
4.2 Loading System and Test Setup	43
4.3 Instrumentation	44
4.4 Frame Alignment	45
4.5 Material and Section Properties	47
4.6 Frame Loading	47

TABLE OF CONTENTS (Continued)

	<u>Page</u>
5. EXPERIMENTAL RESULTS AND COMPARISONS WITH THEORETICAL PREDICTIONS	49
5.1 Experimental Behavior	49
5.2 Comparison of Theoretical and Experimental Curves	54
5.3 Discussion	57
6. ANALYTICAL FRAME BUCKLING STUDIES	58
6.1 Introduction	58
6.2 Frame Buckling Curves	58
6.2.1 Variable Column Length	58
6.2.2 Effect of Beam Yield Stress	62
6.3 Discussion	63
7. PRIMARY BENDING EFFECT	65
7.1 Introduction	65
7.2 Primary Bending Moment	66
7.2.1 Three-Story, Pinned-Base Frame	66
7.2.2 Six-Story, Pinned-Base Frame	68
7.2.3 Variable Beam Length	69
7.2.4 Constant Relative Stiffness	70
7.3 Discussion	71
8. PARTIAL BASE FIXITY	73
8.1 Introduction	73
8.2 The Effect of Partial Base Restraint	75
8.2.1 Three-Story Frame	75
8.2.2 Six-Story Frame	76
8.3 Discussion	78
9. INTERACTION BETWEEN FLOORS	80
9.1 Introduction	80
9.2 Variable Base Restraint	81
9.2.1 Three-Story Frame	81

TABLE OF CONTENTS (Continued)

	<u>Page</u>
9.2.2 Six-Story Frame	83
9.2.3 Distributed Load	83
9.3 Discussion	85
10. SUMMARY AND CONCLUSIONS	86
11. TABLES	90
Table 4.1 Section Properties	91
Table 4.2 Data From Tension Tests	92
Table 5.1 Buckling Load Summary	92
Table 6.1 Comparison of Frame Parameters	92
12. APPENDIX	93
Example 1 - Single Member	93
Example 2 - Two-Story, Single-Bay Frame	94
13. NOMENCLATURE	98
14. FIGURES	101
15. REFERENCES	165
16. VITA	168

LIST OF FIGURES

	<u>Page</u>	
2.1	Moment-Curvature Relationships	102
2.2	Frame Behavior	102
2.3	Beam-Column Behavior, Double Curvature	103
2.4	Beam-Column Behavior, Single Curvature	103
2.5	Load-Deflection Relationships	104
2.6	Tangent Modulus Frame Buckling, No Hinge Unloading	105
2.7	Tangent Modulus Frame Buckling, Hinge Unloading	106
2.8	Small Lateral Load Method	107
2.9	Story Shear Equilibrium	108
2.10	Theoretical Frame Buckling Load, Test 1	109
2.11	Variable Proportionality Constants	110
3.1	Positive Sign Convention	110
3.2	Main Program	111
3.2	Main Program, Continued	112
3.3	Subroutine, Begin	113
3.4	Subroutine, Initial Coefficient Matrix	114
3.5	Subroutine, Load Matrix and Beam Corrections	114
3.6	Subroutine, Column Corrections	115
3.7	Subroutine, Solution for Incremental Deformations	116
3.8	Subroutine, Incremental Beam Moments	117
3.9	Subroutine, Incremental Column Moments	117
3.10	Incremental-Iteration Comparison, Wood's Frame	118
3.11	Incremental-Iteration Comparison, Heyman's Frame	119
4.1	Frame Geometry	120

LIST OF FIGURES (Continued)

	<u>Page</u>	
4.2	Frame Loading	120
4.3	Test Setup, Diagram	121
4.4	Test Setup	122
4.5	Deflected Frame	122
4.6	Pinned-Base	123
4.7	Bases for Test Bed	123
4.8	Dial Rotation Gage	124
4.9	Electrical Rotation Gages	124
4.10	Load Console	125
4.11	Load Pumps	125
5.1	Load-Lateral Sway Relationships	126
5.2	Deflection Comparison, Test 1	126
5.3a	Beam Moments, West Frame, Test 1	127
5.3b	Beam Moments, East Frame, Test 1	127
5.4a	Beam Moments, West Frame, Test 2	128
5.4b	Beam Moments, East Frame, Test 2	128
5.5	Moment Distribution, West Frame, Test 1	129
5.6a	Bottom Story Joint Moments, Test 1	130
5.6b	Bottom Story Joint Moments, Test 2	130
5.7a	Bottom Story Shear Equilibrium, Test 1	131
5.7b	Bottom Story Shear Equilibrium, Test 2	131
5.8a	Moment-Sway Deflection, Test 1	132
5.8b	Moment-Sway Deflection, Test 2	132

LIST OF FIGURES (Continued)

	<u>Page</u>	
5.9	Deflected Frame, Arrested Position	133
5.10	Yield Pattern, Location 3, Joint A, Test 2	133
5.11	Yield Pattern, Load Point, East Frame, Test 1	134
5.12a	Moment Comparisons, Tests 1 and 2, East Frame	135
5.12b	Moment Comparisons, Tests 1 and 2, West Frame	136
5.13a	Beam Deflections, Experimental and Predicted, Test 1	137
5.13b	Sway Deflections, Experimental and Predicted, Test 1	137
5.14a	Beam Deflections, Experimental and Predicted, Test 2	138
5.14b	Sway Deflections, Experimental and Predicted, Test 2	138
5.15	Bending Moments, Experimental and Predicted, Test 1	139
5.16	Bending Moments, Experimental and Predicted, Test 2	140
6.1	Frame Buckling Loads, Column Slenderness Ratio	141
6.2	Load-Response Curves, Column Slenderness Ratio	142
6.3	Restrained Columns	143
6.4	Frame Buckling Loads, Beam Yield Stress	143
6.5	Load-Response Curves, Beam Yield Stress	144
7.1	Frame Buckling Loads, Primary Bending, $n = 3$	145
7.2	Load-Response Curves, Primary Bending, $n = 3$	146
7.3	Effect of Primary Bending, $n = 3$	147
7.4	Load-Response Curves, Primary Bending, $n = 6$	148
7.5	Effect of Primary Bending, $n = 3$ and $n = 6$	149
7.6	Non-Dimensionalized Comparison, $n = 6$	149
7.7	Frame Buckling Loads, Beam Length	150
7.8	Load-Response Curves, Beam Length	151

LIST OF FIGURES (Continued)

	<u>Page</u>
7.9 Non-Dimensionalized Curve, Beam Length	152
7.10 Frame Buckling Loads, Constant Relative Stiffness	152
7.11 Load-Response Curves, Constant Relative Stiffness	153
8.1 Partial Base Fixity	154
8.2 Load-Response Curves, Partial Base Fixity, $n = 3$	155
8.3 Frame Buckling Loads, Partial Base Fixity, $n = 3$	156
8.4 Frame Buckling Loads, Foundation Modulus, $n = 3$	156
8.5 Load-Response Curves, Partial Base Fixity, $n = 6$	157
8.6 Frame Buckling Loads, Partial Base Fixity, $n = 6$	158
9.1 Load-Response Curves, Variable Base Restraint, $n = 3$	159
9.2 Frame Buckling Curves, Variable Base Restraint, $n = 3$	160
9.3 Load-Response Curves, Variable Base Restraint, $n = 6$	161
9.4 Frame Buckling Curves, Variable Base Restraint, $n = 6$	162
9.5 Buckling Load Comparison, Variable Base Restraint	162
9.6 Load-Response Curves, Distributed Load, Variable $n$	163
9.7 Frame Buckling Loads, Distributed Load, Variable $n$	164
A-1 Joint and Member Designation, Example 2	164

ABSTRACT

The dissertation studies the general strength and behavior of unbraced, multi-story, rectangular, planar, steel frames under static gravity loading. A particular problem is the inelastic frame buckling behavior of such structures.

The inelastic behavior of symmetrical multi-story frames under symmetrical gravity loading is described. The present state of knowledge as to the analysis of these frames is outlined. A method to compute inelastic buckling loads for multi-story frames is proposed. This method is a limit-type procedure which employs small lateral loads on the frame to represent the eccentricities in the actual frame. The formulation of a computer solution for the proposed method of analysis is developed.

The results of two multi-story frame buckling tests are presented. The test specimens are three-story, single-bay, pinned-base frames. The correlation between the theoretical inelastic frame buckling loads and the experimental ultimate load values is excellent.

Analytical studies are conducted to examine the effects on the frame buckling loads caused by varying the structural parameters. The frames in the studies are single-bay and multi-story. They are designed on a strength basis to fail at an ultimate load equal to the beam mechanism load. Curves are developed which show the reduction, if any, in the beam mechanism load caused by frame buckling.

The changes in the frame buckling load caused by the primary bending moments are computed and are shown to be significant. The effects on the frame buckling load caused by varying the number of stories in a frame are evaluated. The beneficial effects of partial base fixity are examined. The rotational restraints provided by the lower stories on the top stories of multi-story frames are approximated and the corresponding frame buckling loads are obtained. The implications which the analytical studies have on a proposed design procedure for unbraced multi-story frames are discussed.

## 1. INTRODUCTION

The problems that are encountered in the design of multi-story buildings are relatively recent as the following paragraph illustrates. 1.1

"...What can be considered the first true skyscraper, though steel was not used in it, was W. LeB. Jenney's 10-storey Home Insurance Building erected in Chicago between 1883 and 1885. The frame consisted of round cast-iron columns, wrought-iron built-up box columns and wrought-iron I-beams bolted together by means of angles, webs and gusset plates to form a continuous frame. All parts of the exterior walls were carried on shelf angles fixed to the spandrel beams so that the outermost floor beam carried not only its share of the floor load but one bay of the exterior wall up to the beam above. This method of construction made the very high building of the future possible. Developments after this were rapid. Baumann and Huehl's Chamber of Commerce Building, 1888-89 was fully framed, the 13-storey frame weighing 32,000 tons. Jenn's Sears and Roebuck Store, built a year later, was 57,900 sq. ft. in extent and 8 storeys high; his Manhattan Building of 1891 was of 16 storeys and in this he introduced cantilever beams fixed to columns on a line well inside the line of the party wall so as to avoid overloading the footings of the existing flanking building. Almost all the problems ever to face the designer seem to have been met and solved in Chicago by 1891...."

However, as innovations were introduced into the construction technique, new problems arose and the designer had to solve them. Two of the major changes that occurred were the use of low-carbon steel as a building material and the adoption of a new framing technique. Continuous columns were run from the foundation to the roof, and moment resisting connections were employed to join the beams and the

columns into a relatively rigid framework. When this type of construction was introduced in about 1900, the lateral wind loads on the face of the building were assumed to be transferred through the floor system to massive masonry end walls and through them to the foundation. Shortly thereafter, diagonal bracing was found to be a more effective and a more economical method of carrying the wind loads, and it was adopted. The diagonal braces, together with the adjacent in-panel beams and columns, were considered to behave as a vertical truss system in transmitting the lateral forces to the foundation. The massive end walls could be eliminated, but relatively rigid masonry wall construction was still used throughout the building.

These changes in building technology led to changes in the techniques of analysis. Approximate methods, such as the cantilever and portal methods, were advanced. There seems to be no individual to whom credit can be given for either of these methods of analysis. In the early 1920's, Hardy Cross<sup>1.2</sup> introduced an iterative solution for the slope-deflection equations. This was the moment distribution method and it is used extensively in elastic analysis. Since the late 1940's, the plastic design approach has come into more extensive use. It is interesting to note that the first work of importance in this area was done in 1913 by Kazinczy,<sup>1.3</sup> and that some of the assumptions of the portal method have their counterpart in the multi-story plastic design approach.

Paralleling the advancements in analytical procedures, there have been innovations in the architectural treatment of multi-story

buildings. The present trend is to construct buildings with spacious, column-free, interior areas. These areas are then subdivided by lightweight, movable partitions. The exteriors of the buildings are enclosed with glass and membrane panel-walls. These changes have made the positioning of diagonal wind bracing within the building more difficult. One solution has been to eliminate the diagonal bracing and to use shear walls to house the elevator and service core areas. The shear walls are designed to transmit the lateral loads to the foundations.

If the use of lateral bracing or shear walls is not practical, the rigid frame together with the cladding (the lateral stiffening effects of concrete fireproofing, permanent walls, etc.) must supply the necessary stiffness to prevent excessive lateral sway of the building frame. If the cladding effect is negligible, as can be the case when the fireproofing is sprayed on the steel members, the bare frame alone must supply the necessary lateral stiffness.

The changes described above have refocused attention on the lateral stiffness of building frames. This overall area of study is referred to as a frame stability investigation. If the frame is symmetrical and is supporting only symmetrical gravity loads, then the study is called the frame buckling problem. Both the frame buckling problem and the more general frame stability problem are three-dimensional in scope. Techniques for the elastic analysis of three-dimensional frame stability problems frequently appear in the structural literature, but nothing has been advanced concerning the inelastic analysis for three-

dimensional multi-story frame stability problems. There have been no experimental studies on full-scale, three-dimensional structures.

Most of the two-dimensional studies of frame stability consider the inelastic behavior of the members in the frame. These studies assume that the frame will deflect in only one of the two framing directions, or that there is sufficient lateral bracing in one framing direction so that the sway is restricted to the other direction. Experimental verification on a full-scale structure has been obtained for the methods employed in the two-dimensional multi-story frame stability analysis.<sup>1.4</sup> The frame buckling problem, although a special case of the general frame stability problem, is more difficult to analyze because of the unloading that occurs in the previously yielded fibers in some of the members of the frame. A satisfactory method of analysis has not as yet been developed for either the three-dimensional or the two-dimensional inelastic, multi-story frame buckling problem. Experimental studies have not been conducted on full-sized structures.

This dissertation will examine the inelastic frame buckling problem as applied to rectangular planar building frames of Type 1 AISC construction.<sup>1.5</sup> The behavior of a symmetrical framework under symmetrical gravity loading will be described. A method of analysis will be proposed that will give approximate load-response curves and frame buckling loads for multi-story building frames. The results of two frame buckling tests, which were conducted to verify the proposed method, will be presented. A comparison between the experimental

results and the theoretical predictions will be made. The computer program which is used in the analysis will be described and flow charts will be presented. The computer solution will then be used to examine the changes in the frame buckling load which are caused by varying several of the structural parameters.

## 2. THEORETICAL SOLUTIONS

### 2.1 FRAME RESPONSE

The design of the members in the top stories of tall buildings and in buildings of a few stories is governed by gravity loading and hence frame buckling is restricted to these areas. A usual design procedure is to omit lateral bracing in these stories and to assume that the frame and the cladding provide the necessary lateral stiffness to prevent frame buckling. With the cladding effects constantly being reduced, this practice is now open to question. It will be assumed in this dissertation that the beneficial lateral stiffness effects of cladding are not present, and that the frame receives no lateral support from adjacent out-of-plane members that frame into it. The frame alone must supply the lateral stiffness required to prevent lateral buckling. The values of the frame buckling loads obtained under these assumptions will necessarily be conservative.

The determination of the load-response behavior of a multi-story building frame neglecting the cladding effect is still a very complex procedure. The major factors which affect the strength and the rigidity of a frame and that must be considered in the development of a theoretical solution are:

- 1) Mechanical properties of the materials and the strength and deformation behavior of the members.

- 2) axial load effect on member stiffness
- 3) axial load effect on the sway moment (the P- $\Delta$  effect)
- 4) frame geometry
- 5) rigidity of the connections and the supports
- 6) eccentricities in the loads and the members
- 7) residual stresses from rolling, fabrication and the erection processes.

The procedure is further complicated since factors 5, 6 and 7 are so interrelated that they cannot be experimentally isolated. Also, they directly affect factors 1, 2 and 3. Assumptions, that simplify the analysis procedure, must be made to obtain a workable solution.

In the usual analysis procedure, the joints of the frame are assumed to be rigid and the eccentricities of the members and the loads are not considered. The residual stresses from fabrication and erection also are not considered. They are highly indeterminate and can only be obtained experimentally. The residual stresses from rolling are approximated in computing the moment-curvature relationship of a member (Fig. 2.1). Collectively, these assumptions describe an ideal structure. It is this type of structure on which the equations for most methods of analysis are formulated.

In actuality, there are always some eccentricities in any structure. Their distributions are random and unpredictable. It would not be economical or practical to undertake a testing program to statistically evaluate a meaningful coefficient for the eccentrici-

ties. However, in discussing the general behavior of a structure (Fig. 2.2), the concept of a resulting eccentricity ( $e_o$ ) can be assumed. In the early stages of loading, the effect of the initial eccentricity causes a small lateral sway ( $O'C$ ). As the sway increases with increasing gravity load ( $CD$ ), the P- $\Delta$  effect becomes more significant. The deleterious effect of axial load on the column stiffness also increases the lateral sway. Each of these effects is non-linear and significantly influences the response curve along length  $DE$  and beyond. At a load approximated by point  $E$  on the curve, yielding occurs in a portion of the frame, and the overall stiffness is further reduced. Since there is a lateral deflection when the inelastic behavior begins, the yielding will be at specific locations which are not symmetrically positioned throughout the frame. This non-symmetry, together with the decrease in the stiffness due to the yielding, greatly accelerates the lateral sway of the frame. As the loads are further increased, the yielding spreads. Plastic hinge conditions are approached at certain locations. The overall stiffness is drastically reduced and the frame instability load ( $F$ ) is reached. Beyond this point, deflections increase with little or no increase of load ( $FG$ ). Equilibrium positions are possible if unloading occurs ( $FG'$ ).

If the value of the initial eccentricity ( $e_o$ ) is decreased, the elastic deformations measured from the no load position ( $O'B$ ) will be reduced. The new load-response curve will be steeper than the previous one and will reach a higher load level than  $FG$ . Since the eccentricities are small, the increase in the frame instability load above level  $FG$  should be small. The upper limit for the frame instability

loads will be the frame buckling load (A).

## 2.2 INELASTIC BEHAVIOR

An exact solution involving inelastic behavior should consider the depth of penetration of the yielding at a section, the extent of yielding along the member, the deleterious effects of residual stresses, and the beneficial effects of strain-hardening. These inelastic effects can be considered in a finite difference solution. Since the moment gradients in a multi-story frame are large, the interval between the control points for the finite difference solution should be small. In a multi-story frame analysis, an excessive amount of computer time would be required for this approach under the present (1967) state of computer technology.

Instead, an idealized elastic-plastic moment curvature relationship (Fig. 2.1) will be assumed to give a reasonable approximation for the inelastic behavior.<sup>2.1</sup> The cross-section will be assumed to have a shape factor of unity. The resulting section will behave elastically until the plastic moment capacity ( $M_{pc}$ ) of the section is reached. The section will then rotate plastically under a constant moment. Under these assumptions, yielding does not extend along the member.

The idealized moment-curvature relationship gives a good approximation for the behavior of a beam. For beam-columns the approximation is satisfactory in most cases, especially in parts of the build-

ing frame where frame buckling must be considered. Parikh showed for beam-columns under axial load ratios ( $P/P_y$ ) less than 0.7, with low slenderness ratios, and deflecting in double-curvature (Fig. 2.3) or in single curvature with one end pinned, that the idealized moment-curvature relationship gave moment-end rotation curves which were close approximations to the exact curves.<sup>2.1</sup> If the beam-columns under consideration do not fall within the preceding description (see Fig. 2.4) then the idealized assumption will be inaccurate. An algebraic expression must be developed for the moment-end rotation functions of these members if they are to be considered in the analysis.

### 2.3 EQUILIBRIUM

The load-response curve, that will be used to approximate the actual behavior of a frame, is based on a second-order, elastic-plastic method of analysis. Small deformation theory is assumed and only flexural deformations are considered. In first-order theory, the equations of equilibrium are written for the structure and the members when they are in their undeflected positions. There is no decrease in the stiffness or increase in carry-over factors of the members because of the axial loads.

Second-order theory is used in frame stability analysis. The member and the structure are assumed to be in their deflected positions when the equations of equilibrium are written. The effect of the second-order theory is to consider the additional bending caused by

the axial load and the deformation. This reduces the stiffness of the member and increases the carry-over factor. In the story shear equilibrium equation, the product of the vertical loads and the story sway (the  $P-\Delta$  moment) is introduced by the second-order theory.

The differences between the first-order and the second-order theory are graphically presented in Fig. 2.5 for both the elastic and the idealized elastic-plastic behavior. The first-order elastic curve (OC) is a linear relationship. The second-order elastic curve (OD) is non-linear and reaches an ultimate or frame instability load. If the elastic-plastic behavior is combined with first order theory, the resulting curve (OB') is linear and piecewise continuous. Discontinuities occur at the formation of each hinge. The curve approaches the first-order mechanism curve (BB') as an asymptote. The second-order elastic-plastic curve (OA) is non-linear and is also piecewise continuous. An ultimate load is reached at one of the discontinuities caused by the formation of a plastic hinge. The general shape of the curve is similar to the exact curve (OG') and comparisons with experimental curves show that it is a good approximation for the actual behavior.<sup>1.4</sup>

#### 2.4 PREVIOUS STUDIES

The literature on methods of analysis to determine frame buckling loads under elastic loading is quite extensive.<sup>2.2</sup> The classical approach is to assume an ideal frame with the loads applied

at the connections. For low values of load, the structure remains in the undeflected mode. At the critical load, a second or deflected equilibrium position is possible. The elastic frame buckling load is the lowest load at which bifurcation of the equilibrium position is possible. This analytical approach is similar to the computation for the Euler buckling load of a column.

In building frames of the usual dimensions, frame buckling will occur after some of the members are loaded into the inelastic range. Methods for the determination of inelastic frame buckling loads have been quite restricted in their approach. Those that employ relatively exact moment-curvature relationships have been limited in application to single-bay, single-story frames.<sup>2.2,2.3,2.4,2.5,2.6,2.7,2.8</sup> An energy approach has been used in the inelastic frame buckling analysis of multi-story frames.<sup>2.9</sup>

In the general inelastic stability analysis for multi-story frames, theoretical approaches with less rigorous moment-curvature relationships, although not as sophisticated, have been employed for a more extensive group of problems.<sup>2.1,2.10,2.11</sup> Wood used an elastic-plastic moment-curvature relationship in an analysis to show that the instability load of a multi-story frame is significantly reduced when plastic hinges are introduced into the frame.<sup>2.12</sup>

An empirical relationship has been developed by Merchant to predict inelastic multi-story frame buckling loads.<sup>2.13</sup> It is based on computations of the elastic buckling load and the ultimate load

from simple plastic theory. It shows some agreement with frame buckling loads for tests on model size structures. A similar relationship, determined from analytical and experimental values, is included in the AISC Specification.<sup>1.5</sup>

## 2.5 INELASTIC FRAME BUCKLING

There are two general approaches for the determination of inelastic frame buckling loads of multi-story structures. One is similar to the tangent modulus theory for the determination of inelastic column buckling loads. The second considers the shape of the load-response curve of the actual structure (Fig. 2.2). The tangent modulus method will be described assuming an elastic-plastic moment-rotation behavior for the members of an ideal structure under symmetrical gravity loading. Under these conditions of symmetry, there can be no lateral deflection and the ultimate load will be the beam mechanism load.

Analogies exist between the classical behavior for inelastic frame buckling and the inelastic behavior of an ideal pinned-end column. In the column, a lateral disturbance is required at the tangent modulus load to initiate lateral deformation. An upper limit for the ultimate load which the column can carry is the reduced modulus load. In the post-buckling loading range for the column, the value of the tangent modulus ( $E_t$ ) is reduced and hence the reduced modulus load or upper limit for the ultimate load is lowered. It has been shown that the tangent modulus load is a good estimate for the ultimate load

of the column. 2.14

A corresponding theory to determine the tangent modulus buckling loads for multi-story frames has not as yet been developed. There is an additional problem of plastic hinges unloading as the frame deflects laterally from its initial configuration. For a tangent modulus solution, there should be no hinge unloading as the initial sway takes place. After the initial sway has occurred, hinge unloading can take place. The sequence for this hinge unloading has not as yet been defined. The following discussion is intended to describe the elastic-plastic frame buckling behavior and to serve as a basis of comparison in describing the proposed method to compute inelastic frame buckling loads.

Yielding can occur in the beams and columns of an ideal structure before the tangent modulus frame buckling load is reached. To simplify the presentation, it will be assumed that hinges do not form in the columns. Physically, this can be accomplished through the design procedure for obtaining the member sizes of the columns. Because of the symmetry in the ideal frame, hinges will form initially at the ends of the beams, or a yielded zone will form through the central region of the beams. A special case exists when concentrated loads are placed at the centers of the beams (Fig. 2.6a). The load-response behavior for the special case will be described first.

In the elastic loading region (Fig. 2.6a), the maximum moments occur under the concentrated loads at the centers of the beams. The ultimate load for the elastic frame is shown at level a. The

elastic frame buckling load is used to approximate the value of this ultimate load. The first plastic hinge forms at a concentrated load (Fig. 2.6b). This will lower the ultimate load in an actual frame to the level at b. For the assumed elastic-plastic moment-curvature relationship, there would be no reduction in the ultimate load since the plastic hinge location corresponds to the location of the inflection point in the sway deformation mode of the structure. After a small increase in load, a second hinge will form (Fig. 2.6c) and the ultimate load is further reduced to a level at c. Failure occurs by one of two modes. In the first mode, additional loads are applied and frame buckling occurs at level c. Unloading of the plastic hinges should not occur. In the second mode, additional plastic hinges form (Fig. 2.6d) before the load at level c is reached. Because of the symmetry, they will form at the ends of the beams and a beam mechanism failure will take place. Since there will be no additional rotational restraint provided by the beams to the columns, frame instability will also occur and the frame will deflect laterally with no unloading of hinges. The relative member sizes will govern which of the two failure modes occurs first.

In the more general tangent modulus buckling behavior, unloading of plastic hinges will probably take place. In the elastic loading region of the frame in Fig. 2.7a, it is assumed that the maximum moments occur at the ends of the beams. At the tangent modulus buckling load, a small increment of vertical load and a lateral disturbance are applied simultaneously. There is a small lateral deflection with no unloading of hinges. With the removal of the lateral disturbance,

the frame stays in a deflected configuration. With further increases in the vertical load, unloading of the windward hinges takes place. For clarity, it is again stated that theory has not been developed to substantiate this description of the tangent modulus frame buckling behavior.

In Fig. 2.7b, a simultaneous unloading of hinges on the left end of all beams has been assumed to occur with the application of an additional vertical load. The load-response curve will follow the indicated curve with an upper limit at b. The upper limit would be the deteriorated critical load of the frame.<sup>2.12</sup> The upper limit at b probably could not be reached before additional yielding takes place. If a hinge formed at location 1 in Fig. 2.7c, the upper limit at b would be lowered to the level at c. With the formation of each additional plastic hinge, there is an accompanying finite reduction in the critical load. This continues until the upper limit is reduced to a level d which is below the level of the load being carried by the frame (Fig. 2.7d). On this basis, the ultimate load will usually coincide with the formation of a plastic hinge. If the difference in load between the tangent modulus frame buckling load and ultimate load is not large, then the tangent modulus frame buckling load can be used as a prediction of the ultimate load. Model tests on portal frames indicate that the difference is small.<sup>2.4</sup>

The second approach for the determination of inelastic frame buckling loads is based on the load-response function of the actual frame. In the discussion for this behavior, the initial eccentricity

( $e_o$ ) in Fig. 2.2 had a direct effect on the value of the frame instability load (F). As the value of the eccentricity approached zero, the frame instability load approached the frame buckling load as an upper limit. This limit process is the basis for the proposed method to compute inelastic frame buckling loads. The value of the tangent modulus frame buckling load will be approximated by the frame buckling load which is obtained from the limit of the frame instability loads as the value of the eccentricities approach zero.

## 2.6 PROPOSED ANALYSIS

A limit type procedure, which considers the variables listed in Art. 2.1, is proposed for the computation of inelastic frame buckling loads. The initial eccentricities in the members and the frame can be considered as a resulting eccentricity ( $e_o$ ) in Fig. 2.8a. It is these eccentricities which give the load-response curve its characteristic shape.

There are two techniques for approximating these eccentricities in an analysis. The first approach approximates the eccentricities by assuming an initially deflected shape for the members<sup>2.15</sup> or for the frame.<sup>2.16</sup> The second approach represents the effects of the eccentricities by a set of equivalent proportional loads on the member<sup>2.15</sup> or on the frame. Neither of these techniques has been previously applied to the inelastic analysis of multi-story frames. The second

approach is used in the proposed method of analysis. A computer program to compute inelastic frame instability loads is formulated in Chapter 3.

The frame in Fig. 2.8b illustrates the technique that will be used to compute inelastic frame buckling loads. The frame is loaded with gravity loads ( $W_i$ ) and small lateral loads ( $H_i$ ) which represent the effect of the initial eccentricities. The small lateral loads are proportional to the gravity loads and are applied at each floor level. If a value ( $\alpha_i$ ) is chosen for the proportionality factor, the corresponding load-response curve and frame instability load ( $W_{CR_1}$ ) can be obtained using the formulation in Chapter 3. A second proportionality factor ( $\alpha_2$ ) is chosen and its corresponding load-response curve and frame instability load ( $W_{CR_2}$ ) are obtained. The frame buckling load ( $W_{CR}$ ) in Fig. 2.8c is the limit of the frame instability loads as the proportionality constants ( $\alpha$ ) approach zero. This limit type procedure is the basis for the proposed method of analysis. In Fig. 2.8c, only two frame instability loads are used in the limit procedure to obtain the frame buckling load ( $W_{CR}$ ). A third frame instability load could be computed to determine the accuracy of the linear approximation. If the accuracy is not sufficient, then a parabolic approximation can be used with the three frame instability loads.

## 2.7 SMALL LATERAL LOADS

Small lateral loads are applied at each floor level to

simulate the effect of the resulting eccentricities in the frame. If it is assumed that the alignment and fabrication errors are the cause of the eccentricities and the other effects are negligible, then a relationship can be developed between the proportionality constant at a floor level ( $\alpha_i$ ) and the average eccentricity between floor levels ( $e_i$ ). This is the basis for using proportional lateral loads applied at each floor level.

For a frame in its deflected position (Fig. 2.9a), the shear equilibrium equation for the columns at any story with an eccentricity ( $e_i$ ) is given by

$$\Sigma M_T + \Sigma M_B + \Sigma P (\Delta + e_i) = 0 \quad (2.1)$$

where  $\Sigma M_T$  and  $\Sigma M_B$  are the sum of the moments at the top and bottom of the columns,  $\Sigma P$  is the sum of the axial loads in the columns, and  $\Delta$  is the relative story sway deflection from the zero load position. For an increment of load ( $dP$ ), there will be incremental moments ( $dM$ ) and an increment of deflection ( $d\Delta$ ). The equilibrium equation for the new deflected position (Fig. 2.9b) is

$$\Sigma(M_T + dM_T) + \Sigma(M_B + dM_B) + \Sigma(P + dP) (\Delta + d\Delta + e_i) = 0 \quad (2.2)$$

The incremental equation can be obtained by subtracting the first equation from the second. This gives

$$\Sigma(dM_T) + \Sigma(dM_B) + \Sigma P(d\Delta) + \Sigma dP(\Delta) + \Sigma dP(d\Delta) + e_i \Sigma dP = 0 \quad (2.3)$$

In the proposed analysis, small lateral loads are applied at each floor level in proportion to the loads on the floor.  $\alpha_i$  is the proportionality constant at a floor level. In Fig. 2.9c, the eccentricity effect is represented by an accumulated lateral force and the shear equilibrium equation is

$$\Sigma M_T + \Sigma M_B + \Sigma P\Delta + h\Sigma H = 0 \quad (2.4)$$

For an increment of vertical load ( $dP$ ), there will be an increment of lateral load ( $dH$ ), and an increment of deflection ( $d\Delta$ ). The equilibrium equation for the deflected position (Fig. 2.9d) is

$$\Sigma(M_T + dM_T) + \Sigma(M_B + dM_B) + \Sigma(P + dP)(\Delta + d\Delta) + h\Sigma(H + dH) = 0 \quad (2.5)$$

The incremental equilibrium equation is obtained by subtracting Eq. 2.4 from Eq. 2.5.

$$\Sigma(dM_T) + \Sigma(dM_B) + \Sigma P(d\Delta) + \Sigma dP(\Delta) + \Sigma dP(d\Delta) + h\Sigma dH = 0 \quad (2.6)$$

In comparing the corresponding equilibrium equations of the two systems (Eqs. 2.3 and 2.6), two equalities are evident

$$h\Sigma H = e_i \Sigma P \quad (2.7a)$$

and

$$h\Sigma dH = e_i \Sigma dP \quad (2.7b)$$

Equations 2.7a and 2.7b show that the horizontal loads on the frame should be proportional to the loads on the beams. Since the eccentricities ( $e_i$ ) are very small, then the proportional horizontal loads ( $\Sigma H$ ) should be small with respect to the beam loads ( $\Sigma P$ ).

If the initial eccentricities ( $e_i$ ) within a frame were measured, then the proportionality constants could be computed from Eqs. 2.7a or 2.7b. For the top floor

$$e_1 = h_1 \frac{H_1}{P_1} = h_1 \frac{dH_1}{dP_1} = h_1 \alpha_1$$

or

$$\alpha_1 = \frac{e_1}{h_1} \quad (2.8)$$

For the second floor in the frame and with  $h_1 = h_2 = h$

$$e_2 [P_1 + P_2] = h [H_1 + H_2]$$

$$e_2 [P_1 + P_2] = h [\alpha_1 P_1 + \alpha_2 P_2] \quad (2.9)$$

If  $P_1 = P_2 = P$ , then

$$\alpha_1 + \alpha_2 = \frac{2e_2}{h}$$

$$\alpha_2 = \frac{1}{h} [2e_2 - e_1] \quad (2.10)$$

If  $e_1 = e_2$ , then

$$\alpha_2 = \alpha_1 \quad (2.11)$$

Equations 2.8, 2.10 and 2.11 show that the proportionality constant ( $\alpha_i$ ) should not be the same for all floors.

In the proposed method of analysis, it is not necessary to obtain the initial eccentricity for each member of the frame. The

limit procedure requires a calculation to determine the frame buckling load which is the limit of the frame instability loads as the proportionality constant approaches zero. Equal values of  $\alpha$  can be assumed for each floor. Through a trial and error process, a value  $\alpha$  can be obtained that gives a load-response curve, that is a close approximation for the expected frame behavior. This technique is developed in Fig. 2.10 for the frame in Test 1. The first value of  $\alpha$  is chosen as 1 percent of the floor load. The corresponding load-response curve in Fig. 2.10 is obtained. A second load-response curve is obtained for  $\alpha$  equal to 1/2 percent. The value of the frame buckling load is obtained in Fig. 2.10 for  $\alpha$  equal to zero. The important factor in the proposed method is the determination of the frame buckling load. The obtaining of an exact load-response curve is not essential. Previously, it was shown that the values of  $\alpha$  should not be the same for each floor level. Unequal values could simultaneously be allowed to approach zero. The frame buckling load should be the same value as that computed with equal horizontal loads. This is shown by the limit curves in Fig. 2.11.

The limit curves in Fig. 2.11 are for the frame in Test 1. The top limit curve is the same as that shown in Fig. 2.10d. The values of  $\alpha$  in this curve are equal for all floors. In the middle curve, the value of  $\alpha_2$  is kept constant.  $\alpha_1$  is half that of the top curve.  $\alpha_3$  is twice that of the top curve. In the bottom limit curve  $\alpha_2$  is kept constant while the multiplication factors are reversed for  $\alpha_1$  and  $\alpha_3$ . In the limit as all values of  $\alpha$  simultaneously approach

zero, the values of the frame instability loads approach a common value for the frame buckling load. The largest difference among the three values is 110 pounds.

## 2.8 DISCUSSION OF THE PROPOSED ANALYSIS

In the procedure for computing frame buckling loads, two load-response curves were obtained. Both were similar in shape to the expected load-response of the actual frame. The difference between the frame instability loads for the two theoretical curves was sufficiently close that large errors were not introduced by the limit process as  $\alpha$  approached zero. The accuracy of this procedure was measured by computing a third frame instability load. This was done in Fig. 2.10d. The value of  $\alpha$  was 3/4 percent. An attempt was made to compute a point on this limit curve for  $\alpha$  equal to 1/4 percent. However, hinges formed at both ends of a beam and the associated hinge unloading problem was introduced. This unloading behavior sets a lower bound on the value for  $\alpha$  on the limit curve in the proposed analysis. The limit procedure was shown to be insensitive to changes of  $\alpha$  from floor to floor. The significant point was to select small values for  $\alpha$  so that the frame instability loads obtained were numerically close to the frame buckling load.

### 3. FORMULATION OF THE COMPUTER SOLUTION

#### 3.1 LOAD-RESPONSE CURVES

The proposed method for computing frame buckling loads requires the development of at least two load-response curves. Each point on the load-response curve represents an equilibrium position for the structure under a given loading condition. The individual points on the curve can be obtained by an iteration method or the entire curve can be generated by an incremental procedure. The advantage of the iteration method is in the minimum amount of computer storage capacity required. The advantage of the incremental procedure is that the unloading portion of the load-response curve can be obtained. The slope-deflection method of analysis will be used with the incremental procedure in developing a computer solution to generate the load-response curves.

In the incremental load procedure, the load-deformation response curve is represented by a series of connected chords. At each stage in the computations, an increment of load ( $\delta P$ ) is chosen and the corresponding increment of deformation ( $\delta \Delta$ ) is computed. The accuracy that is required in generating the curve will dictate the size of the load increment to be chosen. Iteration is used to obtain the load increment when a plastic hinge forms.

### 3.2 LOADING AND FRAME GEOMETRY

The computer solution will be limited to rectangular, planar, multi-story frames with rigid beam-to-column connections. The base of the frame can be pinned, fixed, or of a type to simulate the support given to the top stories of a building frame by the stories below. The loads are applied in the plane of the frame and can be applied in two stages; an initial loading, and the succeeding incremental loads. Within either stage the loads are proportional. The horizontal loads are applied at the floor levels. The vertical loads are applied as distributed beam loads and or as two symmetrically placed, concentrated beam loads. Loads can be also applied directly to the columns. Any combination of these loads can be used in either loading stage. With this diversity, it is possible to simulate most loading conditions used in design practice.

### 3.3 BASIC ASSUMPTIONS

The basic assumptions made in the formulation of the computer solution are the following:

1. Elastic-plastic moment-curvature relationship.
2. A plastic hinge is replaced by a real hinge for the additional load increments.
3. During an increment of loading, all loads are proportional.

4. Strain-reversal does not occur in any yielded fiber.
5. Members are straight and prismatic. Out-of-plane behavior and local buckling are not considered.
6. Member length is from center-of-connection to center-of-connection.
7. Equilibrium equations are written for the members in their deflected positions.
8. Axial shortening of the members is neglected.
9. Axial loads in the beams are negligible.

Assumptions 1 and 8 will restrict the application of the proposed method to moderately high multi-story frames.

### 3.4 EQUILIBRIUM OF INCREMENTAL LOADS

The basic equations for a member in the slope-deflection method of analysis are obtained from the differential equation of a beam-column under transverse load.<sup>3.1</sup>

$$M_{ij} = \left(\frac{EI}{L}\right)_k [C_k \theta_i + S_k \theta_j - (C_k + S_k) \rho_{ij}] - M_{ij}^F \quad (3.1a)$$

$$M_{ji} = \left(\frac{EI}{L}\right)_k [C_k \theta_j + S_k \theta_i - (C_k + S_k) \rho_{ij}] + M_{ji}^F \quad (3.1b)$$

where  $C_k$  and  $S_k$  are the stability functions. The positive sign for the quantities in Eqs. 3.1 is shown in Fig. 3.1. The stability functions,  $C_k$  and  $S_k$ , are determined from

$$C_k = \frac{u(u + \cot u - u \cot^2 u)}{1 - u \cot u} \quad (3.2a)$$

and

$$S_k = \frac{u(u - \cot u + u \cot^2 u)}{1 - u \cot u} \quad (3.2b)$$

where

$$u = \frac{\pi}{2} \sqrt{\frac{P_i}{P_E}} \quad (3.3)$$

and  $P_E$  is the Euler load of the column. For any load increment ( $\delta P$ ), the axial load in a column ( $P_{i+1}$ ) during the load increment is estimated from the load ( $P_i$ ) being carried by the column at the beginning of the increment.

$$P_{i+1} = P_i \frac{P_i + (0.5)\delta P}{P_i} \quad (3.4)$$

Equations 3.1a and 3.1b assume elastic material properties and satisfy member equilibrium and compatibility requirements. The slope-deflection equations for the pertinent members can be grouped to satisfy joint equilibrium and story shear equilibrium. Compatibility within the structure is satisfied by solving for the unknown joint rotations and story sway deflections. The story shear equilibrium equation is written for the columns in their deflected position.

$$\Sigma M_{ij} + \Sigma M_{ji} + h\Sigma H + hp_{ij} \Sigma P = 0 \quad (3.5)$$

The development of the controlling relationships for the incremental load procedure is basically the same as that above. For an increment of load the stability factors ( $C_k$  and  $S_k$ ) are assumed to be constant and the axial load in a column is computed from Eq.

3.4. The slope-deflection equations for a member after an increment of load has been applied are

$$\begin{aligned} (M_{ij} + \delta M_{ij}) &= \left(\frac{EI}{L}\right)_k [C_k(\theta_i + \delta\theta_i) + S_k(\theta_j + \delta\theta_j) \\ &\quad - (C_k + S_k)(\rho_{ij} + \delta\rho_{ij})] - (M_{ij}^F + \delta M_{ij}^F) \end{aligned} \quad (3.6)$$

$$\begin{aligned} (M_{ji} + \delta M_{ji}) &= \left(\frac{EI}{L}\right)_k [C_k(\theta_j + \delta\theta_j) + S_k(\theta_i + \delta\theta_i) \\ &\quad - (C_k + S_k)(\rho_{ij} + \delta\rho_{ij})] + (M_{ji}^F + \delta M_{ji}^F) \end{aligned}$$

The incremental slope-deflection equations are obtained by subtracting Eqs. 3.1 from Eqs. 3.6.

$$\delta M_{ij} = \left(\frac{EI}{L}\right)_k [C_k \delta\theta_i + S_k \delta\theta_j - (C_k + S_k) \delta\rho_{ij}] - \delta M_{ij}^F \quad (3.7)$$

$$\delta M_{ji} = \left(\frac{EI}{L}\right)_k [C_k \delta\theta_j + S_k \delta\theta_i - (C_k + S_k) \delta\rho_{ij}] - \delta M_{ji}^F$$

For any connection, the sum of the incremental moments for the intersecting members is equal to zero. The story shear equilibrium equation at the end of the load increment is

$$\begin{aligned} \Sigma(M_{ij} + \delta M_{ij}) + \Sigma(M_{ji} + \delta M_{ji}) + h\Sigma(H + \delta H) \\ + h(\rho_{ij} + \delta\rho_{ij}) \Sigma(P + \delta P) = 0 \end{aligned} \quad (3.8)$$

The incremental equilibrium requirement for the story shear is obtained by subtracting Eq. 3.5 from Eq. 3.8.

$$\begin{aligned} \Sigma\delta M_{ij} + \Sigma\delta M_{ji} + h \Sigma\delta H + h \delta\rho_{ij} \Sigma(P + \delta P) \\ + h\rho_{ij} \Sigma\delta P = 0 \end{aligned} \quad (3.9)$$

The basic equations of the incremental procedure are Eqs. 3.7 and 3.9, and the requirement of joint equilibrium.

### 3.5 MATRIX FORMULATION

The deformation method of matrix analysis will be used to formulate the computer solution. The incremental relationships expressed in Eqs. 3.7 and 3.9 serve as a basis in this development. The member stiffness matrix ( $k$ ) relates the member incremental deformation vector ( $\theta^*$ ) to the member incremental stress vector ( $S^*$ ).

$$S^* = k\theta^* \quad (3.10)$$

or

$$\begin{bmatrix} \delta M_{ij} \\ \delta M_{ji} \end{bmatrix} = \left(\frac{EI}{L}\right)_k \begin{bmatrix} k_{ii} & k_{ij} \\ k_{ji} & k_{jj} \end{bmatrix} \begin{bmatrix} \delta\theta_{ij} \\ \delta\theta_{ji} \end{bmatrix} \quad (3.10a)$$

where

$$k_{ii} = k_{jj} = C_k$$

$$k_{ij} = k_{ji} = S_k$$

---

\*Indicates the matrix contains incremental quantities.

The member incremental deformation vector and the incremental displacement vector of the nodal points or joints of the frame ( $\Delta^*$ ) are related by a kinematic matrix (A).

$$\theta^* = A\Delta^* \quad (3.11)$$

or

$$\begin{bmatrix} \delta\theta_{ij} \\ \delta\theta_{ji} \end{bmatrix} = A \begin{bmatrix} \delta\theta_i \\ \delta\theta_j \\ \delta\rho_{ij} \end{bmatrix} \quad (3.11a)$$

Equilibrium between the external load vector for the nodal incremental forces ( $W^*_1$ ) and the member incremental stress vector is obtained by a statics matrix (C).

$$W^*_1 = C S^* \quad (3.12)$$

A relationship between the external incremental load vector and the nodal incremental displacement vector can be established from Eqs. 3.10, 3.11, and 3.12.

$$W^*_1 = (C k A) \Delta^* \quad (3.13)$$

Since it can be shown<sup>2.11</sup> that  $C = A^T$ , the first-order stiffness matrix of the structure ( $K_1$ ) is

$$K_1 = A^T k A \quad (3.14)$$

The total stiffness matrix of the structure ( $K^*$ ) contains second-order terms,  $h\delta\rho_{ij} \Sigma(P + dP)$ , in the story shear equilibrium

equation. Therefore,

$$K^* = K_1 + K_2^* \quad (3.15)$$

where  $K_2^*$  is a matrix containing the additional terms. There are also second-order terms,  $hp_{ij} \Delta P$ , that must be added to  $W_1^*$  to obtain the total load matrix ( $W^*$ ).

$$W^* = W_1^* + W_2^* \quad (3.16)$$

and

$$W^* = K^* \Delta^* \quad (3.17)$$

Since it is assumed that there is no member shortening, storage space can be economized by eliminating and combining specific rows and columns. The second order terms in the  $W_2^*$  and  $K_2^*$  matrices need not be stored separately and can be added to the  $W_1^*$  and  $K_1$  matrices respectively. The unknown terms of the nodal deformation vector in Eq. 3.17 can be obtained by the Gauss-Jordan solution technique or by iteration.

The member total stress vector ( $S_T$ ) at the end of the increment can be obtained from a previously computed total stress vector ( $S_{T-1}$ ) by adding the incremental stress vector ( $S^*$ ) and making the necessary correction ( $\delta M^F$ ) to include the effect of the transverse incremental beam loads.

$$S_T = S_{T-1} + S^* + \delta M^F \quad (3.18)$$

Before making this addition, the total stress vector ( $S_T$ ) is examined to determine if additional plastic hinges have formed during the increment of loading ( $\delta P$ ). If the plastic moment value is exceeded, iteration can be used to obtain a value ( $\delta P_{MOD}$ ) at which the first additional hinge forms. The total stress vector, the total displacement vector, and the load vector can be computed from increments scaled by the incremental load ( $\delta P_{MOD}$ ). The flow charts for the computer analysis are contained in Figs. 3.2 to 3.9. A more detailed formulation is given for two examples in the Appendix.

### 3.6 PLASTIC HINGES

When a plastic hinge forms in the structure, an additional degree of freedom of motion, the relative rotation of the cross-sections on either side of the hinge, is introduced. An additional line and column could be introduced into the stiffness matrix for each additional degree of freedom. This would be very uneconomical of computer storage space. Instead, the member stiffness matrix will be modified when hinges form without changing the nodal deformation vector. The relative rotation of the sections on either side of the hinge will not be computed.

After a hinge has formed in a member, the relative rotation of the sections on either side of the hinge occurs at a constant moment ( $M_{pc}$ ). For all additional increments of loads, the plastic hinges

are replaced by real hinges. The reduction in  $M_{pc}$  due to increases in the axial load in a column is considered in the next article.

When a hinge forms at the end of a member, the incremental slope-deflection equations can be adjusted to reflect the change in member stiffness.

$$\delta M_{ij} = 0 = \left(\frac{EI}{L}\right)_k [C_k \delta\theta_I + S_k \delta\theta_j - (C_k + S_k) \delta\rho_{ij}] - \delta M_{ij}^F \quad (3.19a)$$

$$\delta M_{ji} = \left(\frac{EI}{L}\right)_k [C_k \delta\theta_j + S_k \delta\theta_I - (C_k + S_k) \delta\rho_{ij}] + \delta M_{ji}^F \quad (3.19b)$$

where  $\delta\theta_I$  is the incremental rotation on the member side of the plastic hinge. The rotation ( $\delta\theta_I$ ) can be solved for in Eq. 3.19a and substituted in Eq. 3.19b to yield

$$\delta M_{ji} = \left(\frac{EI}{L}\right)_k \left[ \frac{C_k^2 - S_k^2}{C_k} (\delta\theta_{ji} - \delta\rho_{ij}) \right] + \left[ 1 + \frac{S_k}{C_k} \right] \delta M_{ji}^F \quad (3.20)$$

where numerically  $\delta M_{ij}^F$  equals  $\delta M_{ji}^F$ . This formulation does not require the computation of the additional deformation term ( $\delta\theta_I$ ), and the incremental joint deformation ( $\delta\theta_i$ ) is still obtained.

Matrices can be set up to record the location and the plastic moment capacity of the plastic hinges as they form in the members. In developing the stiffness matrix ( $K^*$ ) of the structure, Eq. 3.15 is first computed. The matrix that records the location of plastic hinges is searched for the location of the hinges. Terms similar to those in Eq. 3.19 are subtracted from the corresponding terms in

Eq. 3.15 and the terms in Eq. 3.20 are added to like terms in Eq. 3.15. The load matrix (Eq. 3.16) is likewise modified. Similar modifications of the stiffness matrix are made for other locations of plastic hinges in a member.

### 3.7 REDUCTION IN $M_{pc}$

The axial load in a column at a plastic hinge does not remain constant but continues to increase. This causes a shifting of the neutral axis in the cross-section towards the tensile flange of the column. Since the tensile area is decreased, there is a corresponding reduction in the moment capacity ( $M_{pc}$ ) at the plastic hinge. This produces an unloading of the moment in the column. The unloading of moment to the supporting members can be considered in the incremental procedure. Equation 3.4 is used in computing  $M_{pc}$  for the increment. With the formation of a hinge at the end of a member, the moment can be stated as

$$M_{ij} = M_{pc_0} \quad (3.21)$$

where  $M_{pc_0}$  is the plastic moment capacity of the member when the plastic hinge forms. For an additional increment of load,

$$M_{ij} + \delta M_{ij} = M_{pc_0} + \Delta M_1 \quad (3.22)$$

where  $\Delta M_1$  is the reduction in the original plastic moment capacity

$(M_{pc_o})$  caused by the increase in the axial load. The incremental equation is obtained by subtracting Eq. 3.21 from Eq. 3.22.

$$\delta M_{ij} = \Delta M_1 \quad (3.23a)$$

and

$$\delta M_{ij} = \Delta M_1 = \left(\frac{EI}{L}\right)_k [C_k \delta\theta_I + S_k \delta\theta_{ji} - (C_k + S_k) \delta\rho_{ij}] - \delta M_{ij}^F \quad (3.23b)$$

The incremental rotation ( $\delta\theta_I$ ) can be solved for and substituted into Eq. 3.19b to yield

$$\delta M_{ji} = \left(\frac{EI}{L}\right)_k \left[ \frac{(C_k^2 - S_k^2)}{C_k} (\delta\theta_{ji} - \delta\rho_{ij}) \right] + \left[ 1 + \frac{S_k}{C_k} \right] \delta M_{ji}^F + \frac{S_k}{C_k} \Delta M_1 \quad (3.24)$$

This equation differs from Eq. 3.20 by the addition of the last term. For the next increment of load, the total moment at the plastic hinge is

$$M_{ij} + \delta M_{ij1} + \delta M_{ij2} = M_{pc_o} + \Delta M_1 + \Delta M_2 \quad (3.25)$$

The incremental equation is obtained by subtracting Eq. 3.22 from Eq. 3.25

$$\delta M_{ij2} = \Delta M_2 \quad (3.26)$$

The equation for this second increment of loading can be obtained from Eq. 3.23a by changing the subscript on the term ( $\Delta M$ ). An equation similar to Eq. 3.23b is then developed. For succeeding increments, the pattern is repetitive. In the matrix formulation, the corrections described at the end of the previous article would first be

made. Then,  $\Delta M_i$  would be added to  $W_1^*$  in the load vector (Eq. 3.16) corresponding to joint i. The terms corresponding to joint j and to the story shear equation would have  $(\Delta M_i)$  S/C added to them. The reduced  $M_{pc}$  values would have to be stored at each stage in the computations to compute  $\Delta M_i$ .

### 3.8 STABILITY CRITERION

The limit of stability of a multi-story frame under gravity loading is attained when the lateral deformations increase with no increase of vertical load. Mathematically, this can be expressed as

$$\frac{\partial P}{\partial \Delta} = 0 \quad (3.27)$$

A similar criterion can be developed for the incremental load procedure. At the instability load, the incremental sway deflection ( $\delta\Delta$ ) in the incremental story shear equilibrium equation would increase with no change in the incremental load. Equation 3.9 would be modified to omit terms containing  $\delta P$  and  $\delta H$ . For a stable structure

$$\Sigma\delta M > h \delta\rho\Sigma P \quad (3.28)$$

This equation states that, if the frame is in a deflected, stable configuration and a small lateral disturbance is applied, the incremental restoring moments ( $\Sigma\delta M$ ) must be greater than the added overturning moment ( $h\delta\rho\Sigma P$ ).

In the computer analysis, a small increment of load is applied to the frame and a compatible set of incremental deformations is computed. If the incremental sway deformations are positive, a stable deflection position is possible. If the incremental sway deformations are negative, then the frame instability load has been exceeded. Points on the unloading portion of the curve can then be obtained by using negative incremental loads. The accuracy in computing the value of the frame instability load is determined by the magnitude of the incremental load. If too large a value of incremental load is used, an additional problem arises. In a real frame, the instability load is gradually reduced as yielding takes place. In the elastic-plastic analysis, the frame instability load is reduced in finite increments with the introduction of each new hinge. The frame instability load is usually reached when a hinge forms. If the deteriorated critical load is within the bounds of  $P \pm \delta P$ , then the computation for the sway deflection will yield negative incremental deformation values for both positive and negative load increments. The unloading portion of the curve can not be obtained unless the load increment ( $\delta P$ ) is reduced.

### 3.9 COMPARISONS WITH AN ITERATION SOLUTION

A comparison is made for the frames shown in Figs. 3.10 and 3.11 between the load-response curves generated by the incremental

2.1  
procedure and those from an iteration method. The solid curve in each figure is the result from the iteration method. The points are from the incremental procedure. The dashed curve in Fig. 3.10 is a second-order, elastic-plastic moment distribution solution.<sup>2.12</sup> The incremental procedure and the iteration method were formulated from slope-deflection equations and there is a close correspondence between them. The table at the top of Fig. 3.10 is a comparison of lateral sway deflection ( $\Delta_i$ ) for the two slope-deflection formulations at a load factor of 1.90. The correlation is extremely good.

The small discrepancies between the incremental and iteration procedures are caused by the techniques used to compute the loads at the formation of a hinge. In the iteration method, small load increments were used to approach the hinge. This tends to understate both the load and deformation at the formation of the hinge. The incremental procedure used only one cycle of iteration to determine the coordinates specifying a plastic hinge. At the frame instability load, the incremental solution for the frame in Fig. 3.10 had a deflection of 4.2 in. The iteration method could not converge to a point in this region. If the increment of load in the iteration method were smaller, this point could be obtained. The accuracy in the incremental procedure could be improved by using more than one cycle of iteration at a plastic hinge.

#### 4. DESCRIPTION OF TESTS

##### 4.1 FRAME DESIGN

Frame buckling tests were conducted on the two frames shown in Fig. 4.1. Proportional loads were applied as indicated in Fig. 4.2. The loads on the top floor were reduced to prevent plastic hinges from prematurely forming in the top beams. Individual members of the frame were designed by plastic design procedures assuming that the frame was braced.<sup>4.1</sup> The beams were designed to fail by a beam mechanism. The columns were required to carry the axial loads and to have a moment capacity that was just sufficient to satisfy the equilibrium requirement at the bottom story beam-to-column connection. Although the ultimate load was defined on the basis of strength as the beam mechanism load, both the beams and the columns were designed to act at their maximum capacities.

Additional requirements were placed on the members and on the frame geometry. The columns were to have a slenderness ratio of 40 and 45 for Tests 1 and 2, respectively. The column axial load ratio ( $P/P_y$ ) at failure was to be 0.4, and the ratios of member sizes and lengths were to approximate those of members in the top stories of multi-story frames. A trial and error process was used to obtain the beam length, member sizes, and the loads. Difficulty was encountered because of the limited number of lightweight, structural

shapes available. Other considerations were the capacity of the loading system, and the spacing of the anchorages in the test area. In order to comply with all of the imposed conditions, the columns had to be of A441 steel. The column section described in Table 4.1 was a 4WF13 structural shape and it was continuous for the height of the frame. The beam section was a 6B16 structural shape of A36 steel. The beam span, center-of-connection to center-of-connection, was 10 ft in both tests. The beam-to-column connections were designed according to Section 2.7 of the AISC Specification.<sup>1.5</sup>

In each of the tests, two identical frames were braced together to function as a unit and to be free of external restraints (Figs. 4.3 and 4.4). The lateral bracing connecting the two frames was a 2 in. channel section (Table 4.1), and it was designed to give adequate lateral support to the beams and columns. The cross bracing members were 3/8 in. diameter rods and they were designed to force the two frames to act as a unit. Premature failure by local buckling was minimized by choosing beam and column sections which satisfied the  $b/t$  ratios used in plastic design under the AISC Specification.<sup>1.5</sup> Lateral torsional buckling of the column section under axial and bending loads was not a problem since the columns were braced. In addition, the section's  $K_T/Ad^2$  value was such that the full in-plane capacity could be achieved without the aid of lateral bracing.<sup>4.1</sup> Instability of the individual column members was not anticipated since their slenderness ratios were low.

#### 4.2 LOADING SYSTEM AND TEST SETUP

Vertical loads were applied to the frames through the tension jacks of the gravity load simulators. The simulators are shown in an undeflected position in Fig. 4.4. The simulators were designed to allow the tension jacks to move freely with the frame as lateral sway took place in the plane of the frame.<sup>4.2</sup> Figure 4.5 shows the frame and the simulators in a deflected position. A common hydraulic fluid hose line was connected to the four tension jacks which applied the loads to the middle and bottom floorbeams. The pressure in the common hydraulic line for the two top floor jacks was regulated to be approximately three-quarters of that for the other loading jacks.

The jack loads were distributed by the tie rods to the ends of the load beams (Fig. 4.3) and through them to the spreader beams. Because of the common hydraulic hose line and the symmetry of the loading system, a load from a jack was divided equally to the two load points at the end of the spreader beam. The loading beam and spreader beams for each story were pre-assembled on the laboratory floor. The alignment was done with a carpenter square and a measuring tape. No further adjustments were required, since under preliminary loading the differences among the dynamometer readings for a particular story were within the reading accuracy of the individual dynamometer. Pins were used in the connections for the tie rods and dynamometers and the linkages formed gave the loading system additional freedom to move laterally with the test frame. In a linkage under tensile load, the point of load application will line up with the resisting point at the opposite end of the linkage system.

The test frames were bolted to the pin base fixtures shown in Fig. 4.6. The base fixtures were in turn bolted to the column pedestals. The column pedestals and gravity load simulators were bolted to the test bed fixtures as shown in Fig. 4.7. These fixtures were held to the test bed floor by  $2\frac{1}{2}$  in. diameter prestressed studs. The vertical line of support for the gravity load simulators did not coincide with that of the prestressed studs of the column pedestal. This caused a moment to be applied to the test bed fixtures. The resulting twisting caused a negligible amount of inward movement of the column base fixtures. As a precautionary measure, braces were welded between the column pedestals in Test 2. This minimized the movement.

#### 4.3 INSTRUMENTATION

The instrumentation for the frame tests was designed to obtain information concerning both the external and internal frame behavior. Transits were used to measure the horizontal movement of points along the outside face of each column. Levels were set up to read the vertical motions of the center of the beams and of the beam-to-column connections. Dynamometers were used to determine the loads applied through each of the load points. The pressure gage readings of the loading console also were used to measure the applied loads.

Electrical resistance wire strain gage readings were taken to determine the distribution of strains at two cross-sections of each beam and each column length. In the bottom story, four gages were used at each cross-section location. At the middle and top floor locations, two gages were used. The above readings, along with data of the material properties, cross-sectional geometry, and frame dimensions, provided input to a computer program. The output consisted of axial loads, shears, and distributions of moments along each of the members. Equilibrium was based on the second-order theory.

Rotations of the pin bases were obtained from readings of mechanical rotation gages (Fig. 4.8). The rotations of the members at the beam-to-column connections were obtained from electrical rotation gages (Fig. 4.9). Horizontal and vertical deflection scales and a strain gage location also can be observed in this figure. Dial gages measured the inward motion of the column pedestals. Records of visual observations of mill scale flaking and other pertinent data were kept.

#### 4.4 FRAME ALIGNMENT

The column pedestals and pin bases were accurately set with a transit and tape. The same procedure was used for the bases to which the gravity load simulators were bolted. The tops of the column pedestals were set level with a steel straight edge and a carpenter level.

The distance between center lines of the column base plates had fabrication errors in both test frames. For example, in Test 2, the dimension between the two parallel frames was 5/16 in. short and the 10 ft dimension between columns was 1/8 in. short. The corresponding dimensions at the first floor level were accurate to 1/16 in. Rather than bend the column legs to fit the accurately set column pedestals, the column base plate holes were enlarged slightly.

The first test was conducted during the 1965 Summer Conference on "Plastic Design of Multi-Story Frames" at Lehigh University. Time requirement and equipment usage did not permit the accurate alignment of the test frame. A plumb bob was used in measuring both the in-plane and out-of-plane alignment of each of the columns. In the second test, the frame was plumbed in the out-of-plane direction by inserting long metal strips between the top of the column pedestals and the bottom of the pin-base fixtures. The frame was plumbed in the in-plane direction by inserting similar wedges between the top of the pin-base fixtures and the bottom of the column base plates. A transit was used to measure the initial out of alignment. The American Institute of Steel Construction in its "Code of Standard Practice" states:<sup>1.5</sup>

"....In the erection of multi-story buildings individual pieces are considered plumb, level and aligned if the error does not exceed 1:500..."

This criterion was satisfied in both tests. However, the measured fabrication errors could be used to predict the direction in which the frame would sway. In the second test, for example, two of the column

tops were out of plumb to the north and the other two to the south. The net effect was self-canceling. From an examination of the eccentricities that existed in the lower stories, it was possible to correctly predict that the frame would sway to the south.

#### 4.5 MATERIAL AND SECTION PROPERTIES

Frame members of each shape size were rolled from the same heat and ingot. The members were cold straightened by gapping. Tension tests were conducted on specimens cut from lengths, arbitrarily selected, from which the test frames were fabricated. The values from the tension tests are summarized in Table 4.2.

A beam bending test was conducted on a 6B16 section to obtain the moment-curvature relationship and to substantiate the plastic moment value computed from the tension test data. Cross-sectional properties were computed on the basis of measurements taken at locations along the members. These values, shown in Table 4.1, agree with the handbook values. The eccentricities in the cross-sectional geometry were within the tolerance limits on rolling as outlined in the AISC Specification.<sup>1.5</sup>

#### 4.6 FRAME LOADING

The loads applied through the tension jacks were controlled at the load console of the hydraulic loading system (Fig. 4.10). The

distribution of the loads on the frame is indicated in Fig. 4.2. During the early stages of loading, pressure increments were set in the top story jacks and then in the lower jacks. This was accomplished with two complete and separate pumping systems (Fig. 4.11). The pressure level in the particular system was maintained through a needle valve. In the later stages of loading, either a pressure increment or an increment of horizontal deflection of the bottom floor level was used as the load increment. The load ratio shown in Fig. 4.2 was maintained throughout both tests.

When the frame buckling load was reached, the frame lost its ability to react against the constant pressure being maintained by the hydraulic pumps. The frame moved laterally while the pressure was being held constant. To obtain an equilibrium position, it was necessary to quickly close the entrance valve to each of the loading jacks. The frame could not immediately resist the "locked-in" pressure and it continued to move laterally. The beams continued to deflect vertically. Since the piston in the jack was being displaced, the "locked-in" pressure was reduced. The frame was then capable of resisting the reduced pressure and an equilibrium position was obtained in the unloading portion of the load-deformation response curve. A ten to fifteen minute period was observed between the application of a load increment and the taking of readings to allow the frame to adjust to the plastic yielding and the lateral movement.

## 5. EXPERIMENTAL RESULTS AND COMPARISONS WITH THEORETICAL PREDICTIONS

### 5.1 EXPERIMENTAL BEHAVIOR

The load-lateral sway deflection curves for the two frame buckling tests are shown in Fig. 5.1. The ordinate for the curves is the quarter point load,  $P$  (non-dimensionalized as  $P/P_B$  where  $P_B$  is the corresponding load required to form a beam mechanism). The abscissa ( $\Delta_h$ ) is the lateral sway deflection at the first floor level. In Test 1, the ultimate load was well defined and two points were obtained on the unloading portion of the load-response curve. In Test 2, only one point was obtained on the unloading portion of the curve. The sway deflection for this point was 1.98 inches. An exact value of the ultimate load for the second test was not obtained. The maximum stable load obtained during the second test is indicated as point 1 on curve 2. At this load an increment of pressure, equivalent to an increase of 1 kip in the load  $P$ , was applied to the tension jacks. The frame deflected and appeared to stabilize under the increased pressure. A minute later, a reading of deflection through the transit showed that the sway of the first floor was increasing rapidly. The frame instability load had been exceeded. The entrance valves for the loading jacks were immediately closed. The frame came to the equilibrium position indicated at point 2. The ultimate load for Test 2, which is listed in Table 5.1, is an approximation

based on using one-half of the final pressure increment. This ultimate load is at the level indicated by the line at 3 in Fig. 5.1. The arrow symbol from point 1 to point 2 is used throughout for the results of Test 2 to designate that the maximum load point is not well defined.

The load-response curves for both test frames are very similar. The frame in Test 2 had more slender columns and therefore had larger lateral deflections in the earlier stages of loading. At values of  $P/P_B$  less than 0.4, the curves are almost linear and the sway deflections are negligible. For a working load ordinate of 0.6, the sway deflection for Test 2 is 0.10 inches. This is equivalent to a bottom story column chord rotation of 0.0013 radians. This rotation is less than the usual maximum working value of 0.002. For values of  $P/P_B$  greater than 0.85, the sway deflections increase excessively.

Figure 5.2 compares the lateral sway deflection to the vertical beam deflection in Test 1. At a working load ordinate of 0.6, the ratio of lateral sway deflection to vertical beam deflection is 1 to 9. The sway deflection is relatively small. At the frame instability load, the ratio is about 1 to 1. In the post-buckling range, both the deflections continue to increase even though the quarter point load ( $P$ ) is reduced. Generally, the shape and relative deformation of the two load-response curves correspond closely to the frame buckling behavior described in Chapter 2.

It should be noted that the sway deflection at the frame instability load is equivalent to a column chord rotation of only 0.0075 radians. This rotation is approximately 4 times the usual working value of 0.002, and it emphasizes the importance of considering lateral stiffness in the design procedure.

The significant effect of yielding on the instability load of the test frames is shown in Fig. 5.3 and 5.4. The plastic moment value indicated was computed from an average stress obtained from tensile coupon tests and a beam test. The first plastic hinges formed in each test at the load immediately before the frame instability load. These hinges were located at the load point on the first floor beam and at the leeward end of the second floor beam. When the frame instability load of Test 1 was attained, plastic hinges had formed at locations 1, 2, 3, and 4 indicated in Fig. 5.3. The moments at the corresponding locations of Frame 2 (Fig. 5.4) indicate a similar yield pattern. Thus, there was general yielding in the beams when the frames buckled.

While the above plastic deformations were occurring in the beams, the load-response behavior of the moments at the ends of the columns underwent a significant change. This is indicated in Fig. 5.5 by the movements of the inflection points of the columns and the general shifting of the beam moment diagrams in the direction of the sway. (The formation of a plastic hinge is designated by a heavy line).

The changes in the column moments and the yielding in the beams are related through the equilibrium requirements at the beam-to-column connections as in Figs. 5.6a and 5.6b. Curve 1 of Fig. 6a indicates that at the frame buckling load a plastic hinge formed in the end of the beam corresponding to joint A. Prior to this load, the column locations at 2 and 3 maintained joint equilibrium by supplying moments opposite in rotational direction to the moment at location 1. In the post-buckling range, the moment at 1 did not change appreciably and, as the column moment at 3 increased to maintain bottom story shear equilibrium, the column moment above the joint decreased in order to satisfy the joint equilibrium requirement. Figures 5.5c and 5.5d show that a similar readjustment occurred in the columns at the joint immediately above A.

At joint B, the beam moment at location 4 began to unload at the load immediately before frame buckling occurred. Prior to this load, the moment at location 6 was opposite to that required to resist the  $P-\Delta$  effect in the bottom story. As the moment in the end of the beam unloaded, the column moment at 6 also unloaded. By so doing, it tended to maintain the required joint equilibrium while also contributing to balance the  $P-\Delta$  moment. The moment in the column at location 5 increased slightly to satisfy joint equilibrium. A similar behavior is also shown in Fig. 5.5c and 5.5d for the joint above B.

The shear equilibrium requirement in the bottom story is shown graphically in Figs. 5.7a and 5.7b. The line inclined at  $45^\circ$

represents the equilibrium condition. Along this line, the algebraic sum of the resisting end moments of the columns balances the overturning P- $\Delta$  moment. In order to obtain a satisfactory balance, the average initial alignment error for each frame ( $e_{avg}$ ) was added to  $\Delta$  in the P- $\Delta$  effect. The difference between the overturning and resisting moments is equal to the distance between the two curves. These differences tend to balance between frames of the same test. The magnitude of the resulting errors is less than the reliability limit of the strain gage readings.

The moments in the beam and columns in the bottom story for the buckling and post-buckling portions of the curves are similar to those of a portal frame on the verge of a combined beam-sway mechanism. The moments where the hinges would form in such a mechanism are plotted in Figs. 5.8a and 5.8b with the sway deflection as the abscissa. The sway deflection at the frame buckling load is indicated for Test 1. The first signal to the approach of the frame buckling load was the unloading that took place at location 4. In the post-buckling range the beams had no moment change and the columns continued to maintain bottom story shear equilibrium. At the last load point of Test 1, a hinge formed in the column at location 3. A mechanism would have occurred, if an additional hinge formed at either location 4 or at location 5 of Fig. 5.6. The  $M_{pc}$  value of the former location is 250 kip-inches, and at the latter it is 285. Figure 5.9 portrays the frame from Test 1 in a deflected position. Figures 5.10 and 5.11 depict the yielding that took place at joint A and the beam load point.

The overall behavior of the two test frames was similar with regard to both internal (Figs. 5.12a and 5.12b) and external behavior (Fig. 5.1). The impetus for the initial lateral sway deflection was the eccentricities that resulted from the fabrication and alignment procedures. The sway deflections increased as the gravity loads were increased. A general deterioration of lateral stiffness resulted from yielding in the beams. This preceded the occurrence of the frame instability load.

## 5.2 COMPARISON OF THEORETICAL AND EXPERIMENTAL CURVES

A theoretical method for predicting frame buckling loads has been proposed. Two frames have been tested and experimental load-response curves have been obtained. The proposed method can be validated by comparing the theoretical predictions and the experimental load-response curves for both external and internal behavior.

The theoretical and experimental curves for center-line beam deflection for Test 1 (Fig. 5.13a) and Test 2 (Fig. 5.14a) show an excellent correlation. In Figs. 5.13b and 5.14b the theoretical and experimental sway deflections of the first floor beam are compared. The theoretical curves are those obtained by arbitrarily setting  $\alpha$  equal to 1/2 and to 1 percent. A direct correspondence between the theoretical and experimental points should not be expected because of the method of selecting  $\alpha$ . The important requirements in

the comparison are that

- 1) the general shape of the curves must be similar,
- 2) the theoretical curves must approach the experimental curve as  $\alpha$  approaches zero, and
- 3) the theoretical buckling load should give a good prediction of the experimental frame buckling load.

The experimental and theoretical frame buckling loads for the two test frames are listed in Table 5.1. The theoretical predictions were computed by the limit procedure illustrated in Fig. 2.10. The percent errors between the theoretical frame buckling load and the experimental ultimate load for Tests 1 and 2 are 2.4 and 2.8 percent, respectively. Requirement 3 is satisfied. The curves in Figs. 5.13 and 5.14 show that requirements 1 and 2 are satisfied by the external load-response functions. Similarly, Figs. 5.15 and 5.16 show that these requirements are satisfied by the internal load-response functions. The theoretical and experimental curves have the same shape and in the limit, as  $\alpha$  approaches zero, the theoretical curve tends to approach the experimental curve.

The only difficulty to mar this otherwise close correspondence is in the order of the hinge formation. The differences in the magnitudes of the loads at the hinge formations are minor. The theoretical solution shows that hinges form almost simultaneously at the ends of the beams, as indicated by the 1 and 2 on the curves of

Fig. 5.13b. The third hinge forms at the first floor load point at the frame instability load. The maximum value at location 5, using the limit technique, would be  $0.85 M_p$ . The fourth hinge forms at the last load point. There are two principal causes for the difference between the theoretical and experimental order of hinge formation. One is the elastic-plastic, moment-curvature assumption in the theoretical analysis. Using this assumption, a section is either elastic or plastic. At the formation of a plastic hinge, there is an abrupt change in the load-response function. Between the formation of plastic hinges, the structure reacts elastically. In an actual structure, the yielding is gradual and there is a corresponding decrease in the lateral stiffness. Since the inelastic behavior is affected by the residual stresses from rolling, fabrication, and erection, the yielding will first begin at a load lower than theoretically predicted and possibly not at the initial hinge location theoretically predicted. The second cause for the difference in the pattern of hinge formation is that in the theoretical analysis  $\alpha$  is assumed to be equal for all floors whereas the resulting eccentricity between the various floors are not equal. A change in the assumed value for  $\alpha$  from floor to floor can alter the distribution of the moments throughout the frame, the load at which the first hinge forms, and the order of hinge formation. To obtain a better prediction for the order of the hinge formation, a theoretical solution would have to predict the above inelastic behavior and consider the resulting eccentricities of the structure. As previously stated, this does not seem to be practical with the present (1967) computer technology.

### 5.3 DISCUSSION

The method proposed for computing the frame buckling load recognizes in the limit procedure that eccentricities exist within a frame. It does not at any stage in the analysis try to evaluate them but rather approximates their effect by a small lateral load applied at each floor level. A justification for the positioning of these lateral loads has been made. The frame buckling load is obtained by having the value of the proportionality constant ( $\alpha$ ) of the small lateral loads, or equivalently the resulting eccentricity at each floor level, approach zero. Within this limit approach, the correspondence between the theoretical and experimental load-response curves is good. The theoretical prediction for the experimental frame buckling loads is excellent. These two tests, although limited in number, verify the proposed method.

## 6. ANALYTICAL FRAME BUCKLING STUDIES

### 6.1 INTRODUCTION

The limit procedure for obtaining inelastic frame buckling loads will be used to develop frame buckling curves and to study the changes in frame buckling loads caused by varying some of the structural parameters. The frames to be used in the analytical study are basically the same as the test frame shown in Fig. 3.1. The two frames for which there is experimental verification of the frame buckling loads will be incorporated, when possible, into the analytical studies. The results from the analytical studies, although for frames reduced in size, are applicable to frames found in practice. A comparison is made in Table 6.1 between the parameters of Test Frame 1 and those of a frame, similarly designed, under a light manufacturing type loading. The agreement between the parameters is good, and therefore the relationships developed by the studies can be implemented in design practice.

### 6.2 FRAME BUCKLING CURVES

#### 6.2.1 Variable Column Length

The variable in the frame buckling curve of Fig. 6.1 is the column length. The abscissa for the curve is the column slenderness

ratio ( $h/r_x$ ). The ordinate of the curve is the frame buckling load, which is non-dimensionalized by the beam mechanism load. The frames are loaded at the quarter points of the beams. For low values of column slenderness, the frame buckling load approaches the beam mechanism load as an asymptote. For the usual range of column slenderness values found in the top stories of multi-story buildings (30 to 50), there is a gradual reduction in the beam mechanism load of 5 to 10 percent with increasing slenderness ratio. The corresponding load factors are 1.61 to 1.53. These compare to a load factor of 1.70 for the beam mechanism load. Beyond a slenderness value of 50, there is a rapid reduction in the beam mechanism load caused by frame buckling. The reason for this reduction can be seen in the load-response curves (Fig. 6.2) which were developed in the computation of the frame buckling loads.

The load-response curves of Fig. 6.2 are for an  $\alpha$  of 1/2 percent. The numbers along the curves refer to the hinge locations on the frame and indicate the load at and the sequence of hinge formation. The column slenderness values ( $h/r_x$ ) are indicated for the individual curves. For low values of column slenderness, the initial slope of the load-response curves is relatively steep. There is a general yielding in the beams and an increase in load occurs between the formation of the first hinge and the frame instability load. For column slenderness values of 50 and greater, there is a large reduction in the slope of the curves during the early stages of loading. The values for the frame instability loads are lower and they coincide

with the formation of the first hinge. At values of column slenderness of 70 and above, the frame fails in the elastic range. The transition is one from inelastic to elastic frame instability as the column slenderness ratio increases.

There is a close similarity between the frame buckling curve (Fig. 6.1) and the buckling curve of a pinned-end column. The load-response curves for  $\alpha$  equal to 1/2 percent indicate that, as in a column, there are three buckling ranges; an inelastic frame buckling range, an elastic buckling range, and a transition range. The boundaries for these ranges are not fixed but are dependent on the frame parameters. For the curve in Fig. 6.1, which was developed for the specific frame shown, the inelastic frame buckling range applies to columns with slenderness ratios less than 50. The elastic frame buckling range is for columns with slenderness ratios greater than 70. The transition range is for columns with slenderness values from 50 to 70.

The concept of effective column length can also be considered in connection with frame buckling. The free-body in Fig. 6.3 shows the columns in the bottom story of a frame. The columns are restrained by rotational springs, which simulate the effect of the restraints provided by the members framing into the respective connections. The column tops are forced to sway as a unit and therefore the individual column cannot be isolated in describing the sway behavior.

For columns with slenderness ratios less than 50, the initial lateral sway of the frame is small. In the early stages of loading, the effective length of the columns is relatively constant. As the loading increases, the lateral sway and the effective column lengths increase. As yielding takes place in the beams, the rotational restraint provided by the beams to the columns is reduced. The spring moduli,  $\beta_1$  and  $\beta_2$ , are not constants but are decreased by yielding. This results in a rapid increase in the effective column lengths. The problem becomes further involved because the reductions in  $\beta_1$  and  $\beta_2$  are not the same, and thus the effective lengths of the columns are not equal. One of the columns will reach an effective length and support loads at which an elastic column having the same effective length would buckle. The column with the larger effective length becomes unstable and exerts a lateral pull through the beam on the other column. The lateral sway increases and both effective lengths are further increased. Failure of the frame occurs thereafter.

The concept of effective length tends to oversimplify the behavior but it does indicate that there are two principal factors involved in determining the shape of the frame buckling curve. They are the column length and the beam restraint. The effective length of the columns is increased by reductions in the rotational restraints of the supporting members and by changes in the geometry caused by the lateral sway of the frame. These are interrelated through the column slenderness. For very slender columns the lateral sway increases rapidly, even in the early stages of loading. The effective

length similarly increases until failure occurs without any yielding. For columns with slenderness values found in the transition range, the initial sway is relatively large and there is a corresponding change in the effective column length. Yielding occurs and the restraints provided by the beams are reduced. Frame instability occurs immediately upon this reduction in the rotational restraint. The overall behavior is controlled by the column slenderness ratio. Yielding accelerates the changes in the effective column length.

#### 6.2.2 Effect of Beam Yield Stress

If the yield stress of the beams is increased while the other parameters are held constant, the frame buckling load will increase. The increase in the beam yield stress allows the rotational restraints provided by the beams to the columns to remain elastic at higher values of load. The curve for the frame buckling loads (Fig. 6.4) shows this increase.

However, there is a corresponding increase in the beam mechanism load. The non-dimensionalized frame buckling curve ( $P_{cr}/P_B$ ) shows a slight decrease for increasing beam yield stress. The increase in the beam mechanism load, which is linear, is more rapid than the increase in the frame buckling load. The load-response curves in Fig. 6.5 show that, after the second hinge has formed in the frames, the columns with the higher axial load ( $F_y = 42$  ksi) have a smaller remaining load capacity. The stability effect in the columns is responsible for the slight decrease in the non-dimensionalized curve.

The frame with the load-response curve corresponding to a yield stress of 42 ksi, has a plastic hinge form in the column at the frame instability load. The column was designed to carry the axial load and to balance the moment equilibrium requirement at the bottom story beam-to-column connection. The plastic moment capacity of the beam was increased 20 percent without a corresponding increase in the column size.

### 6.3 DISCUSSION

The results of the studies indicate that there are three important parameters in a frame buckling analysis. They are the column slenderness ratio, the rotational restraints provided to a column by its supporting members, and the strength of the individual beams and columns. These parameters are interrelated through the design methods used in obtaining the member sizes. The method of column design determines whether a column behaves elastically or inelastically at the frame buckling load. An ideal situation is for plastic hinges to be on the verge of forming in the columns when frame buckling occurs. If a hinge forms prior to this, the effective length of the particular column is greatly increased and the remaining columns in the story will be more heavily stressed in resisting the additional overturning moments.

Considering strength alone, the ultimate load for the frames in the studies is the beam mechanism load. The numerical

values of the frame buckling loads by themselves are not too significant. They should always be compared to the design ultimate load (beam mechanism load) of the frame. If this is not done, incorrect conclusions can result.

In the frame buckling studies of this chapter, only pinned-base frames have been considered. If a base condition other than pinned is used, the effective length of the column in the bottom story will be decreased and the frame buckling load will be increased. Also, the frames considered in this chapter were loaded at the quarter-points of the beam. The frame buckling load will be influenced by the position of the loads on the beams. The effects of the changes in base support and the load position will be examined in subsequent chapters.

## 7. PRIMARY BENDING EFFECT

### 7.1 INTRODUCTION

The studies of frame buckling for building columns fall within the inelastic frame buckling range. Any factor that affects the restraints provided by the beams to the columns will cause variations in the frame buckling loads. An important factor is the positioning of the transverse loads on the beams or the primary bending effect.

The primary bending effect will be studied for a three-story and a six-story building frame. These frames are basically the same as those of the previous studies. The column section in the bottom three stories of the six-story frame is a 5WF16 structural shape of A441 steel. It is designed on the same basis as the columns of the three-story frame. The axial load and the moment equilibrium requirement at the bottom story beam-to-column connection control the column size.

Two concentrated loads will be symmetrically applied about the centerline of each beam in the frame at a distance (a) from the center of the connections. The variable in the study will be the distance (a), non-dimensionalized by the beam length (L). Values of  $a/L$  smaller than 0.20 will not be considered, since the deformations

of the frames are computed assuming that the effects of the shearing forces are negligible.

## 7.2 PRIMARY BENDING MOMENT

### 7.2.1 Three-Story, Pinned-Base Frame

The effect of the primary bending moment on the inelastic frame buckling load is shown in Fig. 7.1. As the two concentrated loads are moved toward the center of the beam, there is a reduction of over 50 percent in the value of the frame buckling load ( $P_{cr}$ ). The primary bending moment then has a significant effect on the inelastic frame buckling load. This reduction varies directly with the increases shown in the curve for fixed-end moments ( $M^F$ ). The ordinates of this curve were computed for two concentrated beam loads of 10 kips each, positioned at a distance ( $a$ ) from the fixed-ends of the beam. The relationship between the reductions in the frame buckling loads and the increases in the fixed-end moments is made more clear by the load-response curves in Fig. 7.2.

The load-response curves show the general yielding that occurred prior to the frame instability loads. In the early stages of loading, the lateral sway deformation was the same for all of the frames. The fixed-end moments for  $P$  equal to 10 kips were shown above to vary widely with the position ( $a/L$ ) of the two concentrated loads on the beams. Hence, the distribution of the moments within the

frames varied considerably, even though the elastic sway deformations of the frames were equal. At a load (P) of 10.3 kips, yielding began first in the frame with an  $a/L$  value of 0.5. The first hinge formed in the frame with an  $a/L$  value of 0.2 at a load of 24.1 kips. The difference in the initiation of yielding is directly related to the fixed-end moments or to the primary bending effect. Previously, it was shown that the effective column length was significantly affected by a reduction in the rotational restraint provided by the beams. Here, it is shown that the primary bending effect is directly related to the yielding and to the reduction in the rotation restraints. The primary bending then has a direct effect on the inelastic frame buckling load.

The numerical reduction in the frame buckling loads caused by the primary bending effect is quite large. However, if the buckling load for each frame is non-dimensionalized by its beam mechanism load, a different result occurs. Both the frame buckling curve and the non-dimensionalized curve are shown in Fig. 7.3. The frame ( $a/L$  of 0.5) with the largest reduction in the numerical value for the frame buckling load has no reduction in the design ultimate load (beam mechanism load) caused by frame buckling. The frame ( $a/L$  of 0.2) with the highest value for the frame buckling load has a 15 percent reduction in the beam mechanism load. The variation in the beam mechanism load with  $a/L$  is also shown in Fig. 7.3. As  $a/L$  gets smaller, the beam mechanism load increases more rapidly than the frame buckling load. This accounts for the reversal in conclusions as to the deleterious effect of primary bending and again points to the importance of

comparing the value of the frame buckling load with the design ultimate load (beam mechanism load).

### 7.2.2 Six-Story, Pinned-Base Frame

The load-response curve for the six-story frame (Fig. 7.4) has a general yielding pattern similar to that for the three-story frame. For most values of  $a/L$ , an extra hinge forms in the six-story frame at location 3. The load on this beam in the three-story frame was reduced to force the initial yielding to occur further down in the structure and not at location 3.

The effects caused by the increase in the number of stories are evident. There is a reduction in the frame instability loads and a much smaller increase of load between the first yielding and the frame instability load. These effects are caused by an increase in the overturning moments,  $\sum P_i (\Delta_i + e_i)$ , due to the greater number of stories. The overturning moments directly affect the column moments, and through the connections of the frame directly affect the beam moments and the rotational restraints provided by the beams to the columns.

The variation of the frame buckling load with  $a/L$  (Fig. 7.5) is generally the same for the six-story frame as for the three-story frame. The largest difference between the frame buckling load values occurs for the frames with  $a/L$  of 0.2. As the  $a/L$  ratio increases,

the difference between the ordinates of the curves decreases. Figure 7.6 shows the non-dimensionalized curves for the three and six-story frames. As the  $a/L$  ratio approaches 0.5, both of the frame buckling curves approach the beam mechanism load.

### 7.2.3 Variable Beam Length

The curve for  $P_{cr}$  in Fig. 7.7 shows the changes in the frame buckling load of the three-story frame caused by varying the beam length. As the beam length increases, the frame buckling load decreases. In the preceding sections, this reduction was related to the fixed-end moment ( $M^F$ ) or the primary bending effect. In this study, the fixed-end moment increases with the beam length and therefore the frame buckling load decreases.

The load-response curves (Fig. 7.7) show the general yielding that preceded the frame instability loads. At the higher values of load, the differences in the slopes of the load-response curves caused by the variable beam lengths become discernable. At a load ( $P$ ) of 18 kips, the lateral deformations of the frames are approximately the same. The fixed-end moments ( $M^F$ ) shown in Fig. 7.7 are for a load ( $P$ ) of 18 kips. They vary linearly with the beam length. At a load of 19 kips, the first hinge forms in the frame with the longest beam span. Yielding first occurs in the frame with the shortest beam span at a load ( $P$ ) of 24.4 kips. Thus, the reduction in rotation restraint is again related to the fixed-end moment, and the

reduction in the frame buckling load is directly affected by the primary bending.

When the frame buckling load is compared to the beam mechanism load (Fig. 7.9), the resulting non-dimensionalized curve  $(P_{cr}/P_B)$  is almost horizontal. The reduction in the beam mechanism load is 8 percent. The dashed curve  $(P_B)$  in Fig. 7.9 gives values of the beam mechanism load. Its variation is similar to that of the frame buckling load  $(P_{cr})$ . The similarity causes the non-dimensionalized curve to be almost horizontal. It should not be expected that the curve will remain horizontal for values of beam length outside of the range studied.

#### 7.2.4 Constant Relative Stiffness

The frame buckling curve  $(P_{cr})$  in Fig. 7.10 is for a constant ratio of beam stiffness  $(I_B/L)$  to column stiffness  $(I_C/h)$ . The beam and column lengths are varied but their ratio is maintained at a value of 0.575. As the beam and column lengths increase, the frame buckling loads decrease. These reductions can be related to the fixed-end moments  $(M^F)$  in Fig. 7.7 and, as in the preceding sections, the reductions can be shown to be a direct result of the primary bending.

The load-response curves in Fig. 7.11 show the primary bending effect in relation to the yielding in the beams. Yielding occurs first in the beams of greatest span. The yielding causes a reduction

in the rotational restraint provided by the beams to the columns and thus directly affects the frame buckling load. An additional factor in these curves is the varying column length. It varies directly with the beam length. The column length affects the overturning moment and results in load-response curves of different initial slope.

The frame buckling loads in Fig. 7.10 are non-dimensionalized by the beam mechanism loads of Fig. 7.9. The point corresponding to a beam length of 10 feet is common to the non-dimensionalized curves of Figs. 7.9 and 7.10. For beam lengths less than 10 feet, the column lengths of Fig. 7.10 are shorter than those of Fig. 7.9. This reduces the overturning effect and results in a small relative increase in the non-dimensionalized value of the frame buckling loads in Fig. 7.10. For beam lengths greater than 10 feet, the column lengths increase and there is a relative reduction in the non-dimensionalized value of the frame buckling loads. The variations in the non-dimensionalized values caused by the changes in column lengths numerically are small but if they are compared to the average reduction in the ultimate load of 8 percent, the variations become more significant.

### 7.3 DISCUSSION

Primary bending has a significant effect on inelastic frame buckling loads. A reduction in the frame buckling load of over 50

percent was obtained in the study of Article 7.2.1. The primary bending or fixed-end moment was shown to be related to the initiation of yielding in the frame. The yielding caused a reduction in the rotational restraint provided by the beams to the columns and a corresponding increase in the effective length of the columns. As the value of the fixed-end moments increased, there was a decrease in the values of the frame buckling loads.

The study reemphasized the importance of comparing the value of the frame buckling load to the design ultimate load (beam mechanism load) of the frame. This caused a reversal of the initial conclusion as to the deleterious effect of the primary bending. The effect on the frame buckling load caused by changes in the column length, which was considered in the study on constant relative stiffness, was found to be small.

## 8. PARTIAL BASE FIXITY

### 8.1 INTRODUCTION

In this study, the beneficial effect that partial base fixity has on the buckling load of a frame will be examined. In the previous analyses, the frames were supported on pinned-base fixtures. It was assumed that a pinned-base provided no rotational restraint to the frame. A support condition of this type can be approached with a carefully machined, ball-bearing mounted, column-base fixture. However, in building practice a pinned-base support is usually constructed by setting the anchor bolts of the column base plates on a line coinciding with the bending axis of the column. Rotational restraint is inherent in this type of construction but its beneficial effects are usually assumed to be negligible.

The effect of partial base fixity will be evaluated by obtaining load-response curves and non-dimensionalized frame buckling curves for the basic three-story and six-story frames. They will be supported on bases with rotational restraint. The variable in the study will be the modulus ( $\beta$ ) of the rotational restraint provided by the building foundation. The partial base fixity can be represented graphically (Fig. 8.1a) by a rotational spring at the base of each column. The spring stiffness ( $\beta$ ) is assumed to be equal for all columns.

The degree of restraint provided by a building foundation is defined as the ratio of the partial base restraint moment to the corresponding fixed-base moment under the action of a unit moment, which is applied to the opposite end of the column.<sup>8.1</sup> In Fig. 8.1b, the fixed-end moment ( $M_A^F$ ) is  $\frac{1}{2}$  of  $M_B$ . In Fig. 8.1c, the partial-base restraint moment ( $M_A$ ) is equal to  $-\beta\theta_A$ . The moments at A and B in Fig. 8.1c can be expressed as

$$M_A = C \frac{EI}{L} \theta_A + S \frac{EI}{L} \theta_B \quad (8.1)$$

$$M_B = C \frac{EI}{L} \theta_B + S \frac{EI}{L} \theta_A \quad (8.2)$$

$\theta_B$  can be solved for in Eq. 8.2 and substituted in Eq. 8.1 to yield

$$M_A = C \frac{EI}{L} \theta_A + \frac{S}{C} M_B - \frac{S^2}{C} \frac{EI}{L} \theta_A \quad (8.3)$$

Substitution of  $M_B = 1$ ,  $C = 4$ ,  $S = 2$ , and  $\theta_A = -\frac{M_A}{\beta}$  gives

$$M_A = \frac{\frac{1}{2}}{1 + 3 \frac{EI}{L} \frac{1}{\beta}} \quad (8.4)$$

The degree of restraint ( $\epsilon_B$ ) is

$$\epsilon_B = \frac{M_A}{M_A^F} = \frac{1}{1 + 3 \frac{EI}{L} \frac{1}{\beta}} \quad (8.5)$$

For a fixed-base condition, the modulus ( $\beta$ ) is infinite and the degree of restraint ( $\epsilon_B$ ) is equal to 1. For a pinned-base support,  $\beta$  is 0 and  $\epsilon_B$  is 0. A graphical relationship between the degree of restraint ( $\epsilon_B$ ) and the modulus of the rotational restraint ( $\beta$ ) can be seen in Fig. 8.4.

Quarter-point loading will be used in the study since there is experimental verification for the three-story frame with pinned-base support ( $\epsilon_B = 0$ ). Also, the study on the effect of primary bending showed that frames with low values of  $a/L$  had the largest reductions in the design ultimate or beam mechanism load. Using low values of  $a/L$  then will provide a better measure for the beneficial effects of partial base fixity on the frame buckling load.

## 8.2 THE EFFECT OF PARTIAL BASE RESTRAINT

### 8.2.1 Three-Story Frame

The effect of the degree of restraint on the load-response curves is shown in Fig. 8.2. The foundation modulus ( $\beta$ ) varies from a pinned condition ( $\beta = 0$ ) to a fixed condition ( $\beta = \infty$ ). The numbers at the end of each curve refer to the order of hinge formation, and also correspond to the points on the curve and to the hinge locations in the frame. For low values of the foundation modulus, the yielding pattern in the beams is the same for all frames. As the value of the foundation modulus increases, the lateral stiffness of the structure or the load per unit of sway deformation increases. At high values of the foundation modulus, the load-response curve tends to approach that for the fixed-base frame and the frame instability load approaches the beam mechanism load. Yielding becomes more general in the beams

of the frames with these high values of foundation modulus. Beam mechanisms occur in the bottom two beams of the frame with the fixed-base support.

The effect of partial base fixity on the non-dimensionalized frame buckling load is shown in Fig. 8.3. There is no reduction in the design ultimate load of the frames when the degree of base restraint is greater than 0.4. For values of degree of restraint less than 0.4, the reduction in the design ultimate or beam mechanism load is almost linear. For a modulus value of zero (pinned-base condition), there is an 8 percent reduction in the design ultimate load caused by frame buckling. This variation is shown to an expanded scale in Fig. 8.4. A comparison can be made at any ordinate between values of the foundation modulus ( $\beta$ ) and the degree of restraint ( $\epsilon_p$ ). There is a tendency with the latter abscissa to linearize the variations of the non-dimensionalized frame buckling load. Both curves show a large increase in the frame buckling load for small changes in the abscissa at low values of rotational restraint.

### 8.2.2 Six-Story Frame

The load-response curves (Fig. 8.5) for the six-story frames are similar to those of the three-story frames. The numbering system used for the order of plastic hinge formation is the same as that in Fig. 8.2 with the exception of locations 7 and 8. In the six-story

frames the yielding progresses further upward in the frames since there is no physical restriction placed by a limited number of stories.

At higher values of the foundation modulus, the instability effects are also forced upward in the six-story frames. In the frame with a modulus value of 50,000 kip-in. per radian, frame instability occurs after second hinges have formed in the beams of the bottom two stories. In the fixed-base frame with a modulus value of infinity, the instability occurs even higher in the frame. A second hinge does not form in the bottom beam. Second hinges form in the two beams immediately above the bottom beam. These hinges are shown in Fig. 8.5 at locations 5 and 6. The rotational restraint provided by these beams to the adjacent columns is reduced to zero and the frame becomes unstable. The effect of the reduction in the rotational restraint provided by these beams is shown by the curve for sway deflections. The curve is plotted to the right of the frame. These deflections are for the load at which a plastic hinge forms at location 6. A sharp increase in the column chord rotation can be observed in the fourth and fifth floor columns. This is a direct result of the reduction in the rotational restraint provided by the beam in which hinge number 5 occurred. When the hinge forms at location 6, frame instability results.

The non-dimensionalized frame buckling load curves for the three-story and the six-story frames are shown in Fig. 8.6. There is

a reduction in the beam mechanism load of 8.5 percent for the six-story fixed-base frame ( $\epsilon_B = 1.0$ ). There is no reduction for the three-story fixed-base frame. As the degree of restraint is reduced, the reduction in the design ultimate load of the frames is increased. This reduction increases rapidly for values of  $\epsilon_B$  less than 0.4. The reduction in the ultimate load for the six-story pinned-base frame ( $\epsilon_B = 0$ ) is 25 percent. The slope of the curve in this region again indicates the beneficial effect of even a small amount of base rotational restraint.

### 8.3 DISCUSSION

The two types of column base supports usually employed in design practice are the fixed-base and the pinned-base support. Neither is attainable in actual practice. The non-dimensionalized curves of Fig. 8.6 indicate that the changes in the frame buckling load, which are caused by variations in the foundation modulus ( $\beta$ ), for values of  $\beta$  approaching the fixed-base condition are not significant and that a fixed-base assumption is reasonable. For variations in the value of the foundation modulus near zero, the changes in the non-dimensionalized value of the frame buckling load are significant. A pinned-base assumption then is too conservative. The problem that arises with the pinned-base support is the computation of a value for the effective foundation modulus. This is a function of the column-base support, type of foundation, and the soil condition.<sup>8.2</sup> Additional

research is required to evaluate the interaction of these elements in obtaining an effective modulus for the rotational restraint.

The results of the studies in this chapter show the beneficial effects of partial base fixity. In the study on primary bending, the largest reductions in the design ultimate load occurred for small values of  $a/L$  (0.2 and 0.25). The latter value was used throughout this chapter. In all of the studies the beneficial effects of cladding were assumed to be negligible. The effect of the cladding is to increase the frame buckling load. Based on the curves that were developed in this chapter, it would appear that if a fixed-base support was designed for a single-bay frame and a small cladding effect was assumed to be present, then frame buckling would not cause a reduction in the design ultimate load (beam mechanism load) of the frame.

## 9. INTERACTION BETWEEN FLOORS

### 9.1 INTRODUCTION

In Chapter 8, the beneficial effects of partial base fixity on the frame buckling load were examined. This study was limited to buildings of a few stories that were supported directly on the foundation. An additional area in which frame buckling occurs is the top stories of multi-story frames. The top stories are not supported on pinned-bases nor can their supports be represented graphically by rotational springs. Instead, there is a complex relationship between the top floors and the structure below. The rotational restraints provided to the top stories of a building frame vary with the applied load. They are at their maximum value when loads are first applied. As the load on the frame increases, the rotational restraint decreases. This reduction occurs first through the axial load effects in the columns and then by the inelastic behavior in the supporting members.

The variable support condition will be approximated for the top three stories (Fig. 9.1) of a multi-story frame. The lateral deformation at the base of the columns in the third story will be prevented. The sway of the top three floors will be with respect to this level. The beam at the fourth-floor level will be under the same loading pattern as the beams in the floors above. The rotational restraint

provided by this beam will not be constant since the beam will undergo elastic-plastic behavior. A major difficulty arises in adequately approximating the behavior of the restraining columns. It will be assumed that the rotational restraint provided by these columns remains elastic, that the bases of the columns are pinned, and that the stability functions of the columns in the third floor are applicable to the restraining columns in the fourth floor.

Three studies will be made on frames with the assumed variable support. The three-story and six-story frames studied in the chapter on primary bending will be reexamined. The variable will again be the  $a/L$  ratio but the base support will be provided by the variable restraint. The frame in the third study will be under uniform loading. The variable in this study will be the number of stories in the frame.

## 9.2 VARIABLE BASE RESTRAINT

### 9.2.1 Three-Story Frame

The load-response curves for the three-story frames with a variable base restraint are shown in Fig. 9.1. The numbers to the right of the curves refer to the formation of plastic hinges and to the spacing ( $a/L$ ) of the two concentrated beam loads. Beam mechanisms form in the bottom three floor beams of the frames with  $a/L$  values of 0.4 and 0.5.

As in the previous chapter on primary bending, the elastic deformations are the same for all frames and yielding first occurs in the frame with the largest fixed-end moment ( $a/L = 0.50$ ). The frame with an  $a/L$  value of 0.20 has the smallest fixed-end moment. It behaves elastically to an applied load ( $P$ ) of 24 kips. The rotational restraint provided by the beams to the columns in this latter frame remains elastic through a broader load range and hence its frame instability load is higher. It should be noted that the inelastic behavior of the variable base restraint is also affected by the primary bending.

The reductions in the frame buckling load due to the primary bending effect can be seen in the frame buckling curves of Fig. 9.2. As the values of  $a/L$  increase, the values of the frame buckling load ( $P_{cr}$ ) decrease. The frame buckling loads for the pinned-base frame are shown for comparison. The increase in the frame buckling load caused by the variable base restraint is measured by the differences between the ordinates of the two frame buckling curves. The non-dimensionalized curve ( $P_{cr}/P_B$ ) for the variable base restraint shows no reduction in the beam mechanism load for  $a/L$  values greater than 0.3. These curves further indicate that a pinned-base assumption for the supports of the top stories in a multi-story frame is too conservative and that the restraints which are present give a significant increase in the frame buckling load.

### 9.2.2 Six-Story Frame

The load-response curves in Fig. 9.3 are similar to those of the three-story frame (Fig. 9.1). The effect of the primary bending can be explained in the same manner as was done in the previous chapters. The frame buckling curves in Fig. 9.4 give a comparison between the frames with a variable base restraint and those with pinned-base supports. The differences between the curves show the effect of the base restraint. The curves in Fig. 9.5 compare the non-dimensionalized frame buckling curves for the three and six-story frames with the variable base support. The difference between these curves is due primarily to the difference in the number of stories. These curves indicate that frame buckling is not a serious problem in the first three or four stories of a multi-story frame. The small reductions that might be present would be eliminated if even a small cladding effect is assumed to be acting.

### 9.2.3. Distributed Load

The frame buckling studies to this point have been for frames with two concentrated loads on each beam. In this study, the frames will be loaded with a distributed beam load which is equal in magnitude to the two concentrated loads. The effect on the frame buckling load caused by an increase in the number of stories will be examined. The frames in the study will have the same member sizes as those in the previous studies. All of the frames will be supported

by the variable base.

The load-response curves for the frames are shown in Fig. 9.6. The number of stories ( $n$ ) in the frame is indicated to the right of the curves. The column sections are continuous for three stories. The 5WF16 column section is designed for loads and moments at the sixth-floor level. It has excess capacity when used in the four and five-story frames. This is discernable in the order of hinge formation. The hinge in the column at location 3 for the four-story frame occurs at the frame instability load. In the five-story frame, it occurs after the hinge forms at location 4. In the six-story frame, it forms before the hinge at location 4. The effect of the number of stories can be seen in the slope of the load-response curves. The overturning moment is a function of the number of floors. As the number of floors ( $n$ ) increases, the slope of the curves decreases.

The non-dimensionalized frame buckling curve in Fig. 9.5 has the same shape as the buckling curve ( $P_{cr}$ ). The beam mechanism load is a constant. There is very little reduction in the ultimate strength of the frame due to frame buckling. The reduction of 6.5 percent for the six-story frame can probably be eliminated by a small cladding effect.

### 9.3 DISCUSSION

The non-dimensionalized frame buckling curves indicate that the reduction in the beam mechanism load for the majority of the frames in the study is minor and could be compensated for by a small cladding effect. Frame buckling then is not a serious problem in the top stories of multi-story frames. An exception to this is the six-story frames (Fig. 9.4) with small values of  $a/L$ . These frames had the higher values for frame buckling loads, but when the values were non-dimensionalized by the beam mechanism load, the resulting ratios indicated a significant reduction in the design ultimate load of the frames.

A study is required to determine the story level at which the combined loading, gravity loading plus wind, governs the design of the members of the frame. When this has been determined, a more definitive statement can be made as to the detrimental effect on the design ultimate load of the frame due to frame buckling in the top stories of multi-story frames.

## 10. SUMMARY AND CONCLUSIONS

A method is presented to compute inelastic frame buckling loads for multi-story building frames. Small lateral loads are applied at each floor level to represent the effects of the initial eccentricities within the frame. The small lateral loads are proportional to the loads on the floorbeams. A value is assumed for the proportionality constant and a frame instability load is computed. The frame buckling load is defined as the limit of the frame instability loads as the value of the small lateral loads or initial eccentricities approach zero.

A computer solution is written to compute inelastic frame instability loads. A second-order, elastic-plastic load-response curve is also generated in the computations for the frame instability load. The points on the load-response curve are obtained by an incremental procedure. The incremental procedure has an advantage over the iteration method in that the unloading portion of the load-response curve can be obtained. The incremental formulation also considers the reduction in the moment capacity ( $M_{pc}$ ) in a column due to increases in the axial load of the column after a plastic hinge has formed.

Frame buckling tests were conducted on two, three-story, single-bay frames. The comparisons between the load-response curves of the test frames are good. The frames have load-lateral sway

response curves similar in shape to those of the anticipated frame buckling curves. The ratios of the lateral sway deflection to vertical beam deflection at working load for both tests are small. Frame buckling causes a reduction in the design ultimate load (beam mechanism load) of 9 and 12 percent in Test 1 and 2, respectively.

Comparisons are made between the experimental results and the theoretical predictions. In the limit as the small lateral load approaches zero, the theoretical load-response curves tend to approach the experimental curves. The predicted frame buckling loads are within 3 percent of the ultimate loads from the frame tests.

Analytical studies examine the changes in the frame buckling load caused by varying some of the structural parameters. These studies are for single-bay multi-story frames. The studies show the important effect of the column slenderness ratio, the rotational restraint provided to the columns by the supporting members, the primary bending moment, and the strength of the individual members.

The studies show that the frame buckling problem can be divided on the basis of column slenderness ratio into three ranges; the inelastic frame buckling range, the elastic buckling range, and the transition range. The significant factor in the elastic buckling range is the column slenderness ratio. In the inelastic buckling range, it is the inelastic behavior in the members of the frames. Since building columns have low values of slenderness ratio, multi-

story building frames are included in the inelastic buckling range. In this range the changes in the frame buckling load caused by variations in the column slenderness ratio are small. The important parameter is the rotational restraint provided to the columns by the supporting members. These rotational restraints are significantly reduced by inelastic behavior.

The effect of the primary bending moment on the inelastic frame buckling load is examined by varying the position of the loads on the beams. The primary bending effect is related to the initiation of yielding in the rotational restraints of the columns. This causes an increase in the effective length of the columns and thus directly affects the frame buckling load. When the load-spacing variable ( $a/L$ ) is changed from 0.2 to 0.5 (Fig. 7.1), the frame buckling load is reduced by 50 percent. This shows the significant effect of the primary bending. When the frame buckling loads are compared to the design ultimate load (beam mechanism load) of the frame, an unexpected result occurs. The frame with the lowest value for the frame buckling load has no reduction in the design ultimate load. The frame with the highest value for the frame buckling load has the biggest reduction in the design ultimate load. The value of the frame buckling load in itself is not too important. It is only after the frame buckling load is compared to the design ultimate load that reasonable conclusions can be made.

The rotational restraint provided by the foundation to the frame is examined. The results indicate that if a fixed-base support

is designed for the frame studied, frame buckling is not a problem. If a pinned-base support is designed, then frame buckling must be considered. The frame buckling load is not sensitive to changes in the foundation modulus for modulus values approaching the fixed-base condition. For values approaching the pinned-base condition, small changes in the foundation modulus cause relatively large changes in the frame buckling load. Neither of these extreme support conditions can be fully attained in construction practice. Based on the results of the study, a fixed-base design assumption will give a reasonable value for the frame buckling load, whereas a pinned-base assumption will give a value that is too conservative.

Frame buckling in the top stories of single-bay multi-story frames is also examined. The rotational restraint provided by the lower stories to the top stories is approximated. The studies show that a pinned-base assumption for the support of the top stories is too conservative. The reduction in the design ultimate load in all but two of the frames in the study indicates that, for single-bay frames of less than seven stories, the frame buckling problem is minor and can be compensated for by the effect of the cladding.

In general, the analytical studies for the building frames indicate that, if a proper base restraint is used, the reduction in the beam mechanism load caused by frame buckling is not significant. Additional studies are required for multi-bay frames and to determine the number of stories at which the combined loading will govern the design of the members.

11. TABLES

Table 4.1 Section Properties.

Section	b in.	d in.	t in.	w in.	b/t -	d/w -	r <sub>y</sub> in. <sup>y</sup>	r <sub>x</sub> in. <sup>x</sup>	I <sub>x4</sub> in.	S <sub>x3</sub> in.	Z <sub>x3</sub> in.	f -	
4W13	Nominal	4.060	4.16	0.345	0.280	11.77	14.86	0.99	1.72	11.3	5.45	6.3	1.16
	Measured	4.090	4.145	0.345	0.284	11.85	14.60	1.01	1.717	11.316	5.461	6.265	1.15
6B16	Nominal	4.030	6.25	0.404	0.260	9.97	24.04	0.96	2.59	31.7	10.1	11.6	1.15
	Measured	4.051	6.232	0.379	0.285	10.69	21.87	0.941	2.56	31.10	9.98	11.525	1.15
2 2.3	Nominal	1.0	2.0	0.187	0.187	5.4	10.7	0.30	0.75	0.38	0.38	--	--

Table 4.2 Data from Tension Tests

Section	Specimen No.	$\sigma_y$ ksi	$\epsilon_y$	$\epsilon_{st}$	$E_{st}$ ksi	$\sigma_{ult}$ ksi	Elong. %
4 W 13	1 F*	51.0	.00194	.0190	425	73.7	24.4
	2 W*	49.2	190	216	396	71.5	21.8
	3 F	50.9	195	238	422	73.2	24.5
	4 F	50.7	192	220	430	72.6	23.4
	5 W	49.5	185	190	370	71.4	23.0
	6 F	50.6	183	228	453	73.2	25.4
6 B 16	1 F	35.0**	.00125	.0209	635	-	-
	2 F	33.6	122	192	550	-	-
	3 W	35.5	120	234	-	-	-

\*F = flange

\*W = web

\*\* $\sigma_y = 33.2$  ksi (beam test)

Table 5.1 Buckling Load Summary

Test Frame Number	1	2
Beam Mechanism Load, $P_B$	27.2	27.2
Ultimate Load, $P_U$	24.8	(24.6)
Ratio of $P_U/P_B$	0.91	0.88
Frame Buckling Load, $P_{cr}$	24.2	23.9
Percent Error	2.4	2.8

Table 6.1 Comparison of Frame Parameters

Member	Section	L or h	L/d or h/d	L/ $r_x$ or h/ $r_x$	$P/P_y$	$M_{P_B}/M_{P_C}$	$I_B/I_C$	$I_C L/I_B h$	
T E S T	Beam	6 B 16	10.0	20	46	0.37	1.25	2.78	1.58
	Column	4 W 13*	5.75	17	40				
D E S I G N	Beam	16 B 31	24.0	18	45	0.31	1.35	2.54	1.27
	Column	8 W 40	12.0	18	41				

\*A441 Steel

12. APPENDIXEXAMPLE 1. SINGLE MEMBER

There are two geometric reference systems for the deflected member in Fig. 3.1. One is with respect to vertical and horizontal coordinate systems and the other is with respect to the line joining the end points of the member. A kinematics matrix (A) relates the displacements ( $\Delta$ ) in the general system to those in the member system ( $\theta$ ).

$$\theta = A \Delta$$

$$\begin{bmatrix} \theta_{ij} \\ \theta_{ji} \end{bmatrix} = \begin{bmatrix} 1 & 0 & 1 \\ 0 & 1 & 1 \end{bmatrix} \begin{bmatrix} \theta_i \\ \theta_j \\ -\rho \end{bmatrix} \quad (\text{A.1})$$

The minus sign used with  $\rho$  is consistent with the positive moment convention in Fig. 3.1. The member stiffness matrix (k) is written with respect to member coordinate system. The individual terms can be obtained directly from the slope-deflection equations or any basic method of structural analysis can be used to develop them.

$$S = k \theta$$

$$\begin{bmatrix} M_{ij} \\ M_{ji} \end{bmatrix} = \left(\frac{EI}{L}\right) \begin{bmatrix} C & S \\ S & C \end{bmatrix} \begin{bmatrix} \theta_{ij} \\ \theta_{ji} \end{bmatrix} \quad (\text{A.2})$$

Considering only first order effects, the stress vector (S) above can be related to the nodal force vector (W) by the statics matrix (C).

$$\begin{matrix} W & = & C & S \\ \begin{bmatrix} M_i \\ M_j \\ HL \end{bmatrix} & = & \begin{bmatrix} 1 & 0 \\ 0 & 1 \\ 1 & 1 \end{bmatrix} & \begin{bmatrix} M_{ij} \\ M_{ji} \end{bmatrix} \end{matrix} \quad (A.3)$$

It can be seen that  $A = C^T$ . The stiffness matrix in the general coordinate system can be developed by the standard transformation

$$\begin{matrix} K & = & A^T & k & A \\ \begin{bmatrix} C & S & C+S \\ S & C & C+S \\ C+S & C+S & 2(C+S) \end{bmatrix} & = & \begin{bmatrix} 1 & 0 \\ 0 & 1 \\ 1 & 1 \end{bmatrix} & \begin{bmatrix} C & S \\ S & C \end{bmatrix} & \begin{bmatrix} 1 & 0 & 1 \\ 0 & 1 & 1 \end{bmatrix} \end{matrix} \quad (A.4)$$

where each side is multiplied by a scalar term (EI/L).

#### EXAMPLE 2. TWO-STORY, SINGLE-BAY FRAME

The stiffness matrix will be developed for a two-story, single-bay frame in which there is no axial shortening of the members. The members and nodal points of the frame are systematically numbered in Fig. A.1. The kinematic matrix can be developed by applying a unit, positive deformation to each of the nodal displacements while fixing all of the other displacement terms. The kinematic matrix is the effect on the member displacement terms due to the isolated unit nodal deformations.



Equilibrium is used to develop the relationship between the member stress vector (S) and the nodal force vector (W).

$$\begin{array}{c}
 W \\
 \left[ \begin{array}{c} M_1 \\ M_2 \\ H_1 h_1 \\ M_4 \\ M_5 \\ H_2 h_2 \\ M_7 \\ M_8 \end{array} \right] = \begin{array}{c} C \\
 \left[ \begin{array}{cccccccccccc}
 1 & 0 & 1 & 0 & 0 & 0 & 0 & 0 & 0 & 0 & 0 & 0 \\
 0 & 1 & 0 & 0 & 1 & 0 & 0 & 0 & 0 & 0 & 0 & 0 \\
 0 & 0 & 1 & 1 & 1 & 1 & 0 & 0 & 0 & 0 & 0 & 0 \\
 0 & 0 & 0 & 1 & 0 & 0 & 1 & 0 & 1 & 0 & 0 & 0 \\
 0 & 0 & 0 & 0 & 0 & 1 & 0 & 1 & 0 & 0 & 1 & 0 \\
 0 & 0 & 0 & 0 & 0 & 0 & 0 & 0 & 1 & 1 & 1 & 1 \\
 0 & 0 & 0 & 0 & 0 & 0 & 0 & 0 & 0 & 1 & 0 & 0 \\
 0 & 0 & 0 & 0 & 0 & 0 & 0 & 0 & 0 & 0 & 0 & 1
 \end{array} \right] \begin{array}{c} S \\
 \left[ \begin{array}{c} M_{12} \\ M_{21} \\ M_{14} \\ M_{41} \\ M_{25} \\ M_{52} \\ M_{45} \\ M_{54} \\ M_{47} \\ M_{74} \\ M_{58} \\ M_{85} \end{array} \right]
 \end{array} \quad (A.7)
 \end{array}$$

The stiffness matrix of the structure can now be developed by the transformation  $K = A^T k A$ . To conserve space, the  $EI/L$  term in each element of the matrix is not shown. Since it is assumed that there is no member shortening, the chord rotations ( $\rho$ ) for all columns in any story are equal.

$$K = A^T k A$$

$$K = \begin{bmatrix} (C_a+C_c) & S_a & (C+S)_c & S_c & 0 & 0 & 0 & 0 \\ S_a & (C_a+C_d) & (C+S)_d & 0 & S_d & 0 & 0 & 0 \\ (C+S)_c & (C+S)_d & 2(C+S)_c & (C+S)_c & (C+S)_d & 0 & 0 & 0 \\ S_c & 0 & (C+S)_c & C_c+C_b+C_e & S_b & (C+S)_e & S_e & 0 \\ 0 & S_d & (C+S)_d & S_b & C_d+C_b+C_f & (C+S)_f & 0 & S_f \\ 0 & 0 & 0 & (C+S)_e & (C+S)_f & 2(C+S)_e & (C+S)_e & (C+S)_f \\ 0 & 0 & 0 & S_e & 0 & (C+S)_e & C_e & 0 \\ 0 & 0 & 0 & 0 & S_f & (C+S)_f & 0 & C_f \end{bmatrix}$$

(A.8)

Study of this matrix will show that the largest terms are on the main diagonal and that there is a great amount of symmetry about the diagonal. Instead of reading in the member stiffness and kinematic matrices and then performing the above computation, storage space can be conserved by directly building the above matrix.

13. NOMENCLATURE

A	Kinematic matrix
$A^T$	Transposed kinematic matrix
C	Statics matrix
$C_k$	Carry-over factor
E	Modulus of elasticity
$E_{st}$	Strain-hardening modulus
$E_t$	Tangent modulus
H	Horizontal load
I	Moment of inertia
K	Stiffness matrix of a system
$K^*$	Incremental stiffness matrix
L	Beam length
$L_k$	Member length
M	Bending moment
$M_B$	Moment at the bottom of a column
$M^F$	Fixed-end beam moment
$M_{ij}$	Moment at the i end of member ij
$M_{ji}$	Moment at the j end of member ij
$M_p$	Plastic moment
$M_{pc}$	Plastic moment reduced for axial load
$M_T$	Moment at the top of a column
P	Axial load, concentrated beam load
$P_B$	Beam mechanism load

$P_{cr}$	Buckling load
$P_E$	Euler buckling load
$P_T$	Tangent modulus buckling load
$P_u$	Ultimate load
$P_y$	Yield load
$S_k$	Stiffness factor
$S_T$	Stress matrix
$S_x$	Elastic section modulus, strong bending axis
$S^*$	Member incremental stress vector
$W$	Load matrix
$W_B$	Beam mechanism load
$W_{cr}$	Buckling load
$W_i$	Distributed load, $i^{th}$ beam
$W^*$	Nodal incremental force vector
$Z_x$	Plastic section modulus, strong bending axis
$a$	Distance to the concentrated load
$b$	Flange width
$d$	Depth of section
$dP$	Increment of load
$e_o$	Initial eccentricity
$e_i$	Eccentricity between $i$ and $i+1$ floor
$f$	Shape factor
$h$	Column height

$k$	Member stiffness matrix
$n$	Number of stories
$r_x$	Radius of gyration, strong bending axis
$r_y$	Radius of gyration, weak bending axis
$t$	Flange thickness
$w$	Web thickness
$\alpha$	Proportionality constant
$\beta$	Foundation modulus
$\Delta$	Sway deflection
$\Delta^*$	Nodal incremental displacement vector
$\delta\Delta$	Increment of sway deformation
$\epsilon$	Strain
$\epsilon_B$	Degree of base restraint
$\epsilon_{st}$	Strain-hardening strain
$\epsilon_y$	Yield strain
$\theta_i$	Rotation of $i^{\text{th}}$ connection
$\theta_j$	Rotation of $j^{\text{th}}$ connection
$\theta^*$	Member incremental deformation vector
$\rho_{ij}$	Chord rotation of column $ij$
$\Sigma$	Finite summation
$\sigma$	Stress
$\sigma_{rc}$	Maximum compressive residual stress
$\sigma_{ult}$	Ultimate stress
$\sigma_y$	Yield stress

14. FIGURES

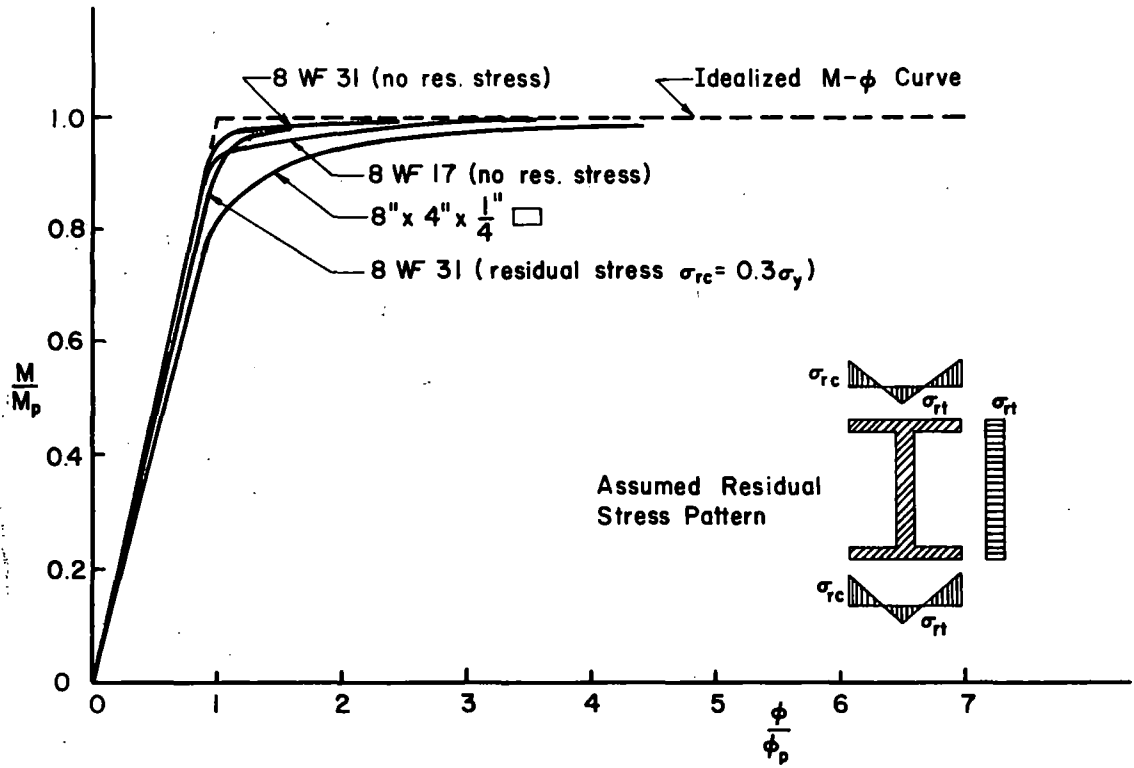


Fig. 2.1 Moment-Curvature Relationships

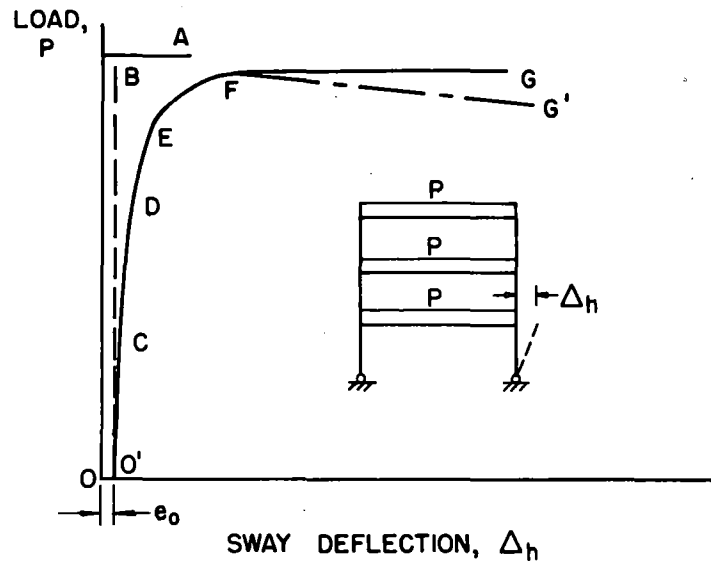


Fig. 2.2 Frame Behavior

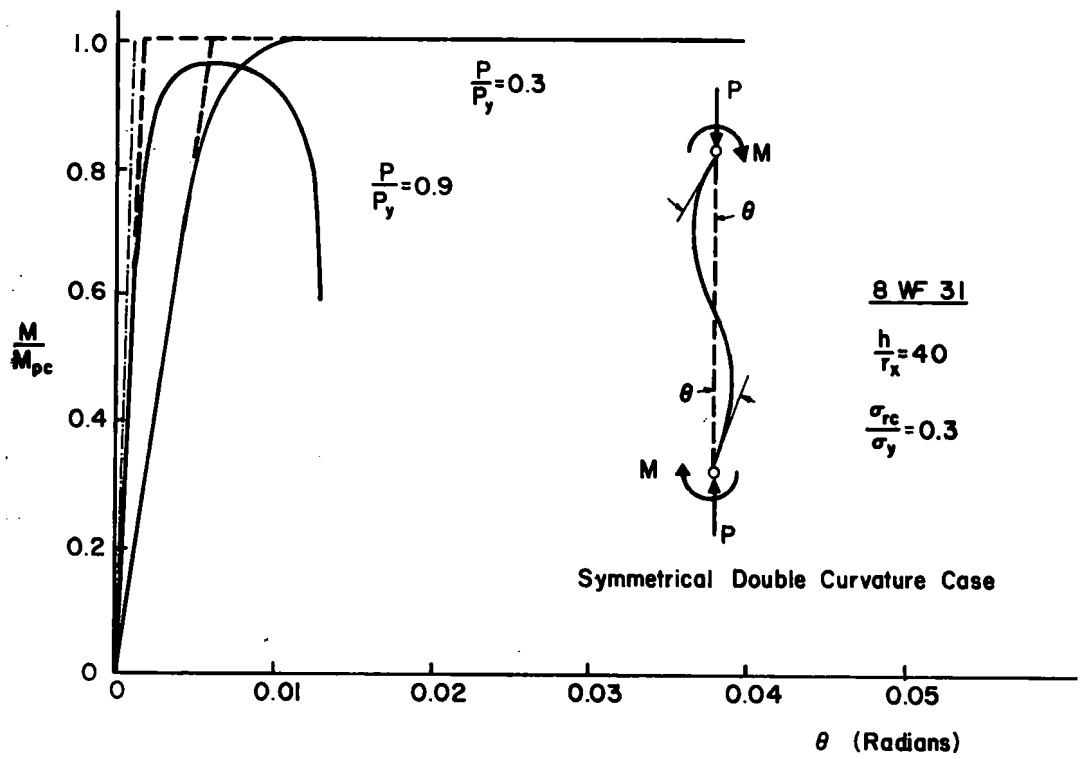


Fig. 2.3 Beam-Column Behavior, Double Curvature

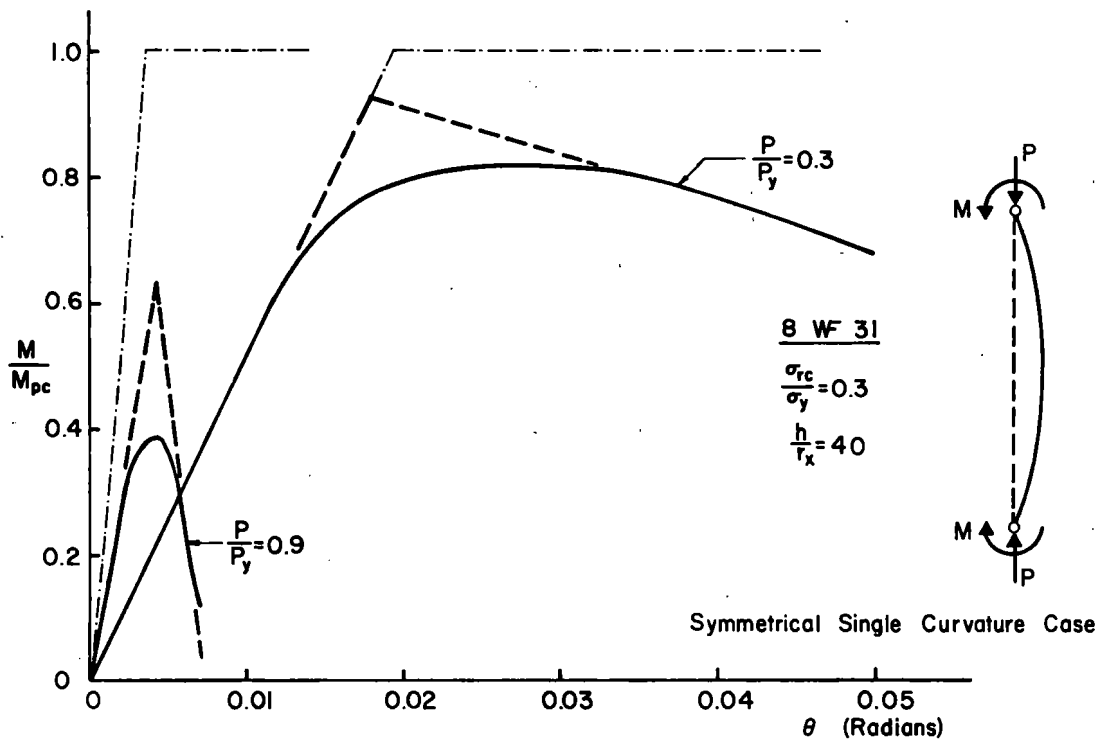


Fig. 2.4 Beam-Column Behavior, Single Curvature

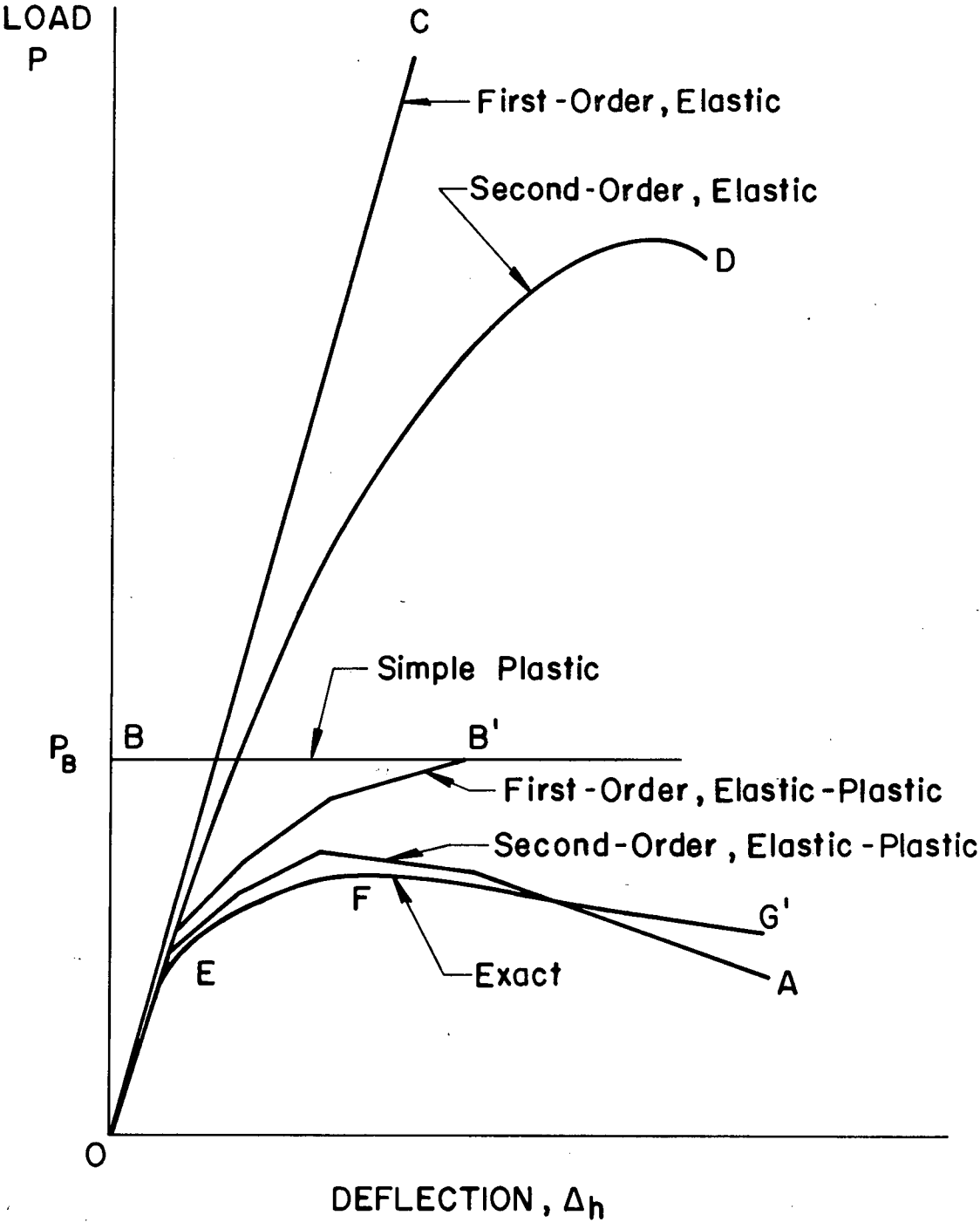
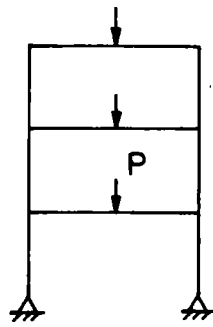
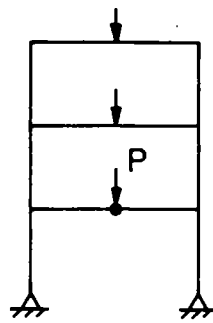
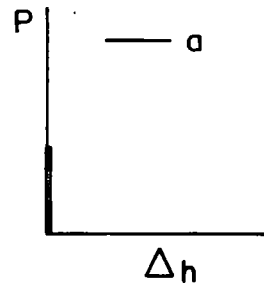


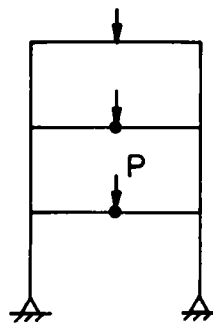
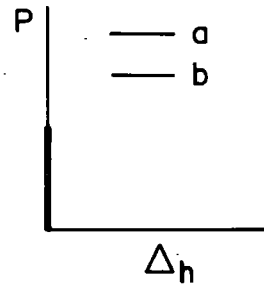
Fig. 2.5 Load-Deflection Relationships



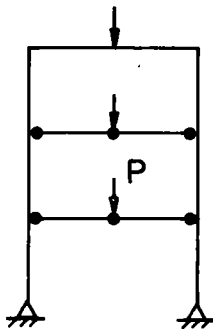
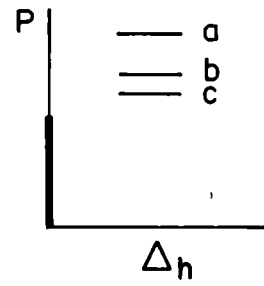
(a)



(b)



(c)



(d)

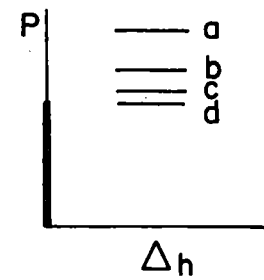
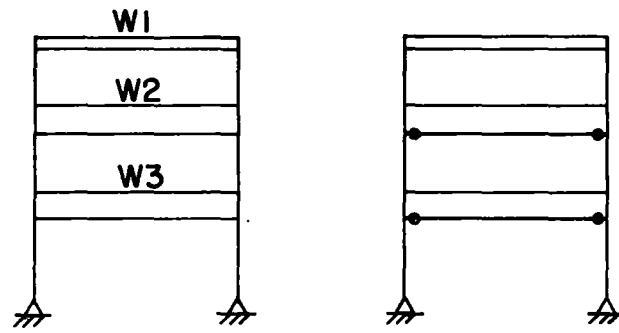
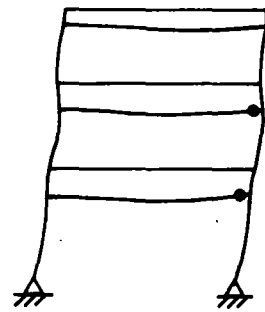
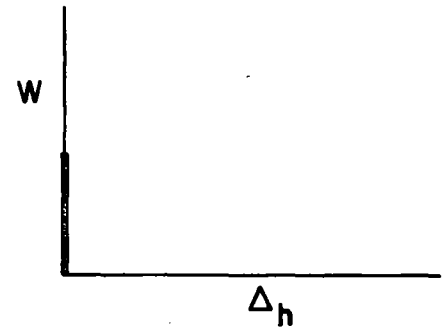


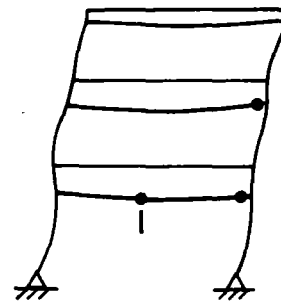
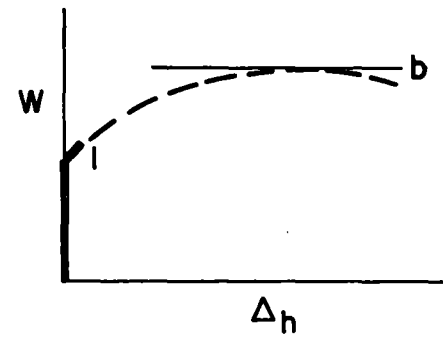
Fig. 2.6 Tangent Modulus Frame Buckling, No Hinge Unloading



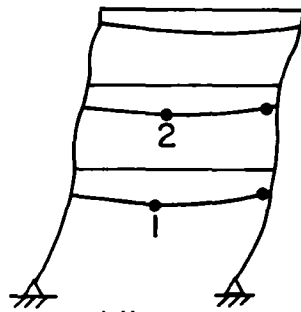
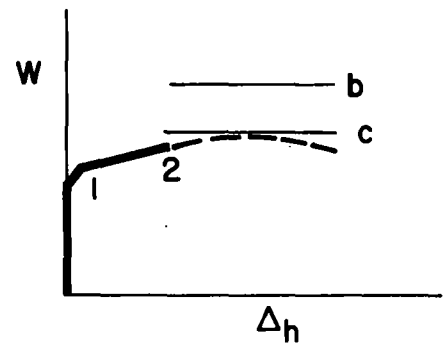
(a)



(b)



(c)



(d)

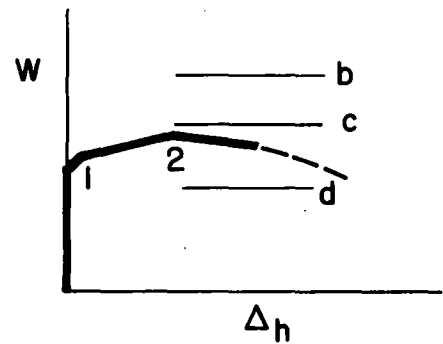
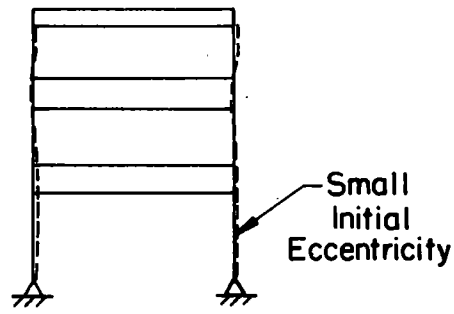
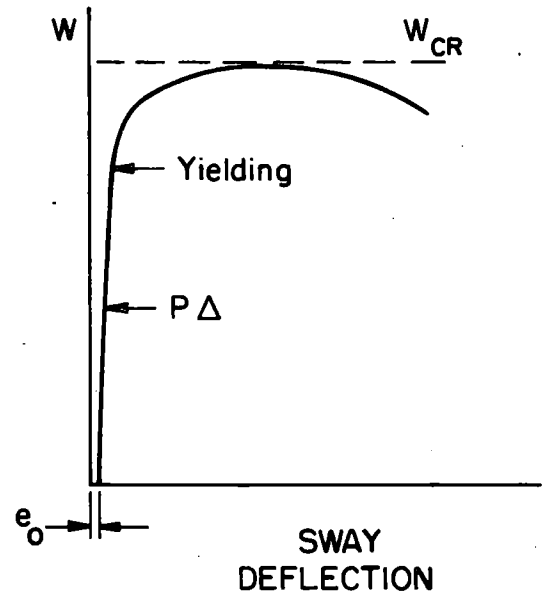


Fig. 2.7 Tangent Modulus Frame Buckling, Hinge Unloading

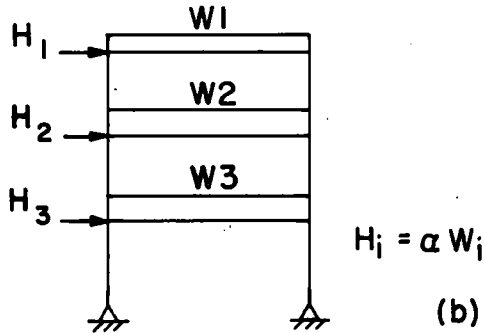
ACTUAL FRAME



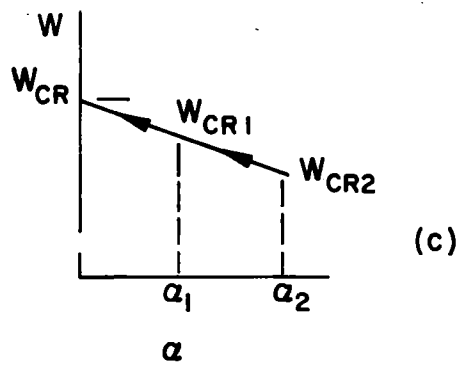
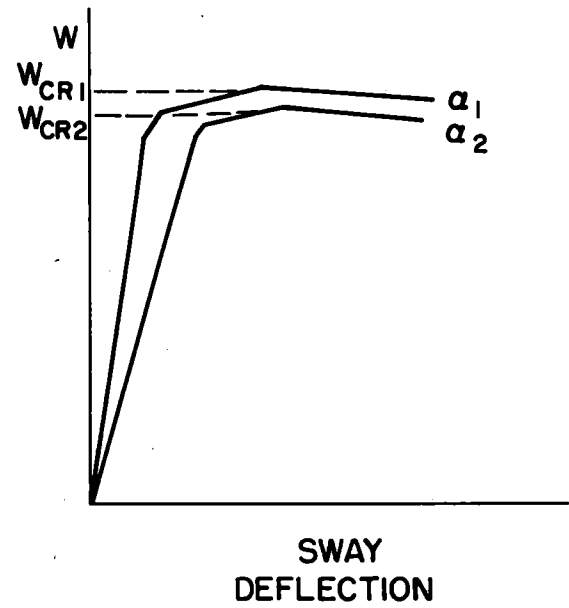
(a)



SMALL LATERAL LOAD METHOD



(b)



(c)

Fig. 2.8 Small Lateral Load Method

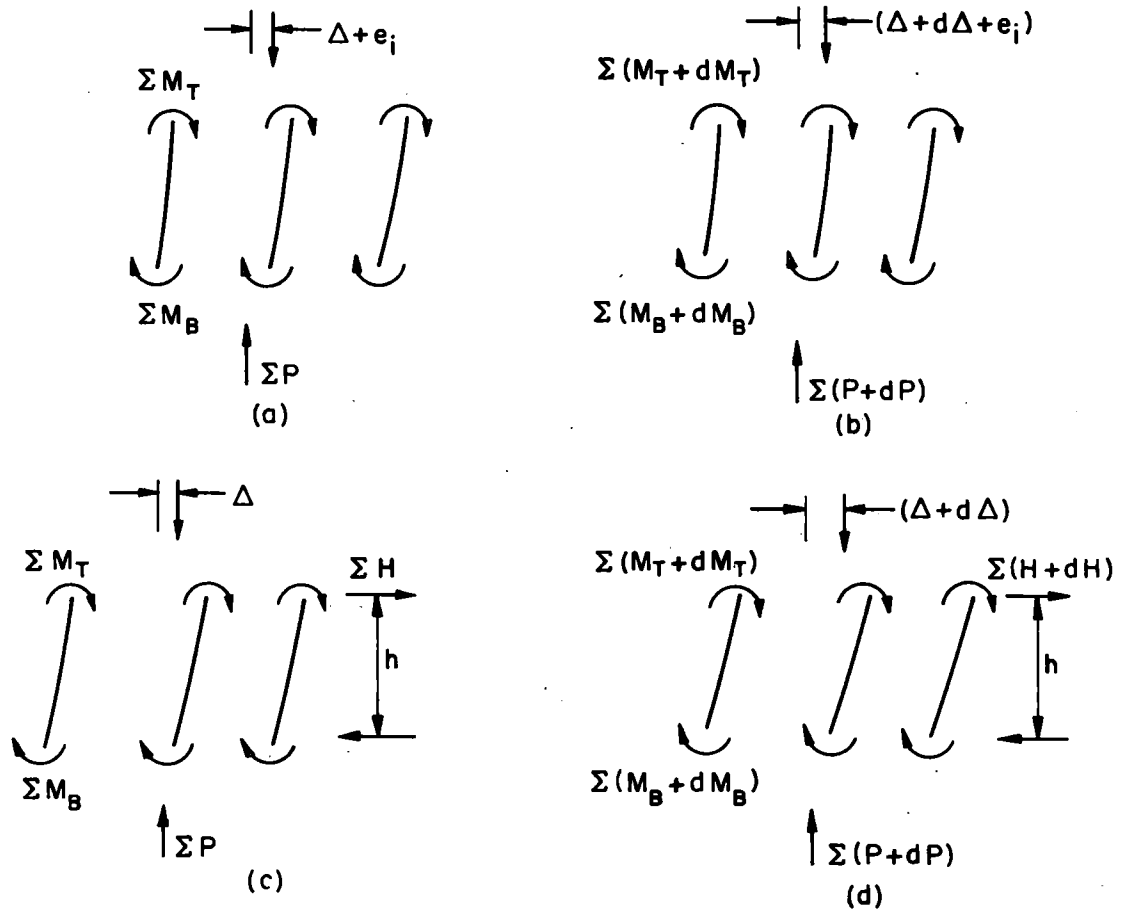


Fig. 2.9 Story Shear Equilibrium

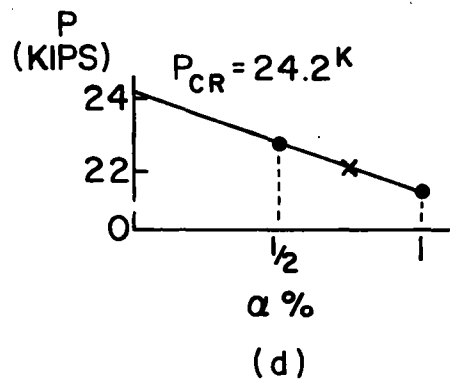
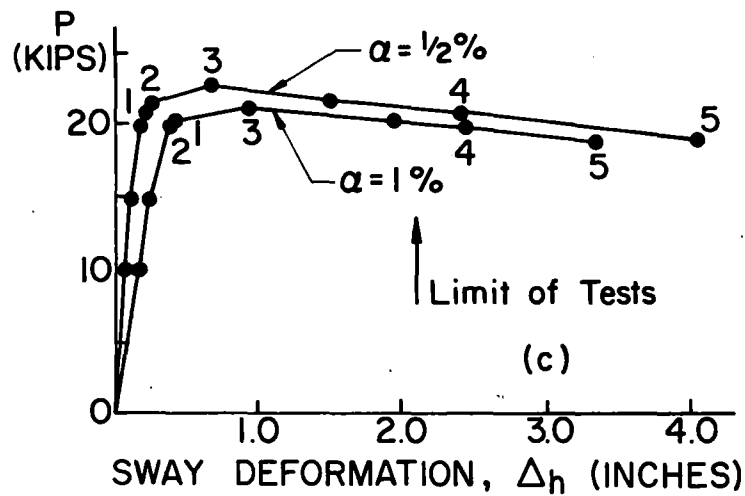
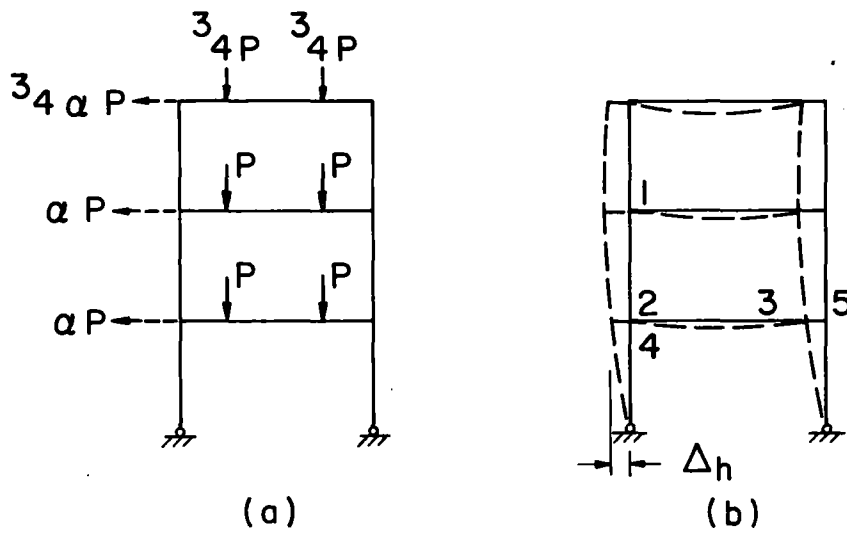


Fig. 2.10 Theoretical Frame Buckling Load, Test 1

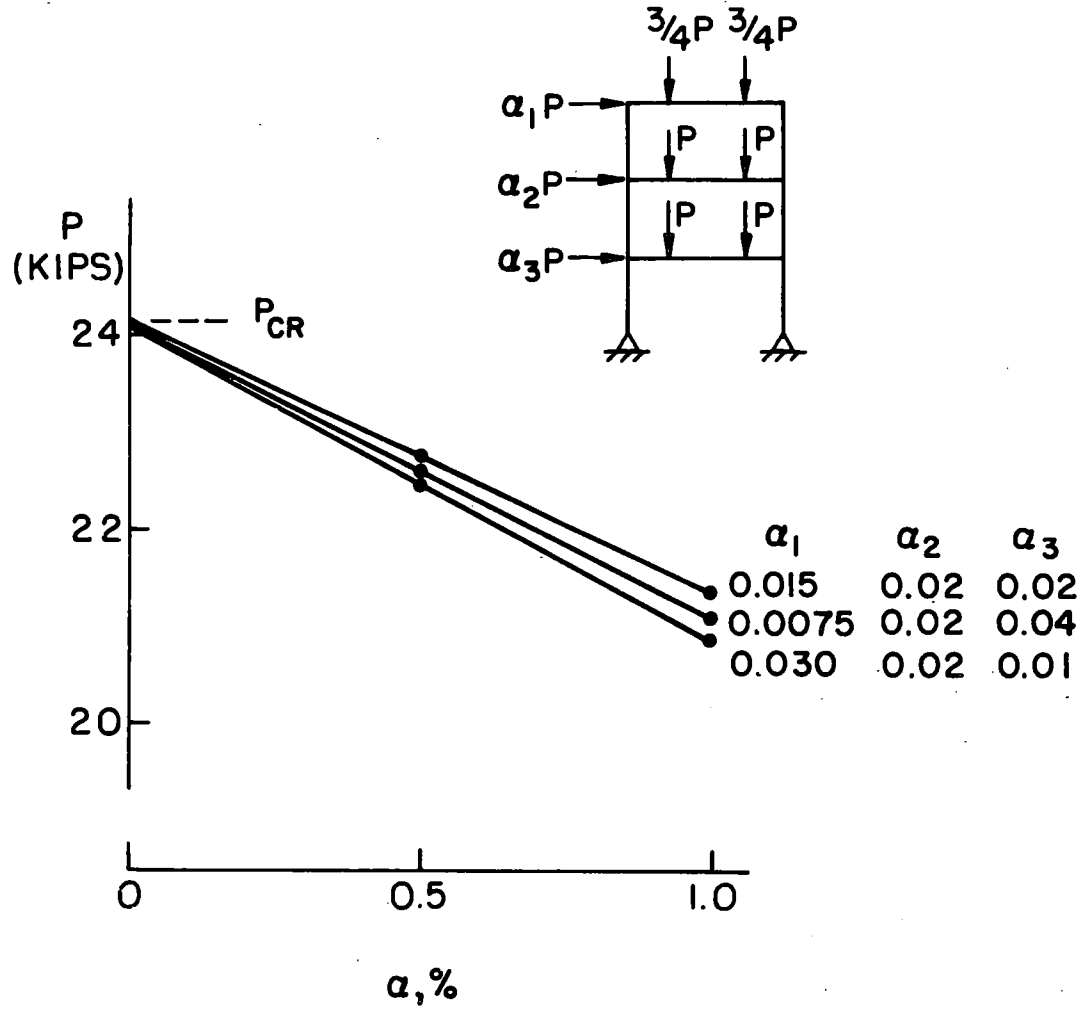


Fig. 2.11 Variable Proportionality Constants

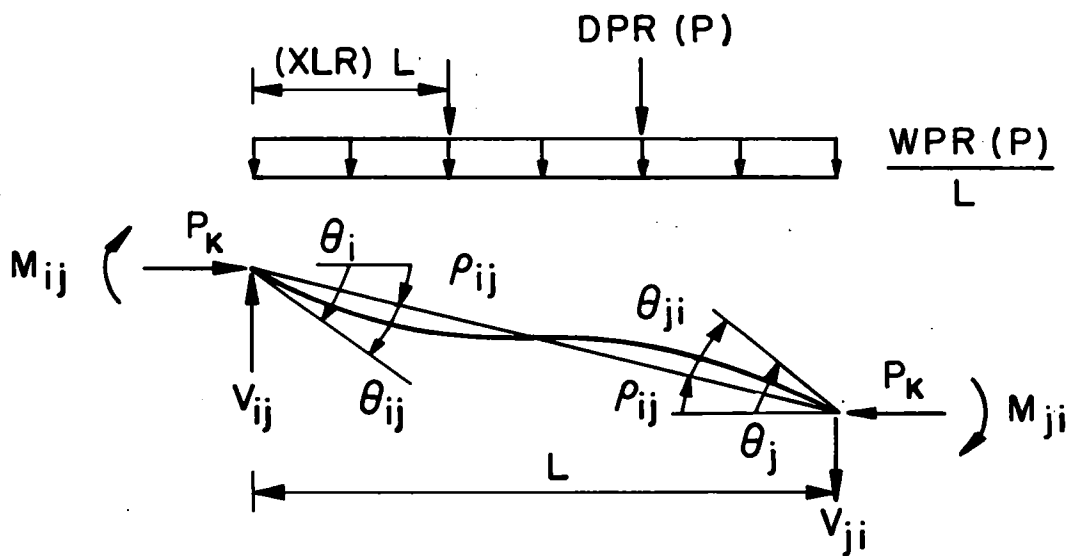


Fig. 3.1 Positive Sign Convention

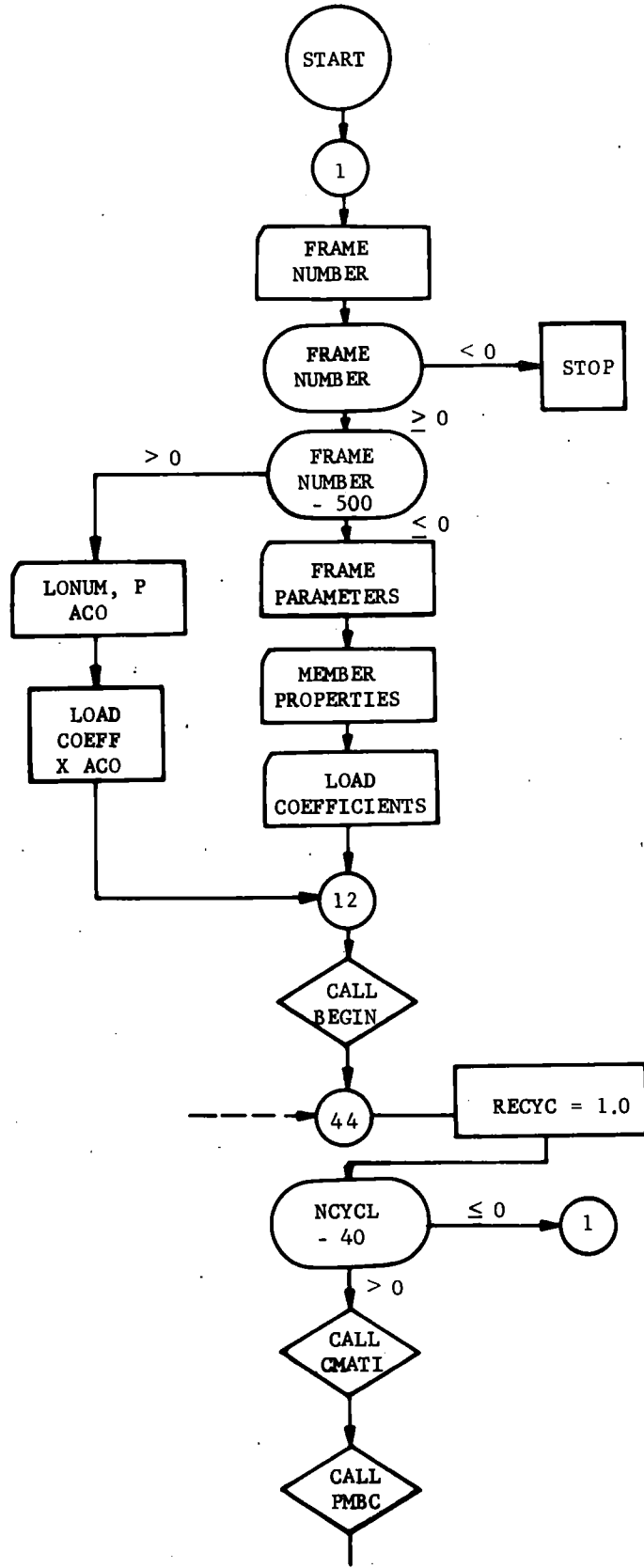


Fig. 3.2 Main Program

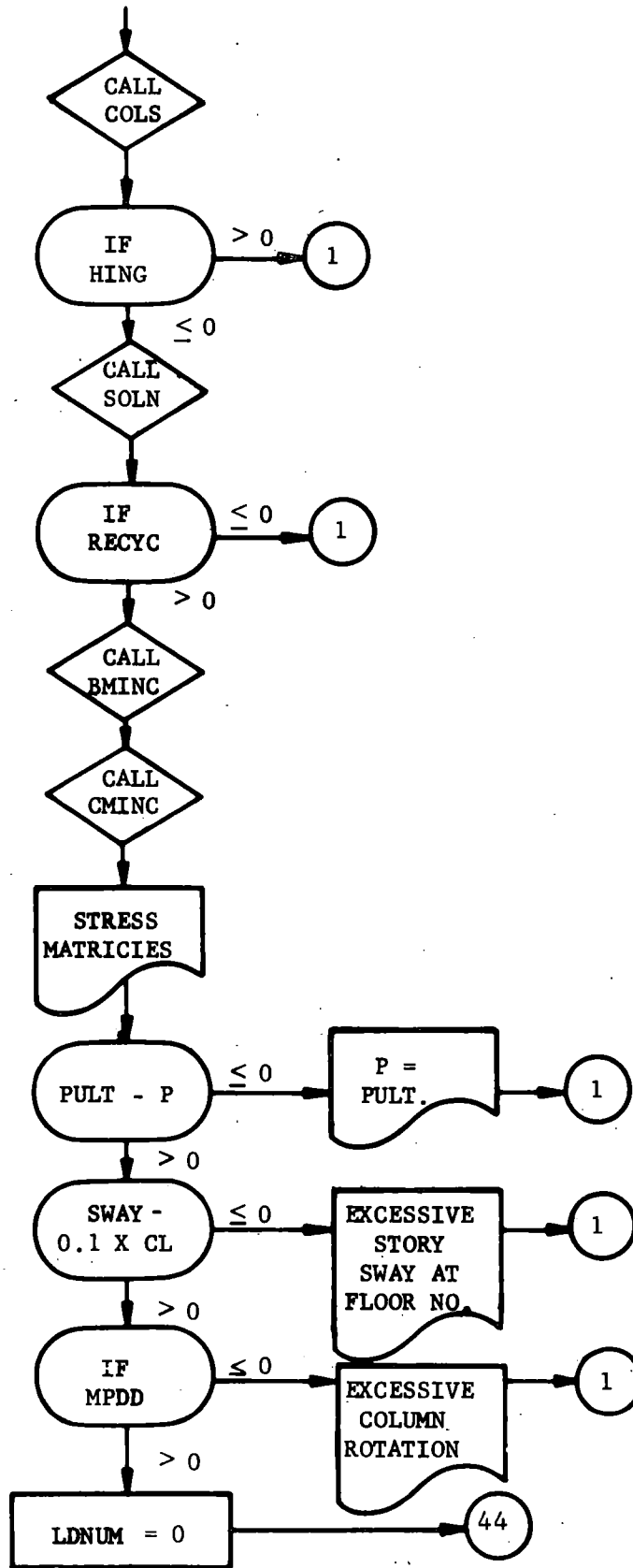


Fig. 3.2 Main Program, Continued

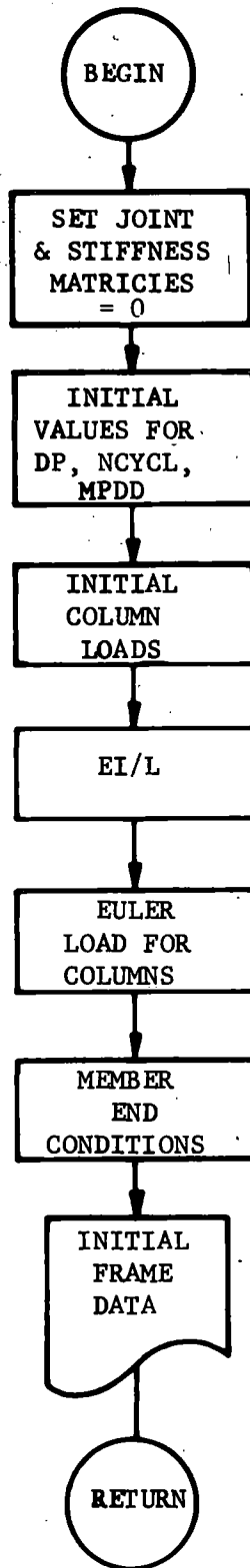


Fig. 3.3 Subroutine, Begin

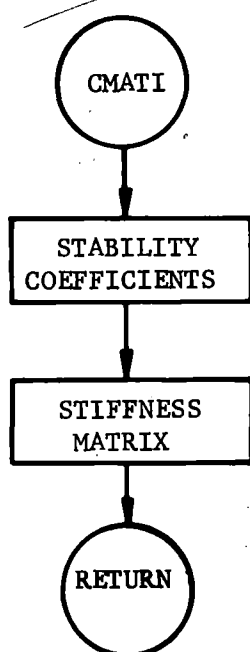


Fig. 3.4 Subroutine, Initial Coefficient Matrix

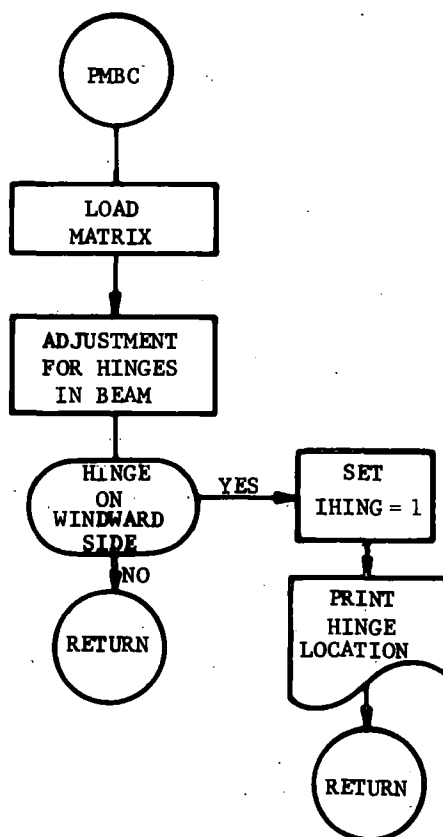


Fig. 3.5 Subroutine, Load Matrix and Beam Corrections

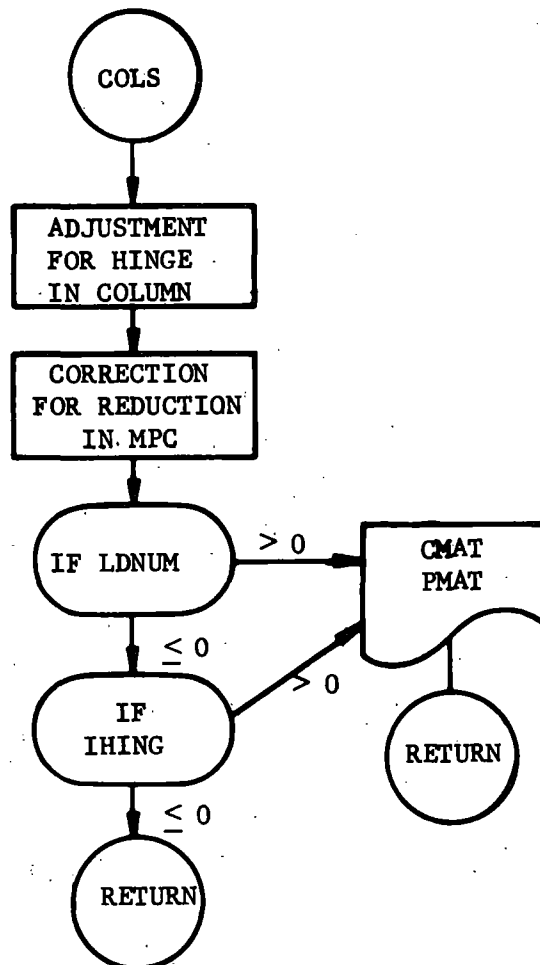


Fig. 3.6 Subroutine, Column Corrections

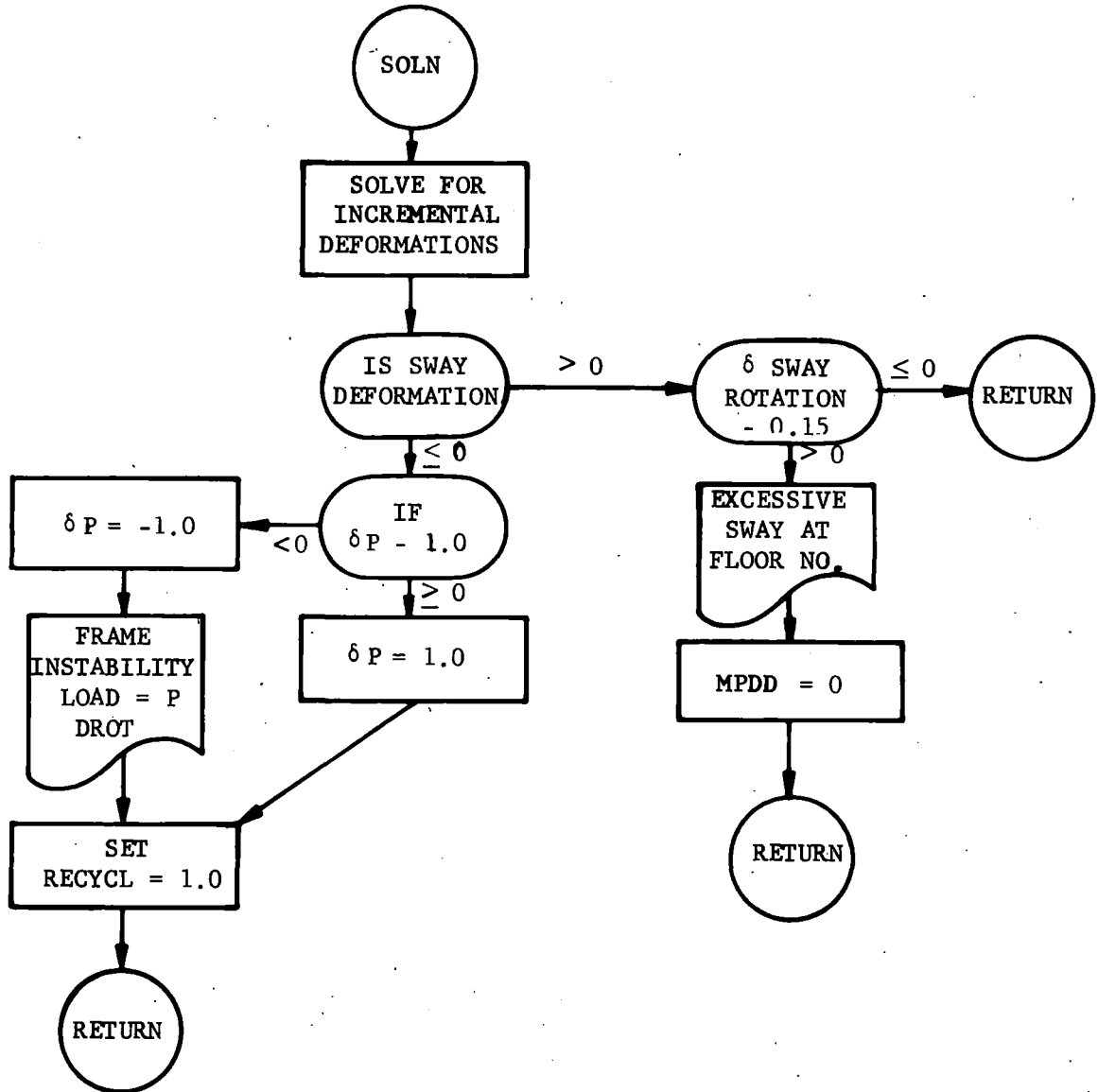


Fig. 3.7 Subroutine, Solution for Incremental Deformations

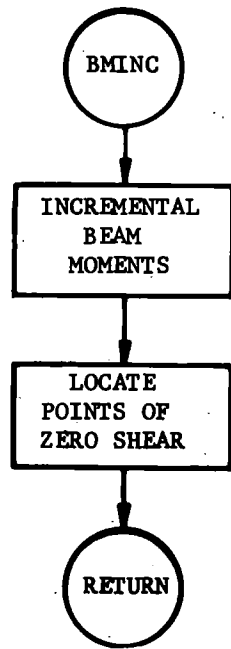


Fig. 3.8 Subroutine, Incremental Beam Moments

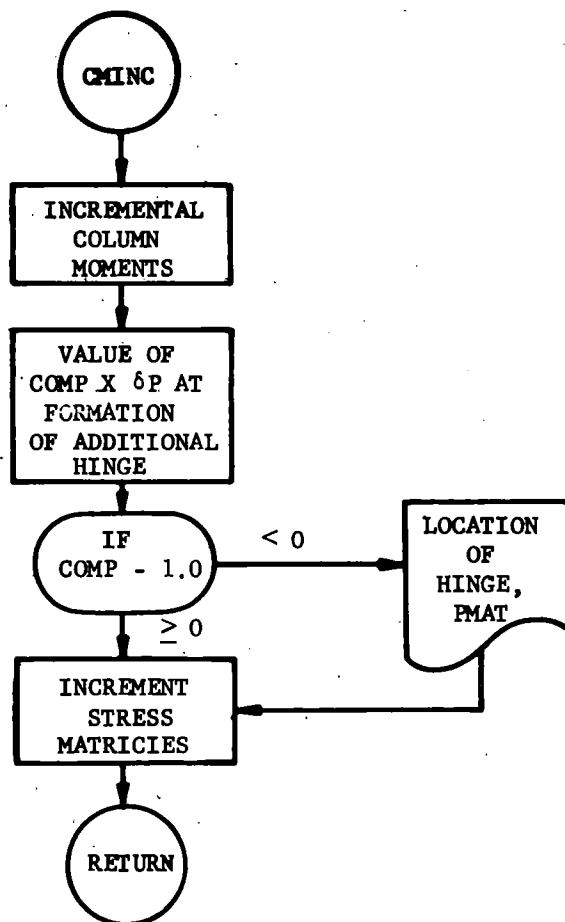


Fig. 3.9 Subroutine, Incremental Column Moments

$\lambda = 1.90$		CF = 4.26			
$\Delta$	1	2	3	4	
Iteration	1.90	1.65	1.12	0.48	
Increment	1.88	1.64	1.11	0.48	

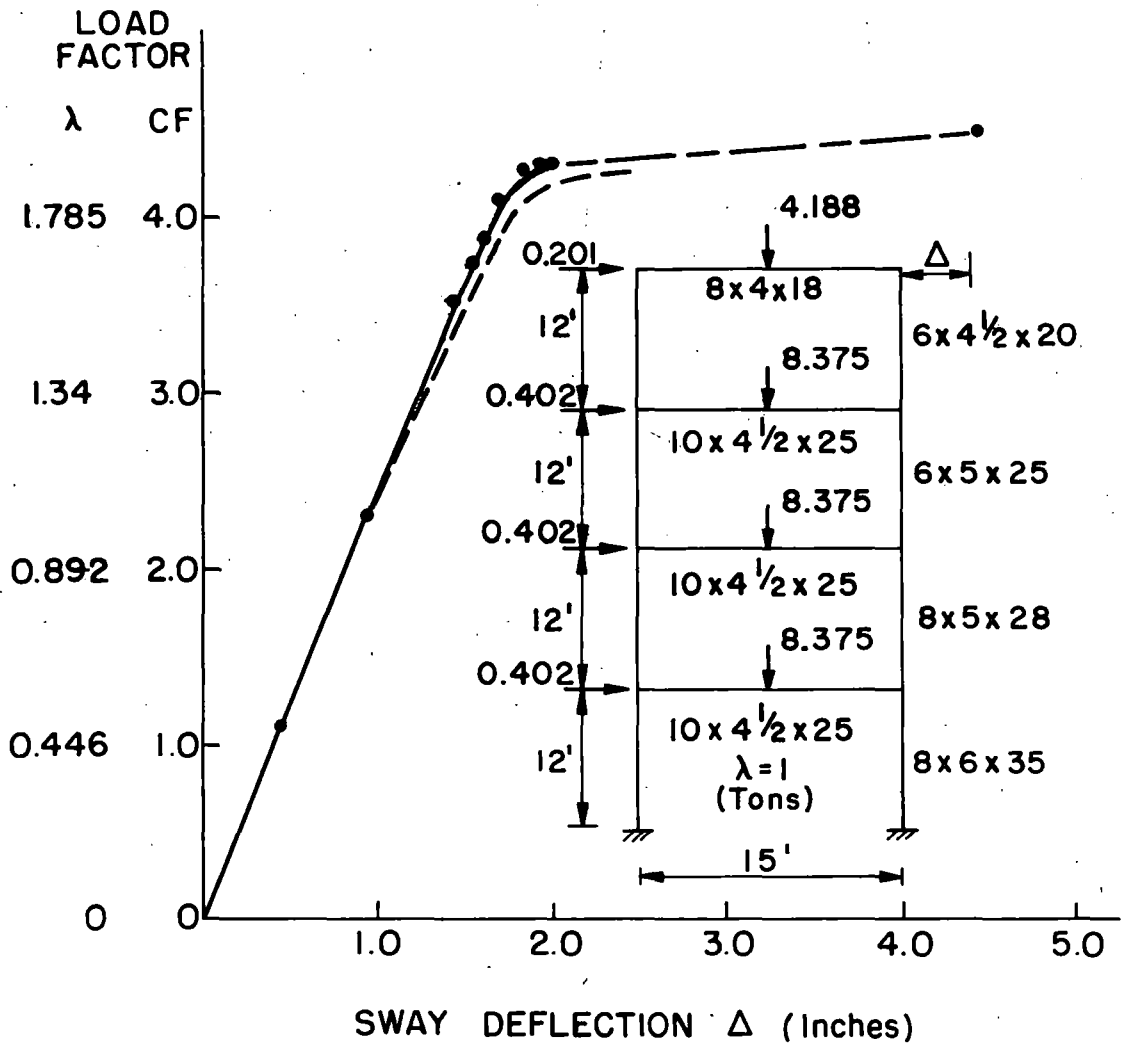


Fig. 3.10 Incremental-Iteration Comparison, Wood's Frame

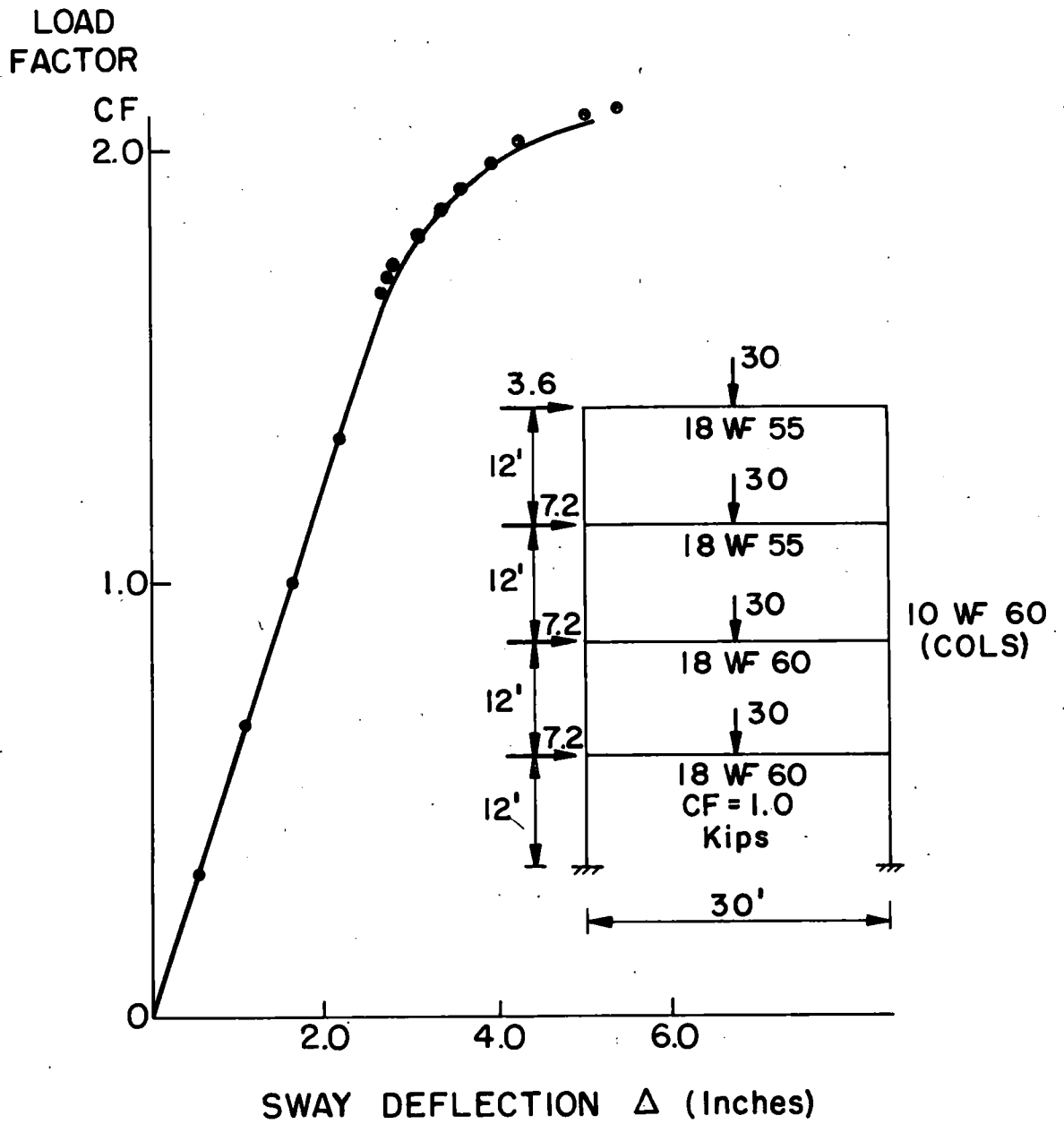


Fig. 3.11 Incremental-Iteration Comparison, Heyman's Frame

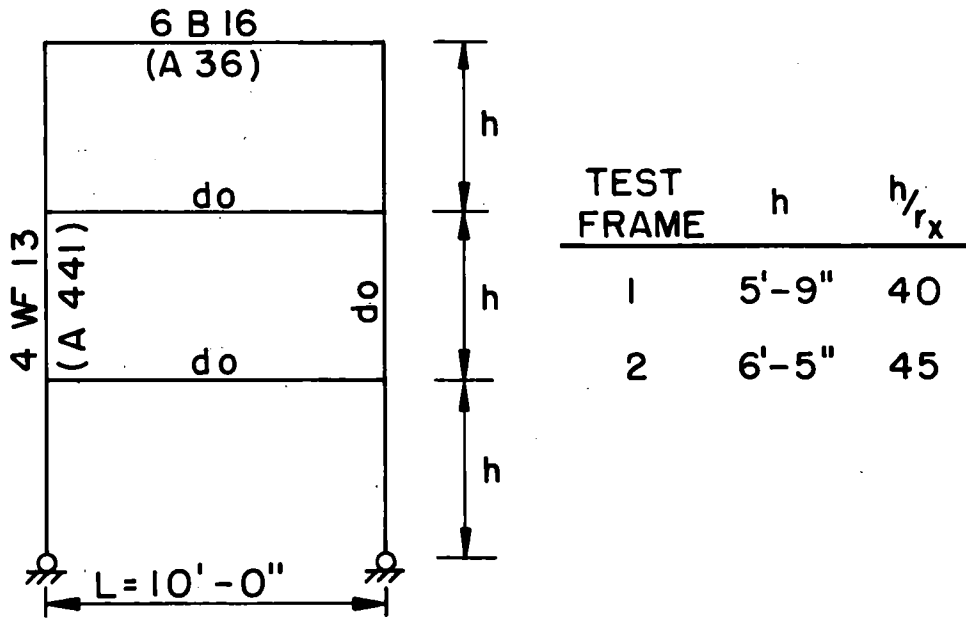


Fig. 4.1 Frame Geometry

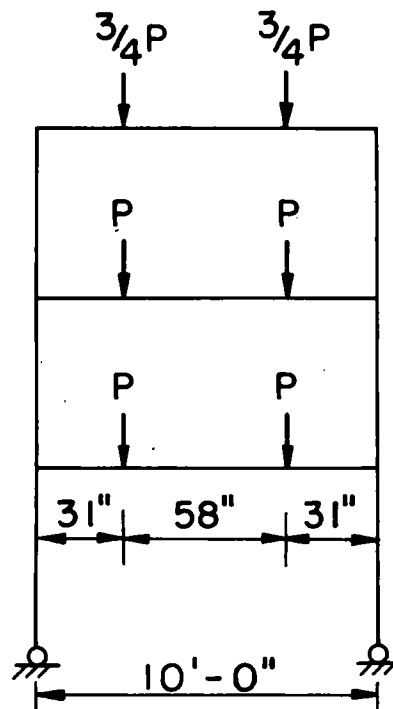


Fig. 4.2 Frame Loading

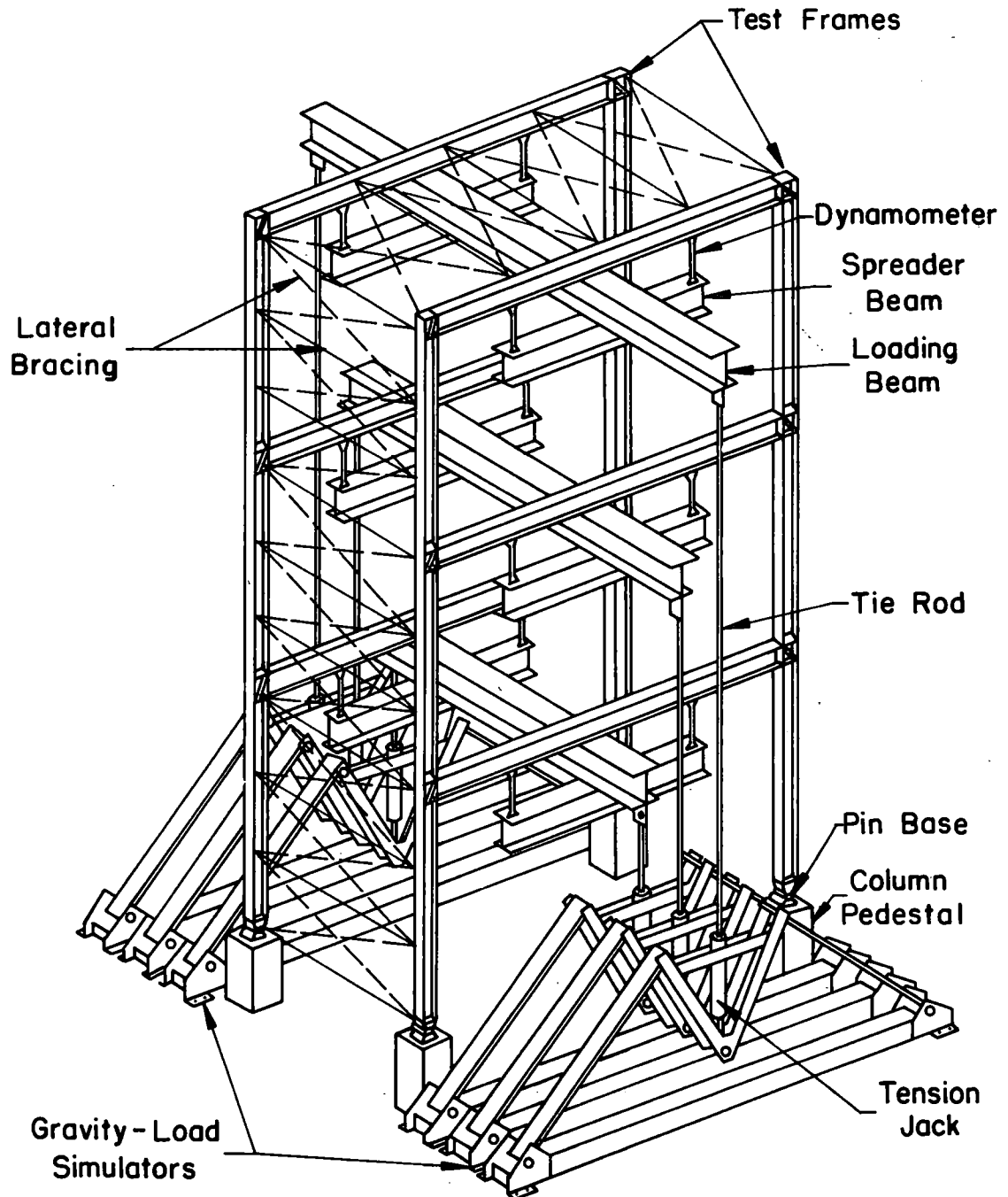


Fig. 4.3 Test Setup, Diagram

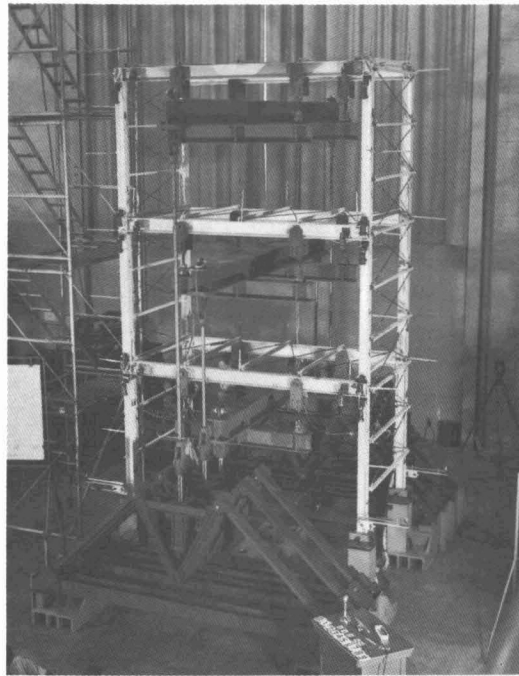


Fig. 4.4 Test Setup

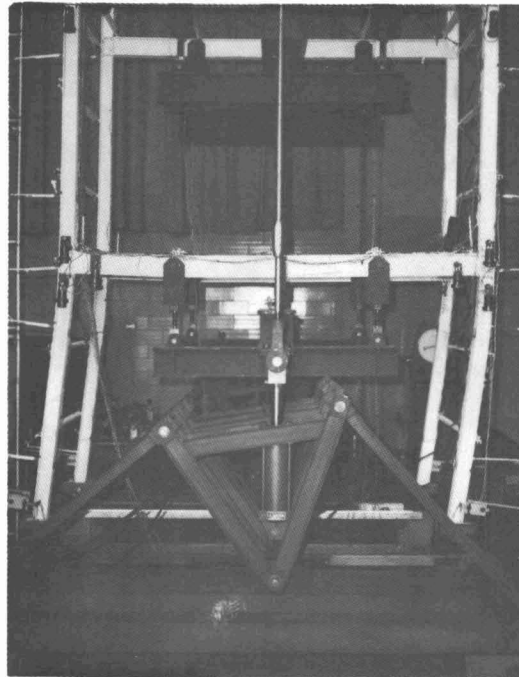


Fig. 4.5 Deflected Frame

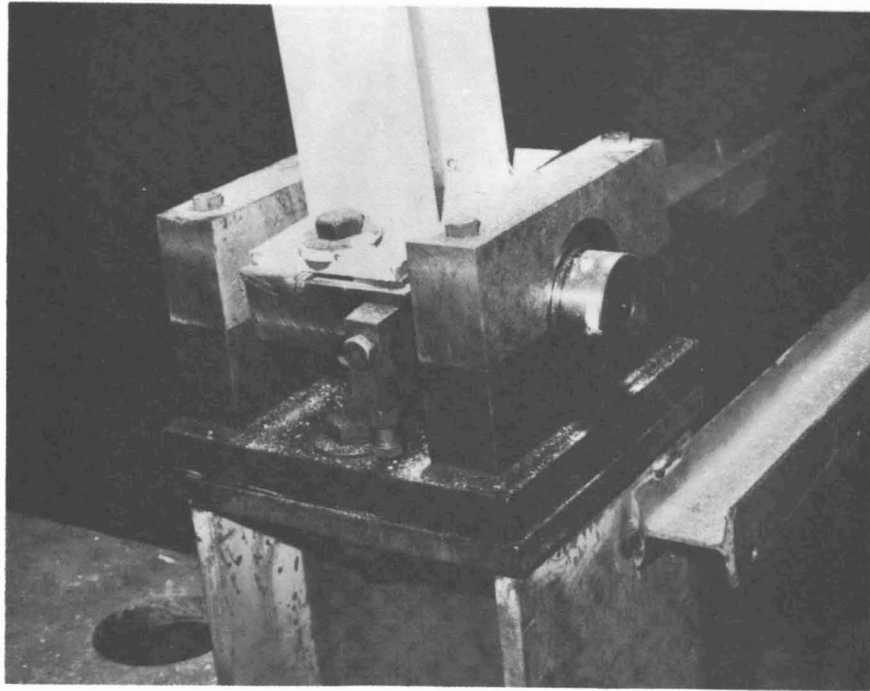


Fig. 4.6 Pinned-Base

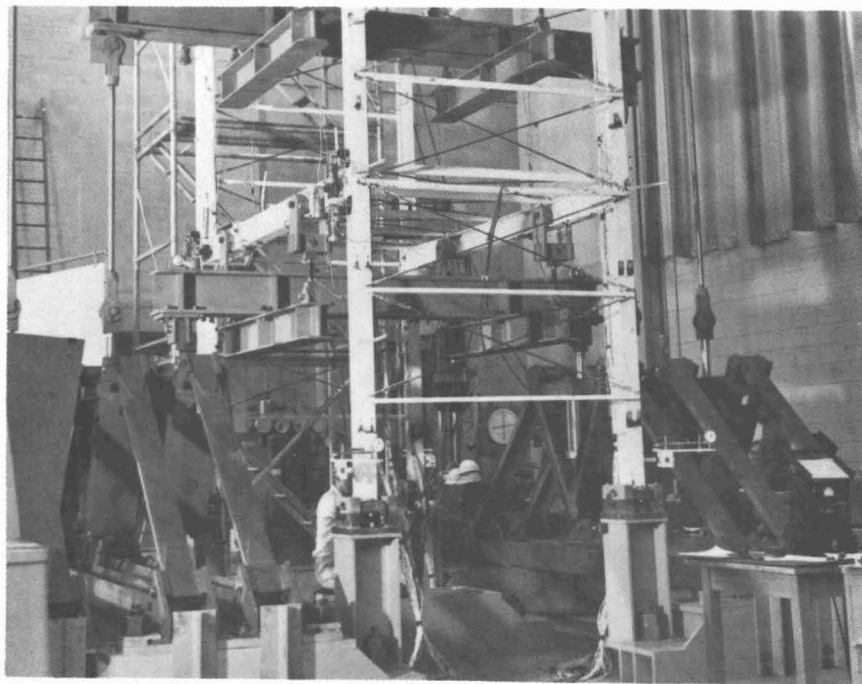


Fig. 4.7 Bases for Test Bed

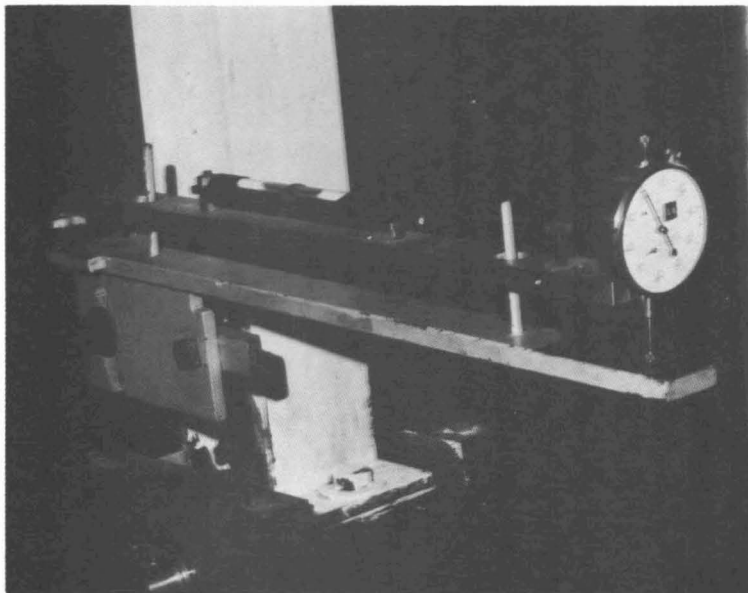


Fig. 4.8 Dial Rotation Gage

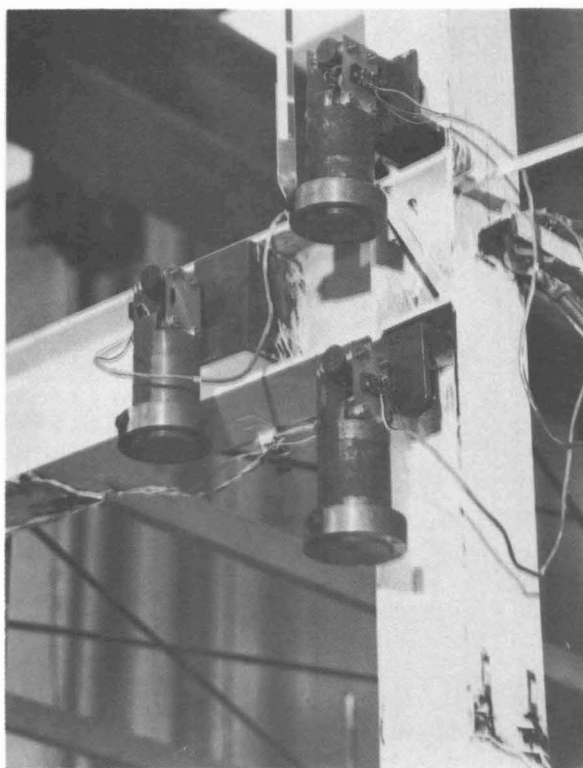


Fig. 4.9 Electrical Rotation Gages

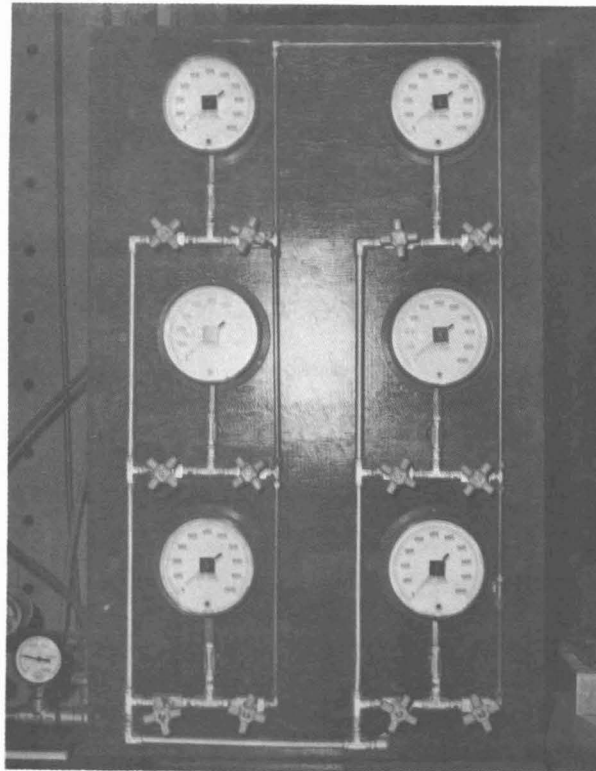


Fig. 4.10 Load Console

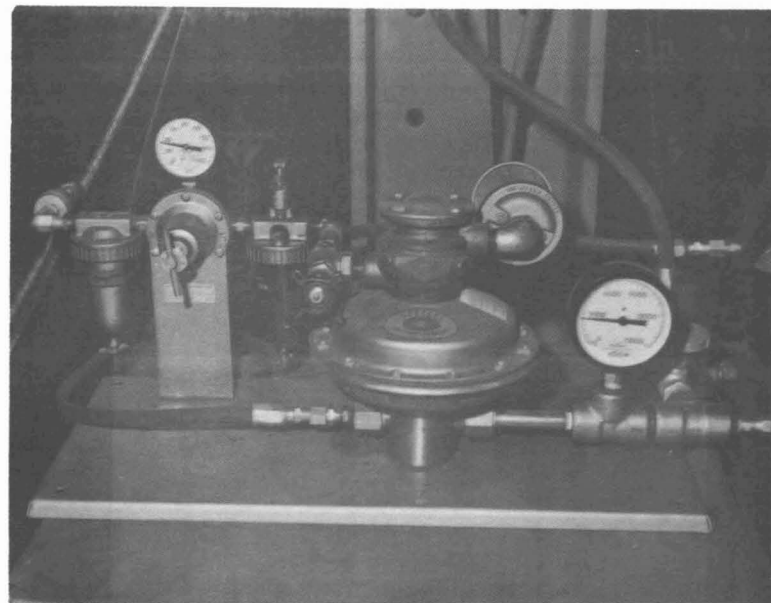


Fig. 4.11 Load Pumps

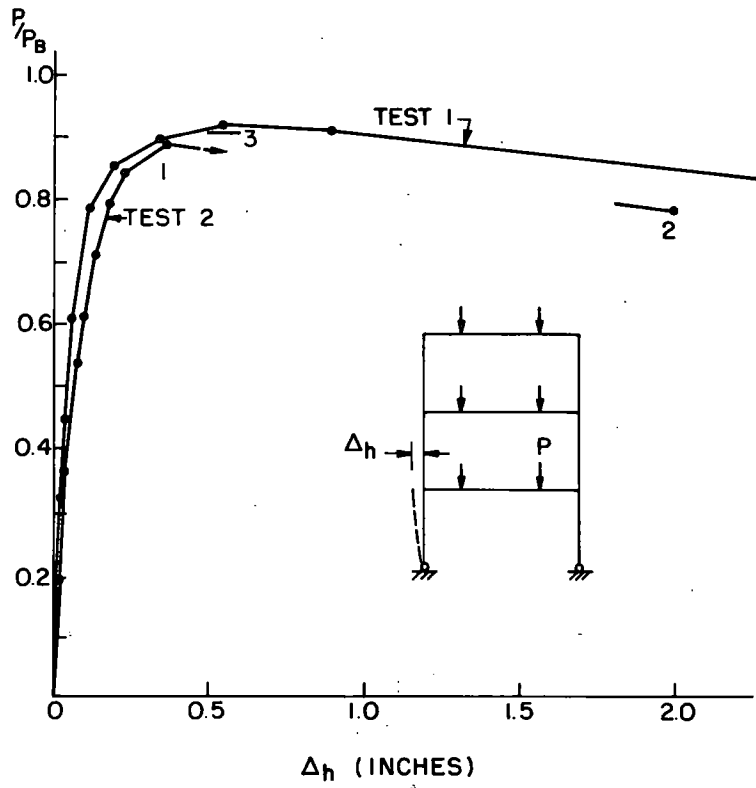


Fig. 5.1 Load-Lateral Sway Relationships

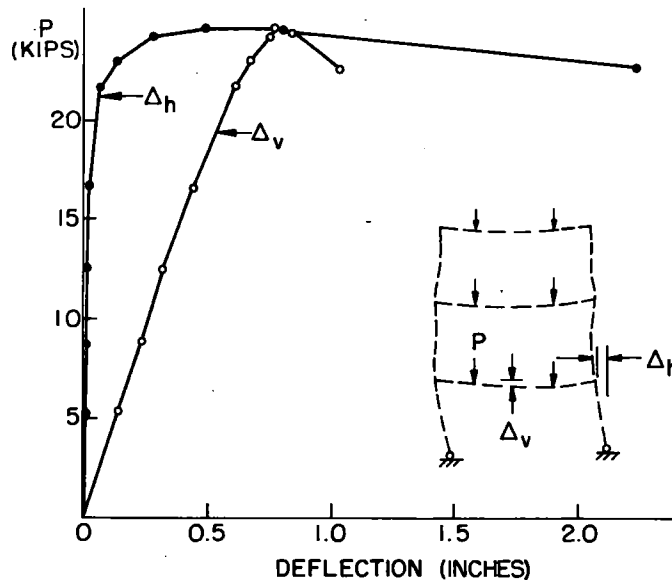


Fig. 5.2 Deflection Comparison, Test 1

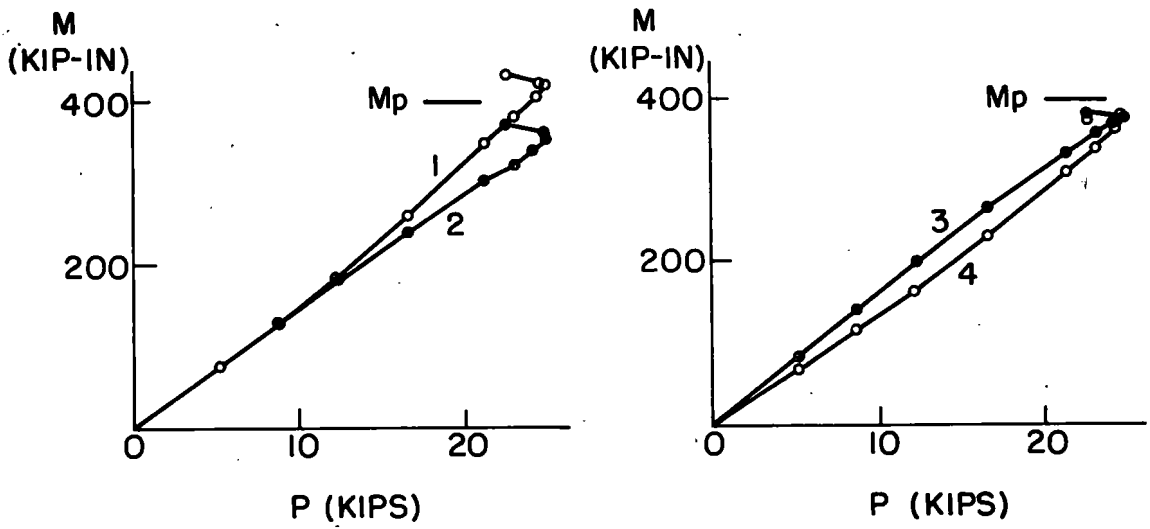


Fig. 5.3a Beam Moments, West Frame, Test 1

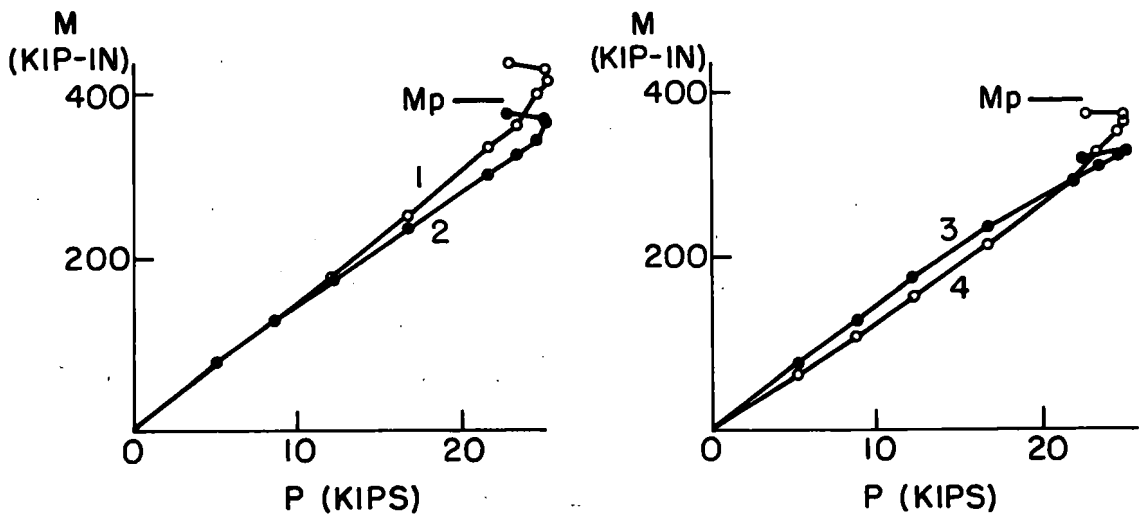
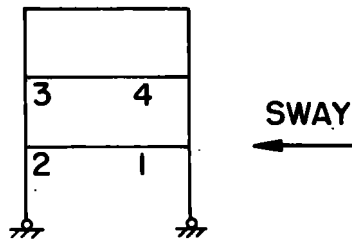


Fig. 5.3b Beam Moments, East Frame, Test 1

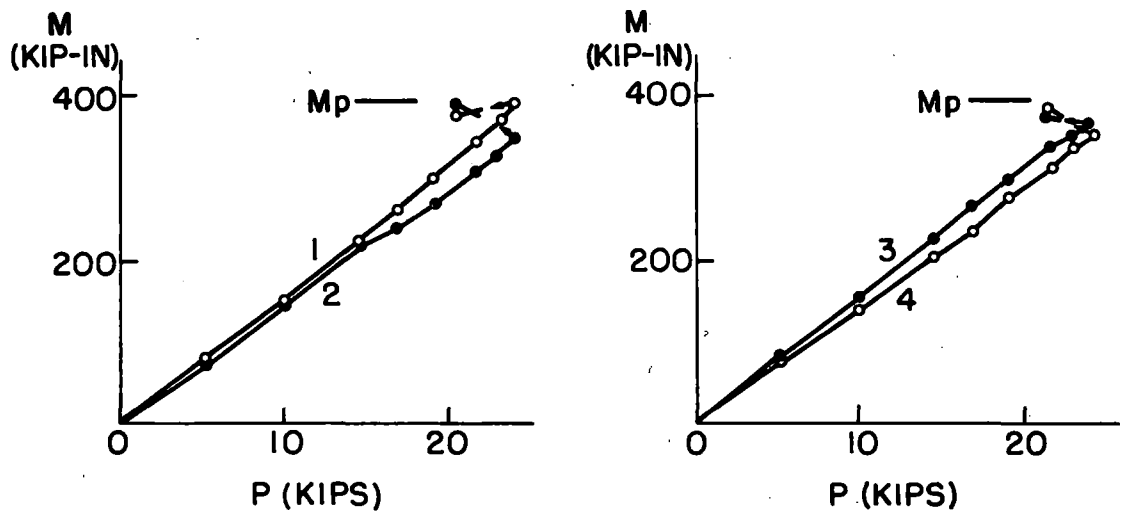


Fig. 5.4a Beam Moments, West Frame, Test 2

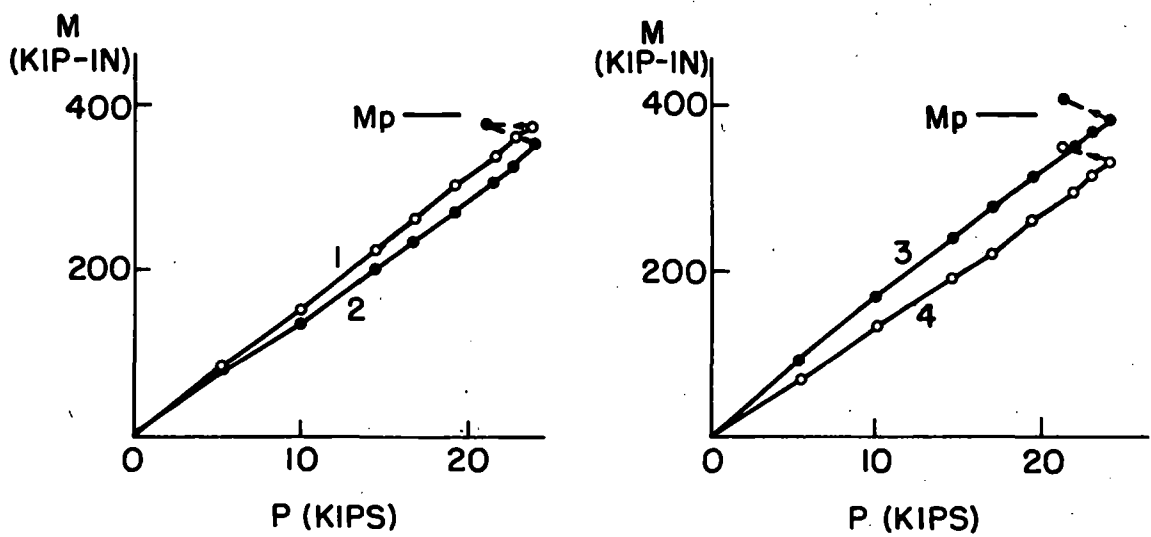
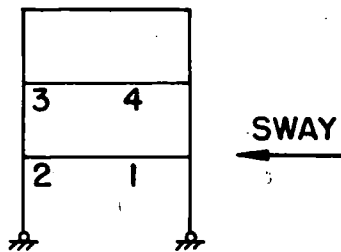


Fig. 5.4b Beam Moments, East Frame, Test 2

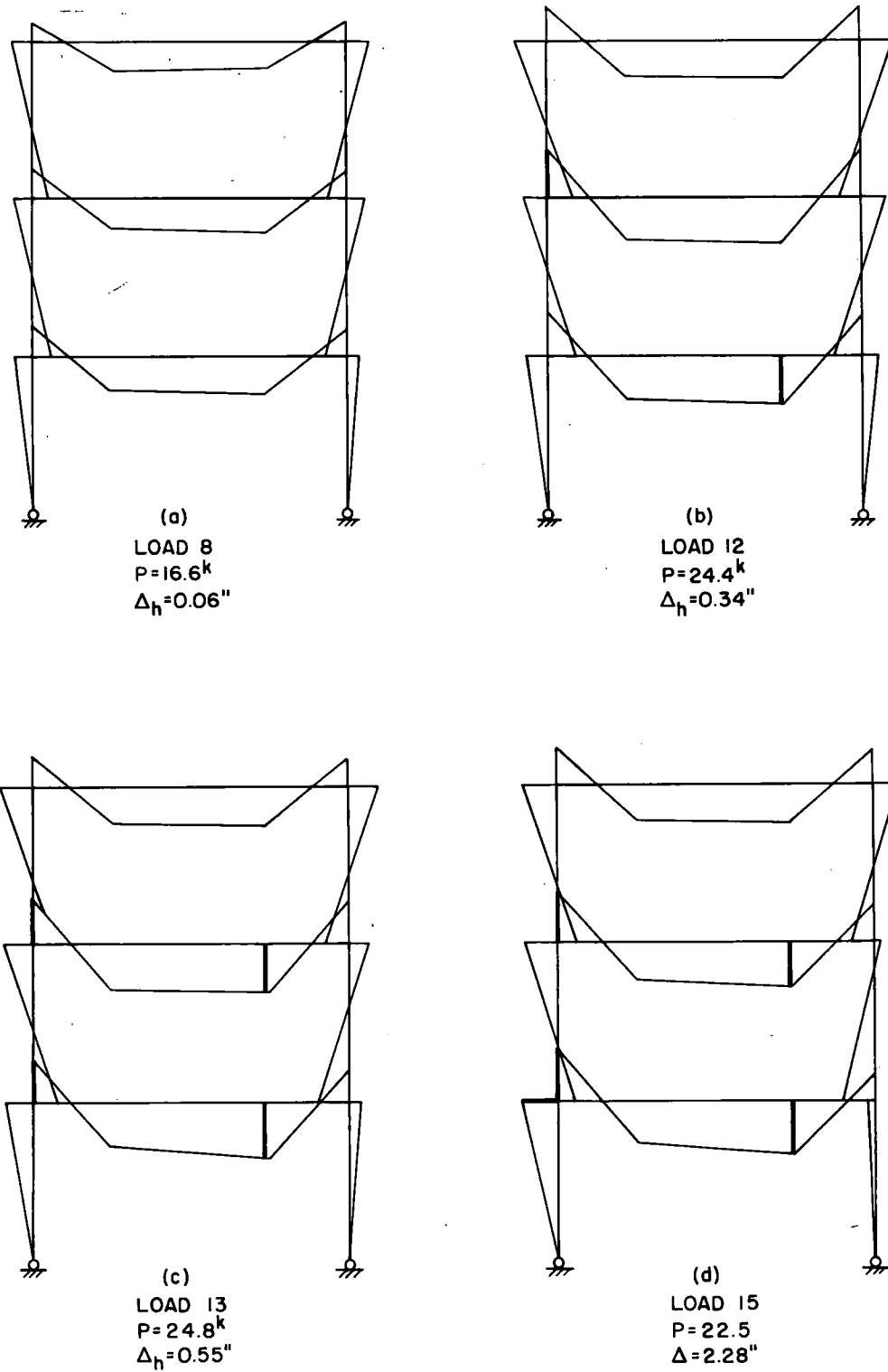


Fig. 5.5 Moment Distribution, West Frame, Test 1

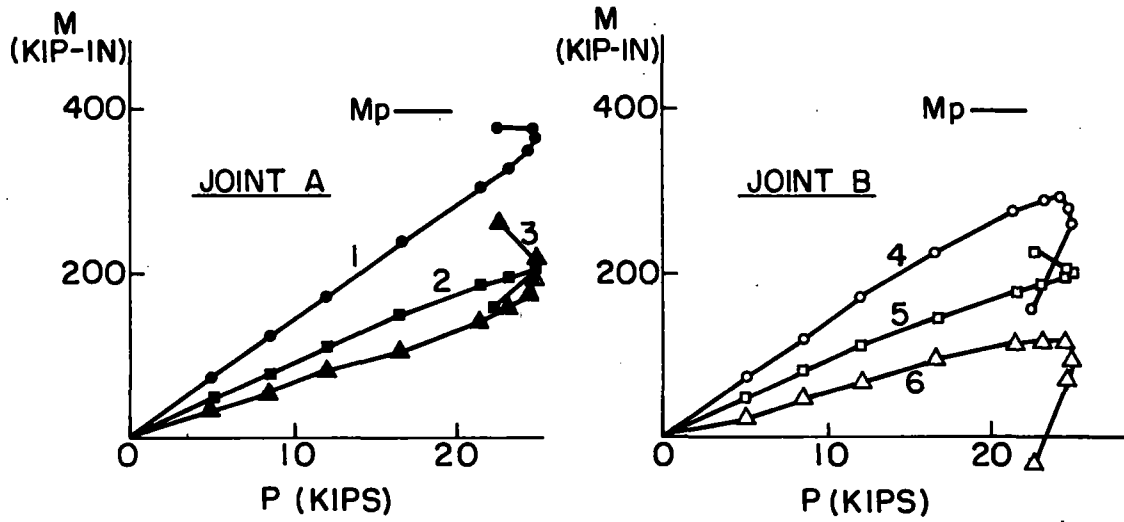


Fig. 5.6a Bottom Story Joint Moments, Test 1

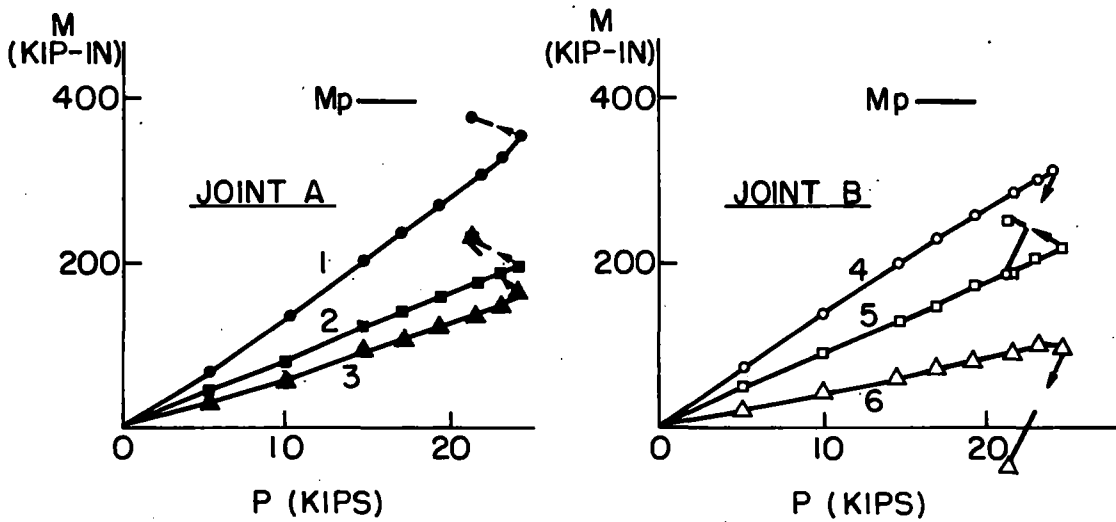
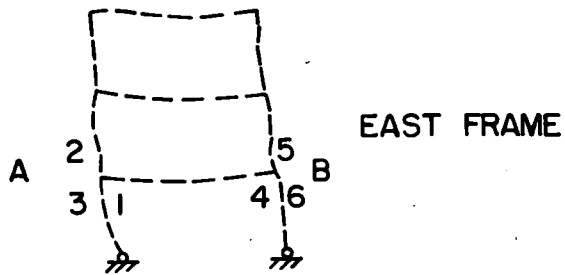


Fig. 5.6b Bottom Story Joint Moments, Test 2

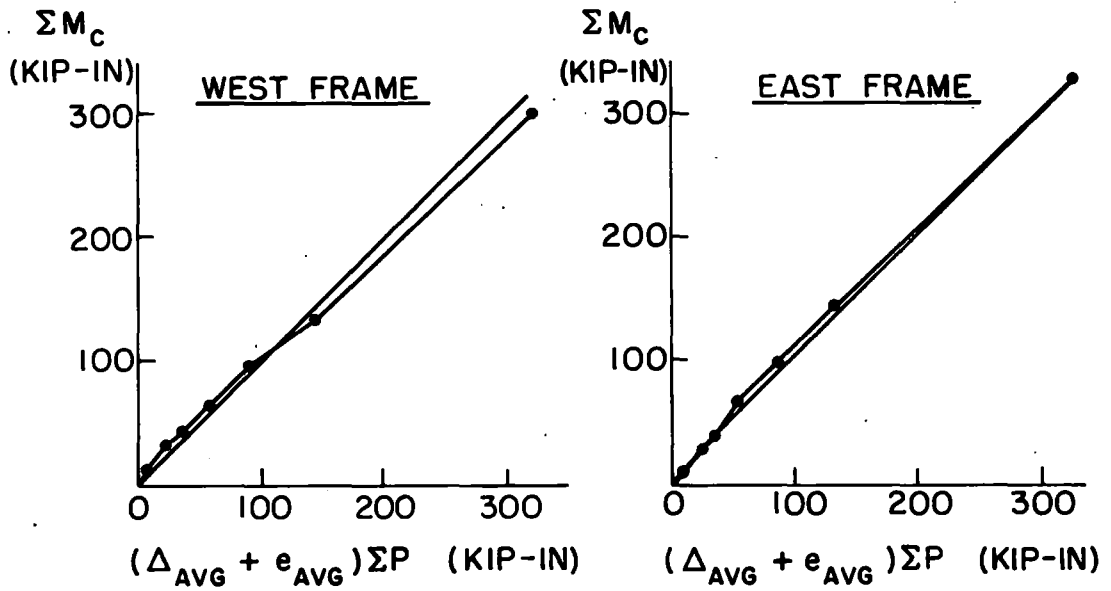


Fig. 5.7a Bottom Story Shear Equilibrium, Test 1

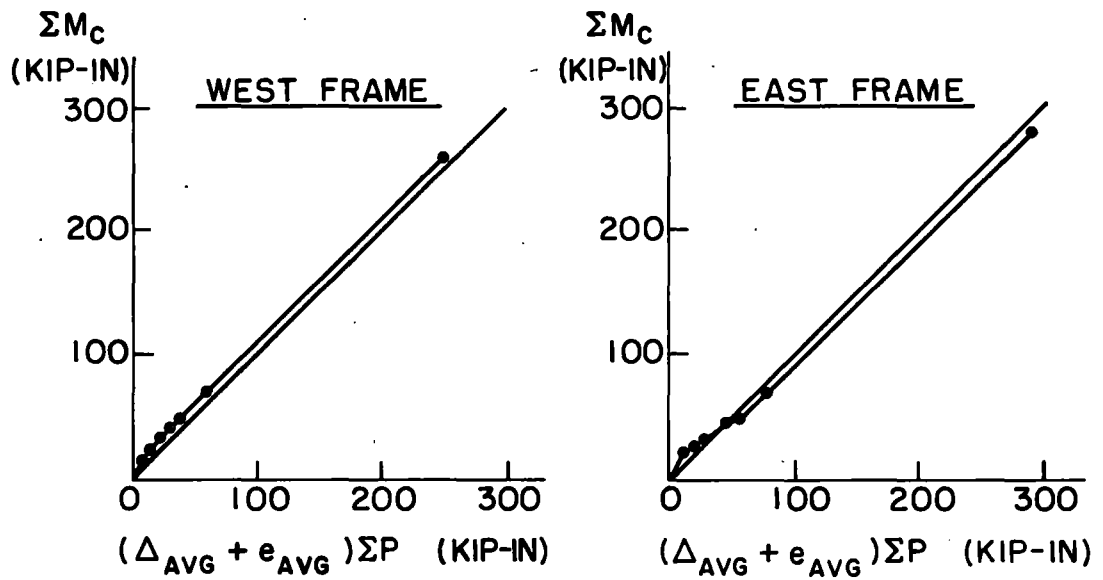


Fig. 5.7b Bottom Story Shear Equilibrium, Test 2

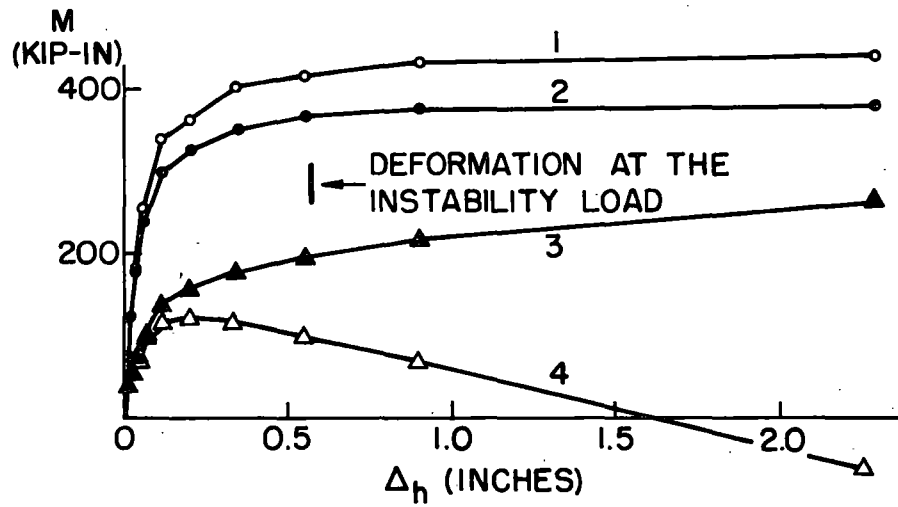


Fig. 5.8a Moment-Sway Deflection, Test 1

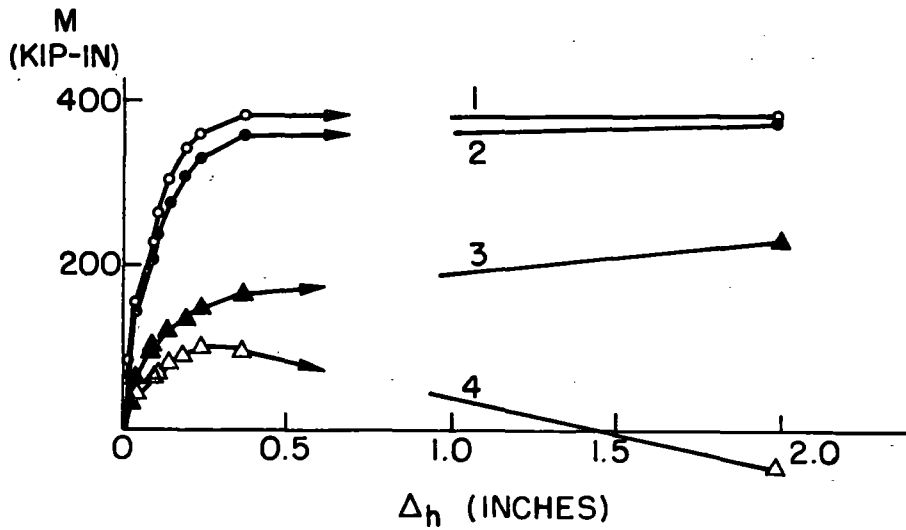
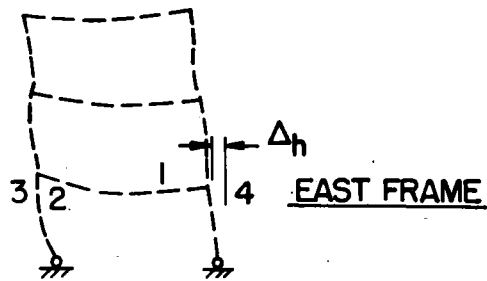


Fig. 5.8b Moment-Sway Deflection, Test 2

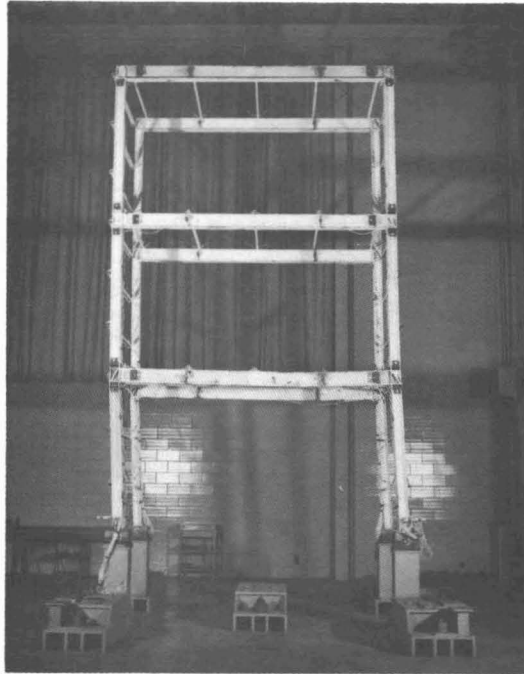


Fig. 5.9 Deflected Frame, Arrested Position

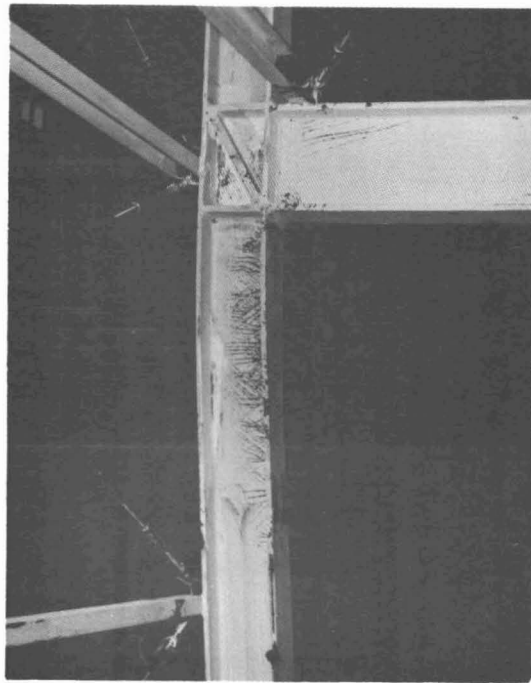


Fig. 5.10 Yield Pattern, Location 3, Joint A, Test 2

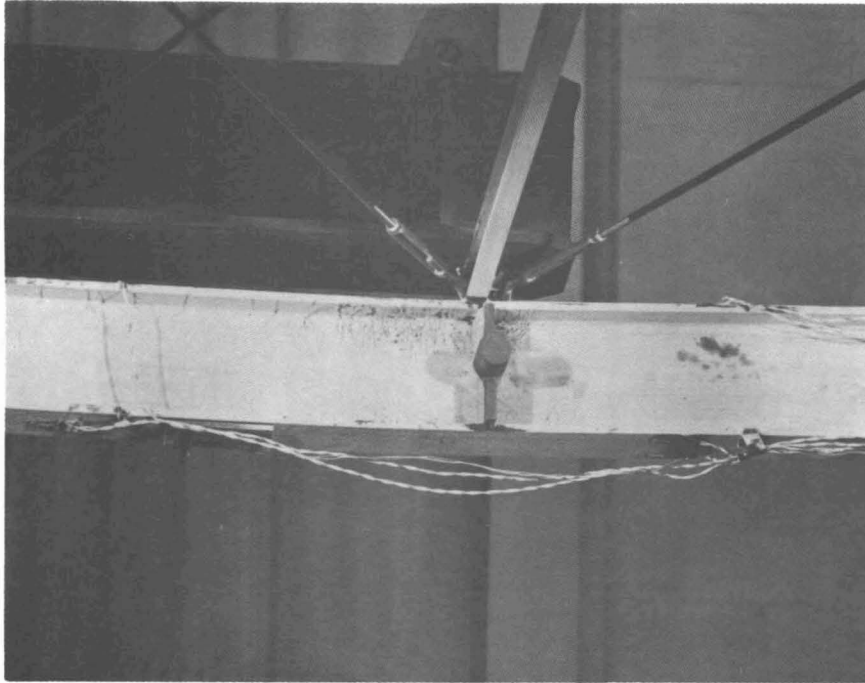


Fig. 5.11 Yield Pattern, Load Point, East Frame, Test 1

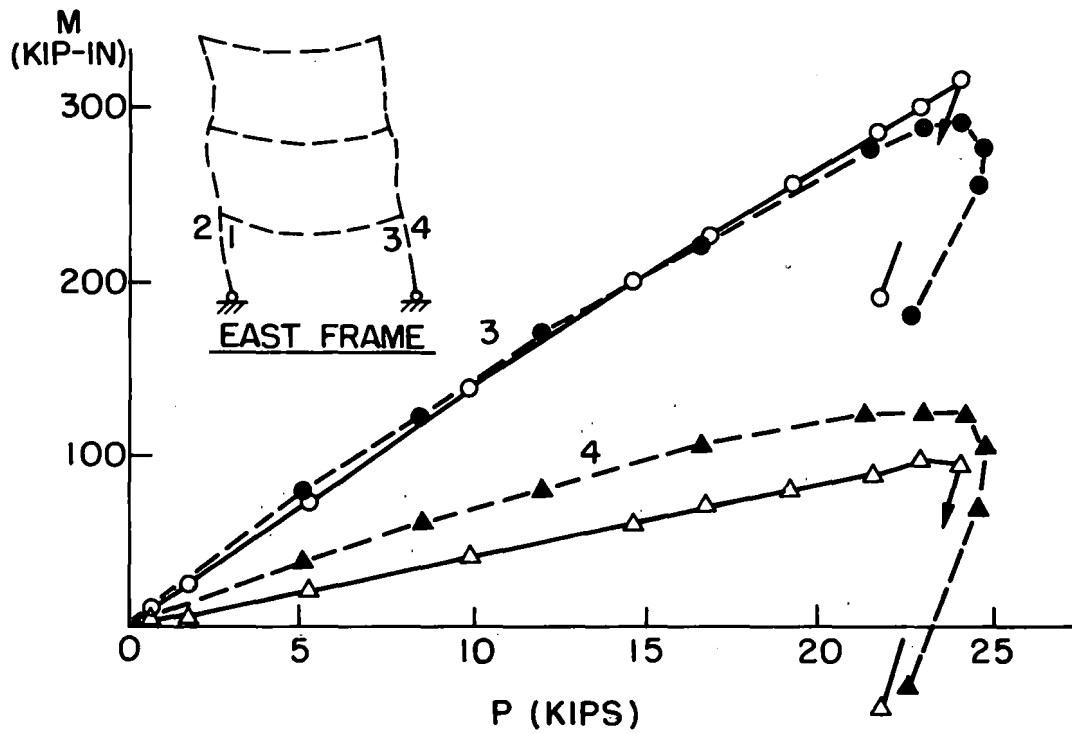
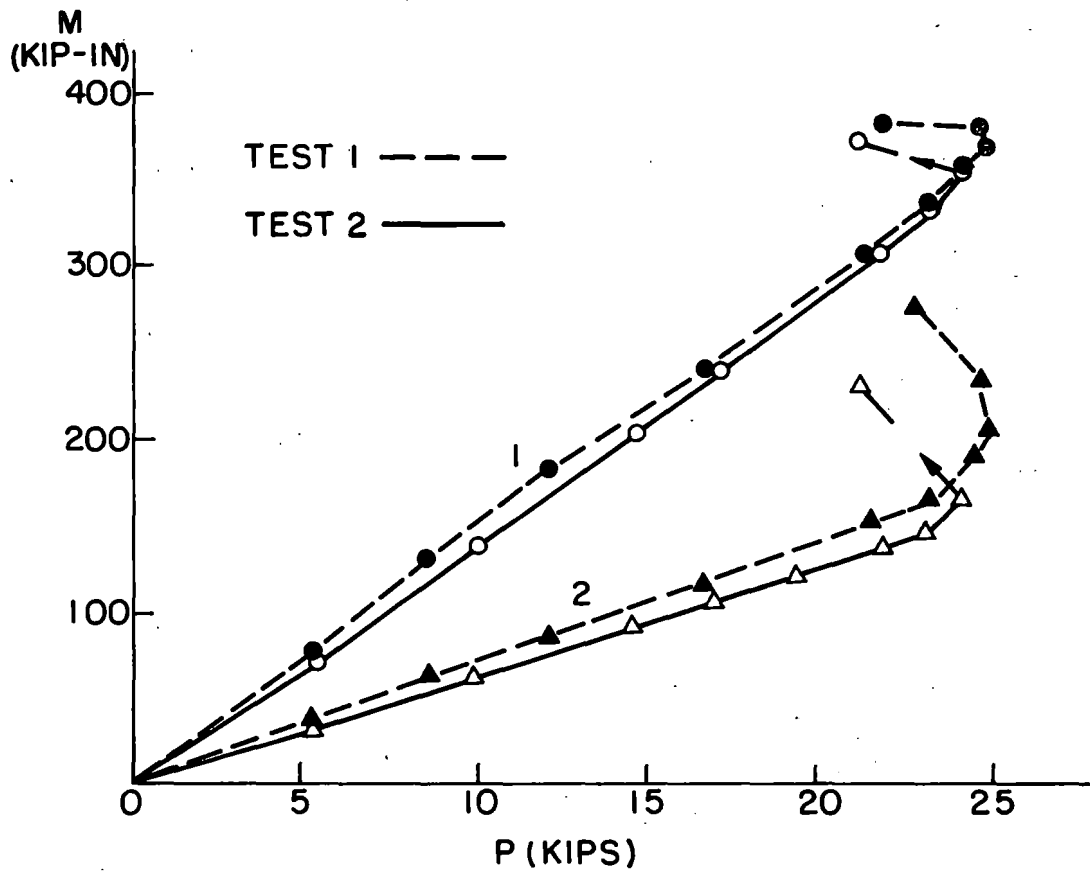


Fig. 5.12a Moment Comparisons, Tests 1 and 2, East Frame

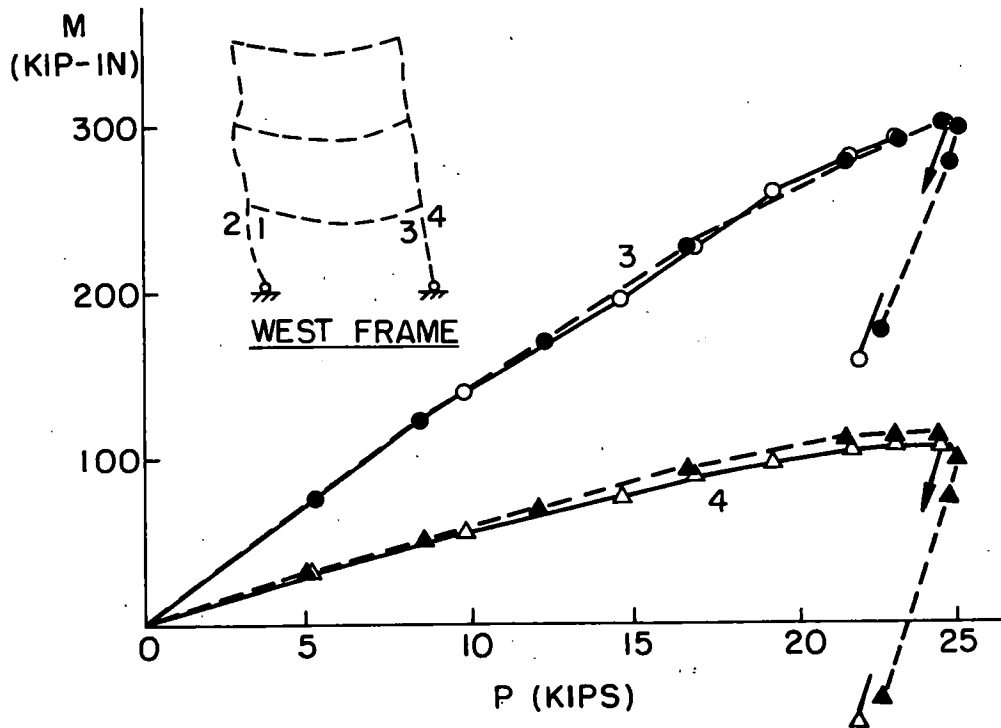
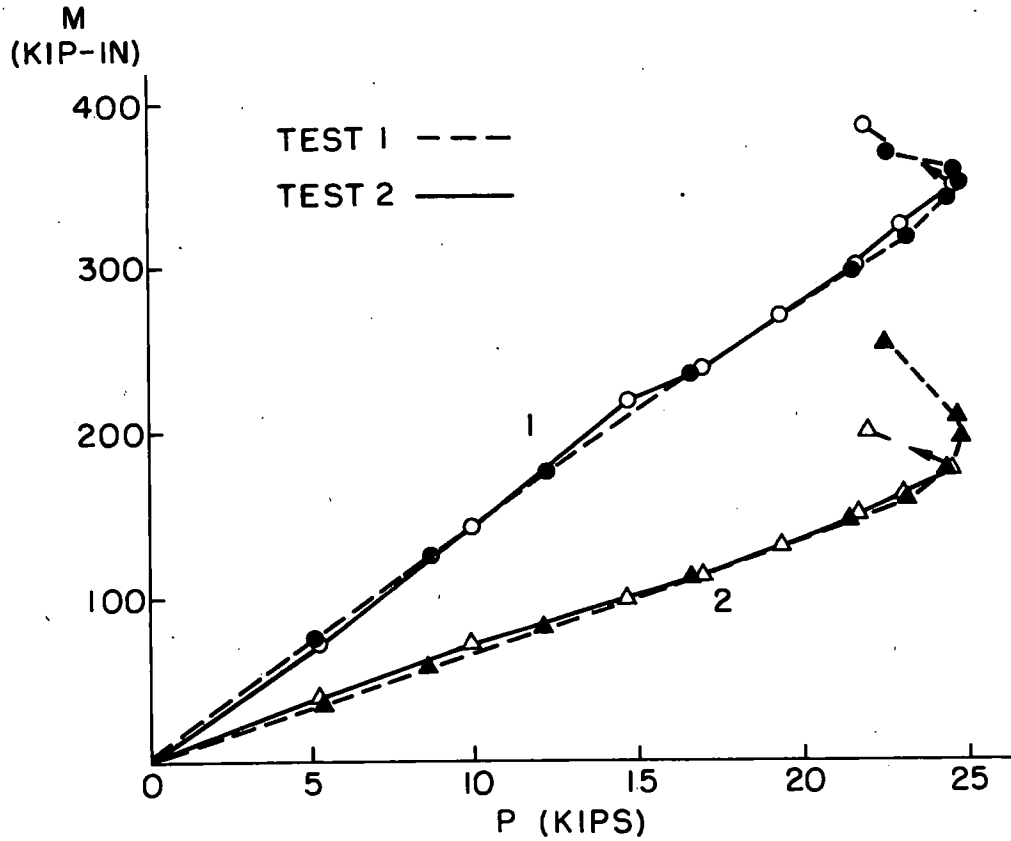


Fig. 5.12b Moment Comparisons, Tests 1 and 2, West Frame

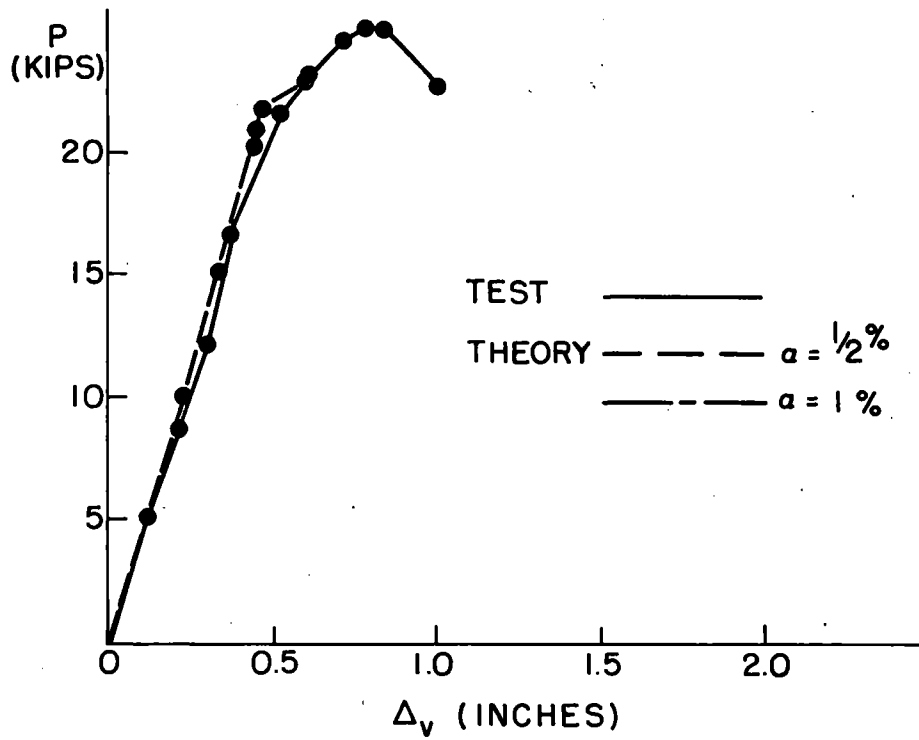


Fig. 5.13a Beam Deflections, Experimental and Predicted, Test 1

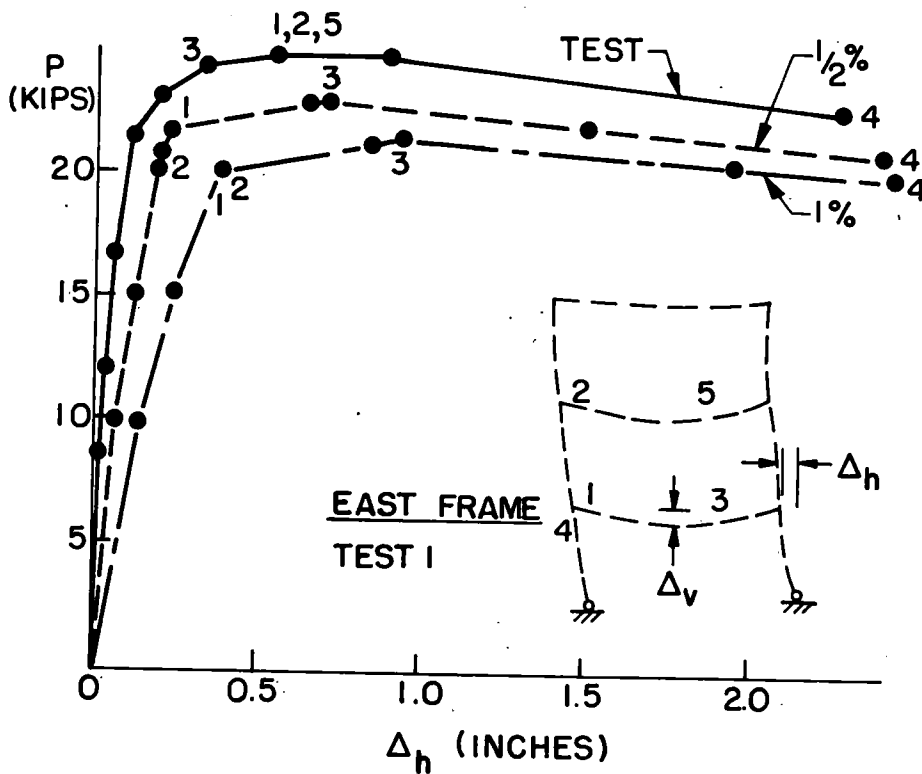


Fig. 5.13b Sway Deflections, Experimental and Predicted, Test 1

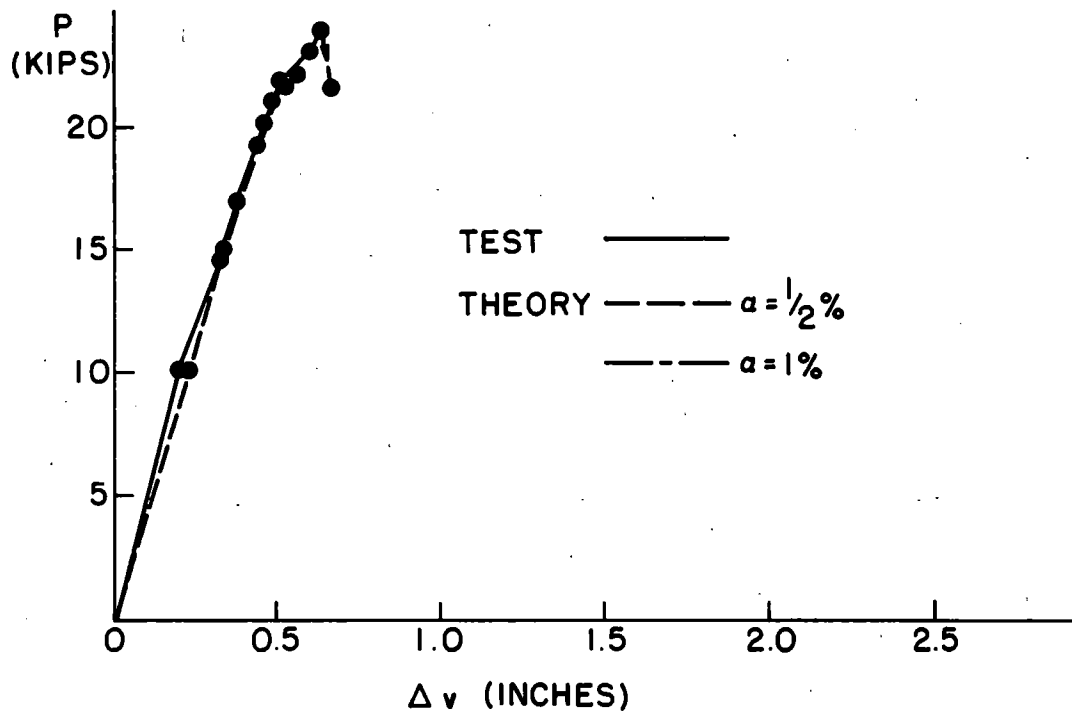


Fig. 5.14a Beam Deflections, Experimental and Predicted, Test 2

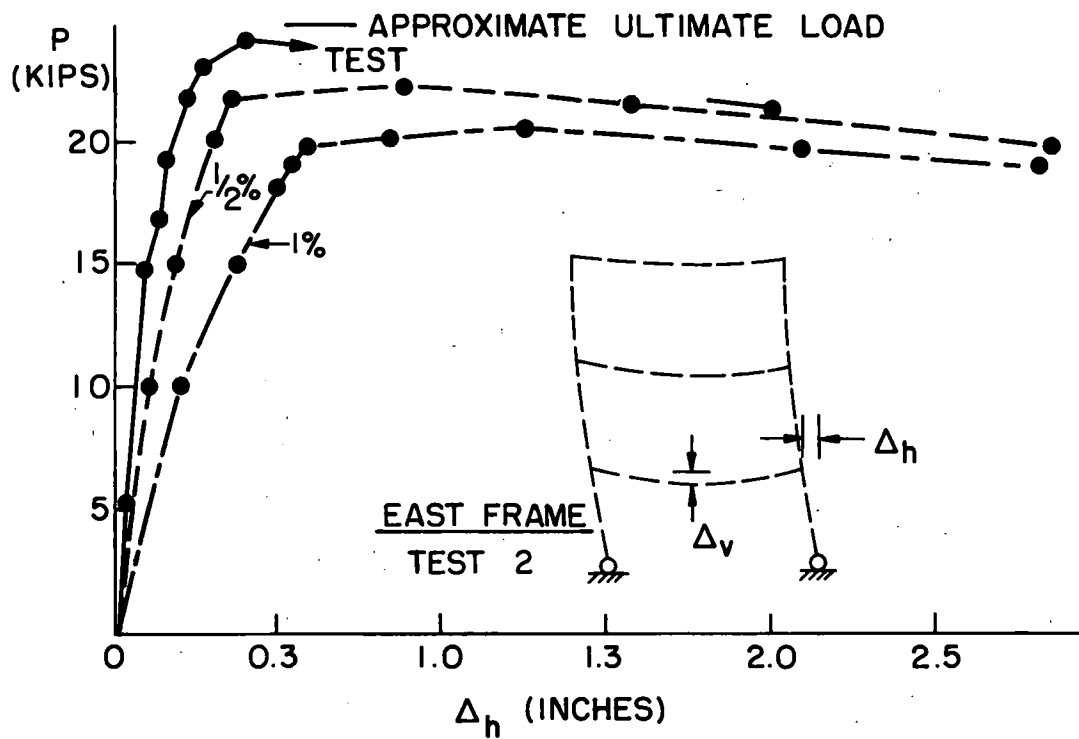


Fig. 5.14b Sway Deflections, Experimental and Predicted, Test 2

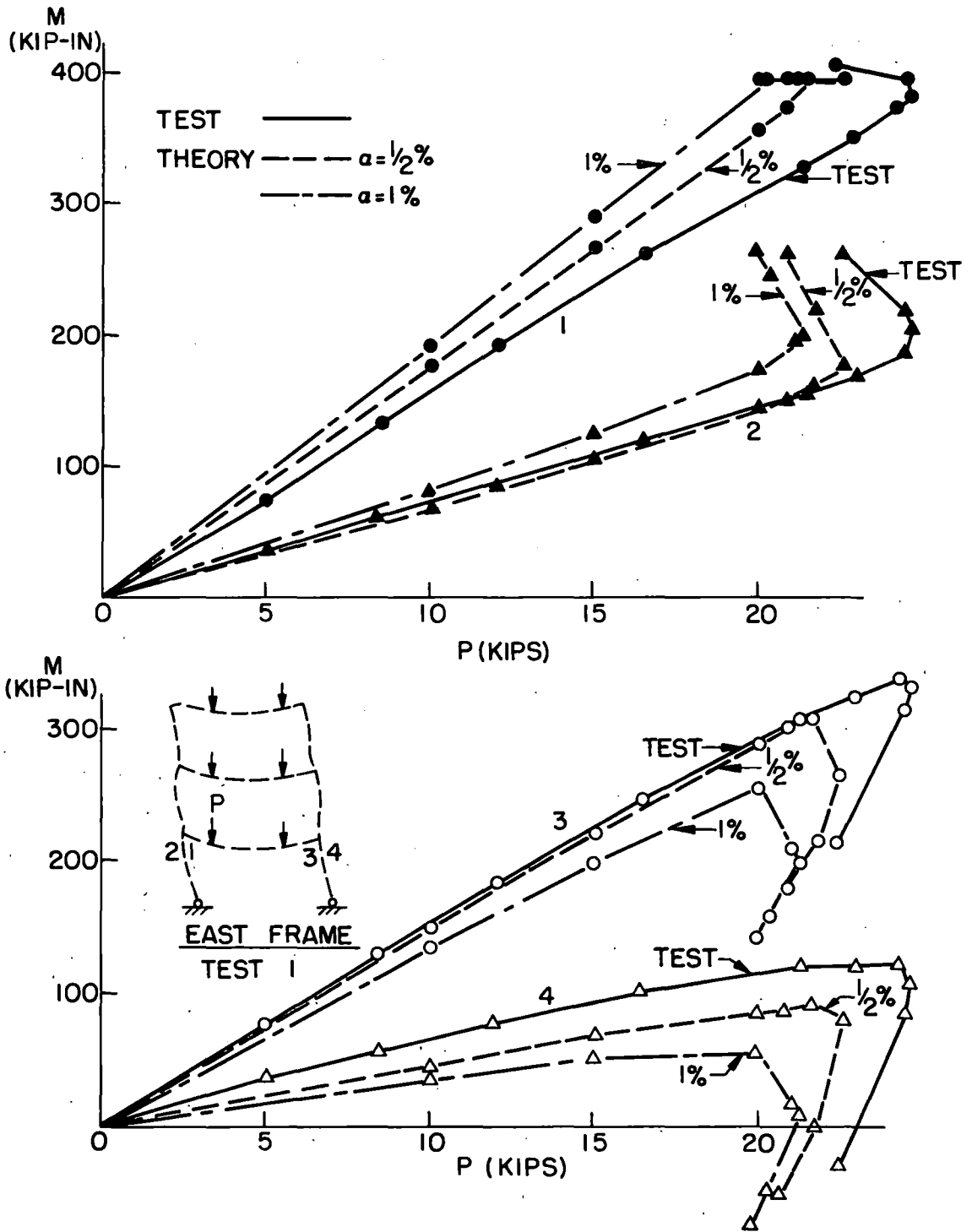


Fig. 5.15 Bending Moments, Experimental and Predicted, Test 1

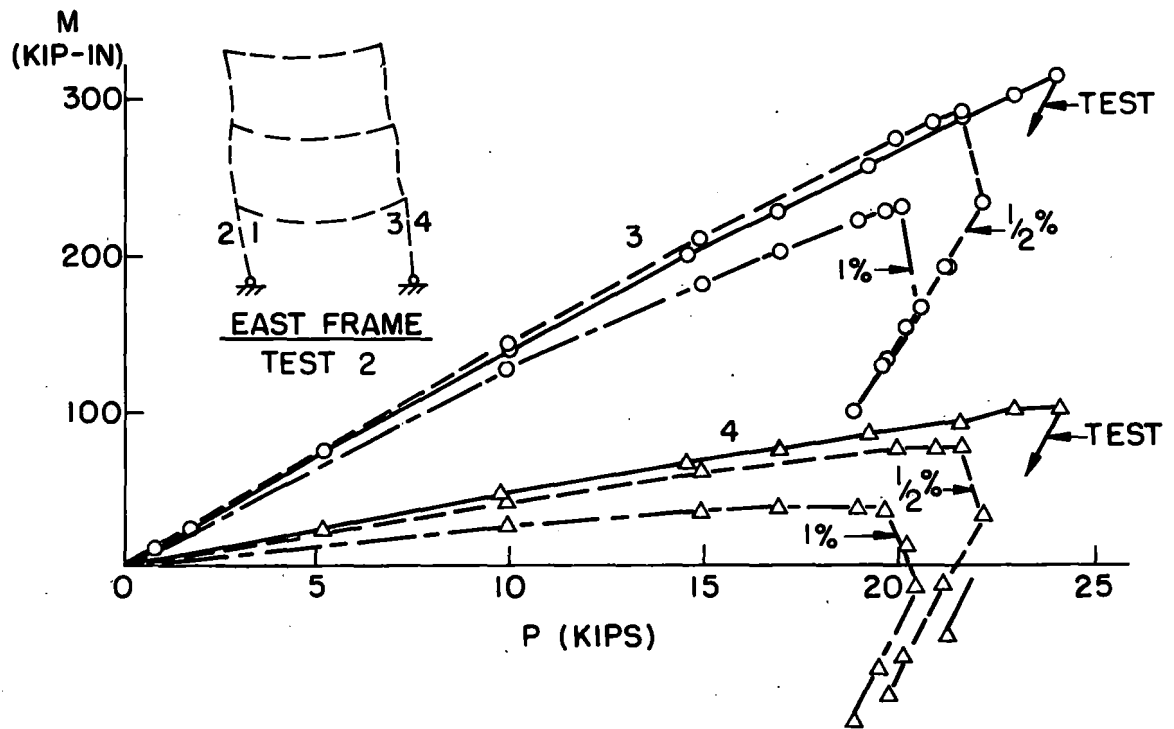
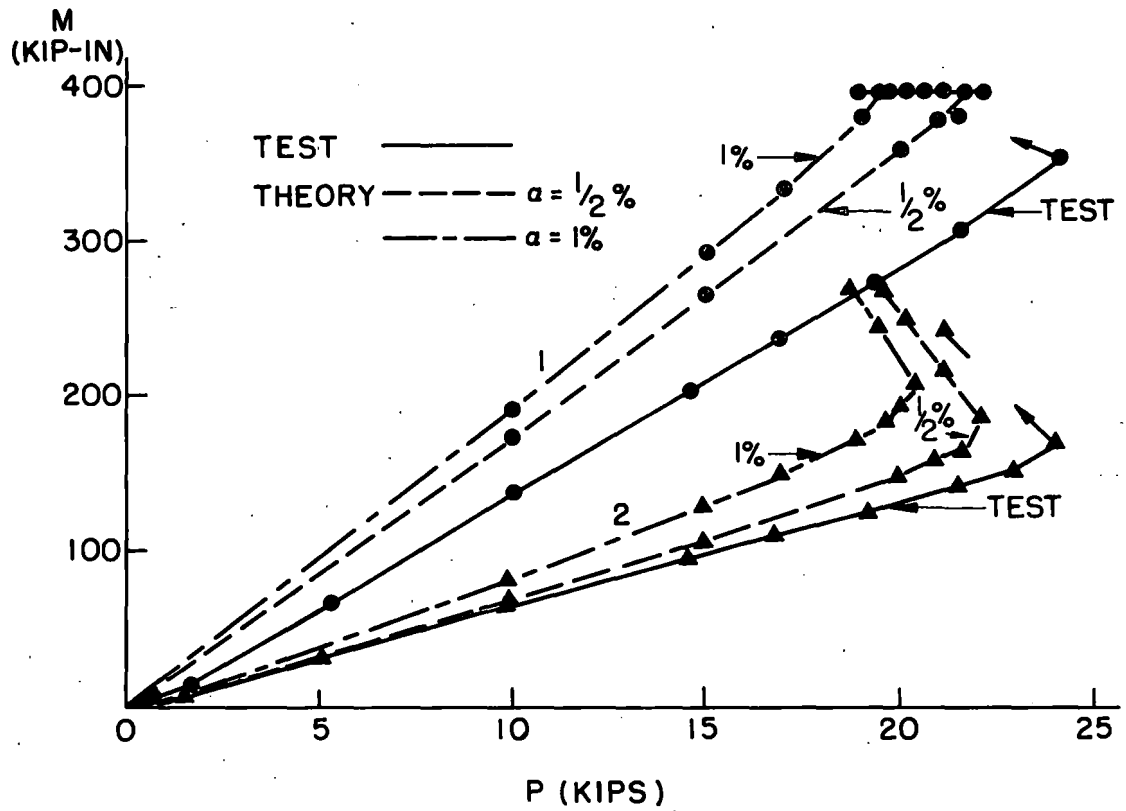


Fig. 5.16 Bending Moments, Experimental and Predicted, Test 2

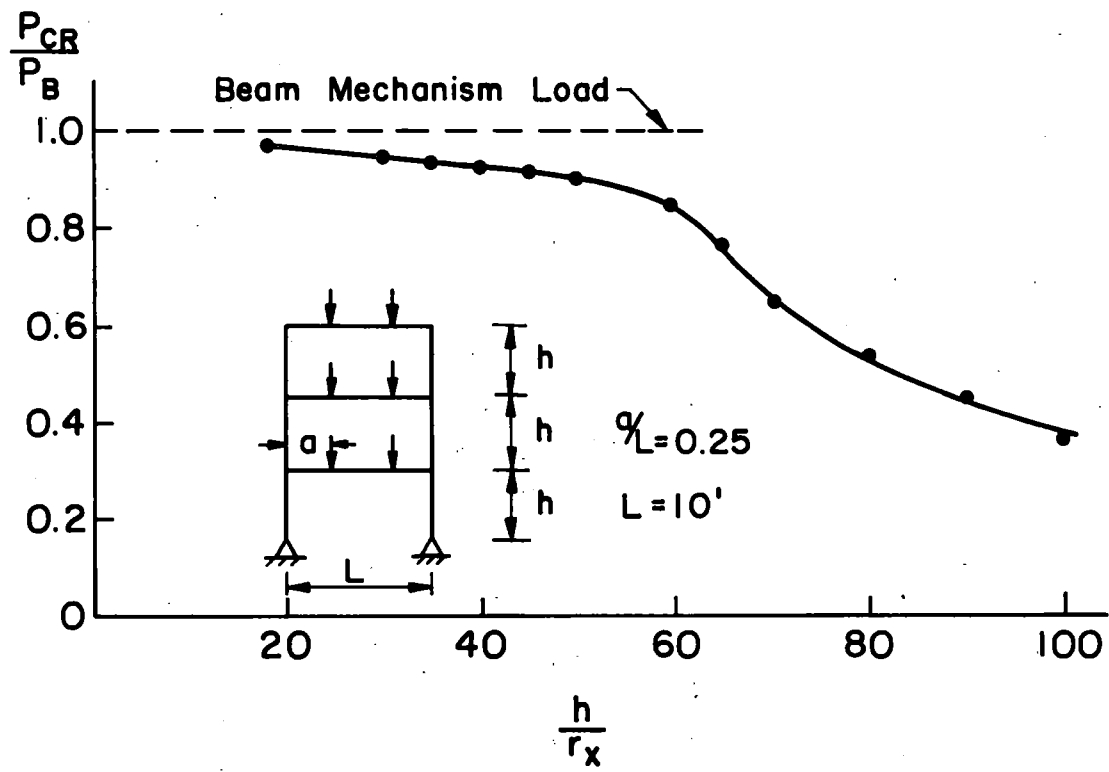


Fig. 6.1 Frame Buckling Loads, Column Slenderness Ratio

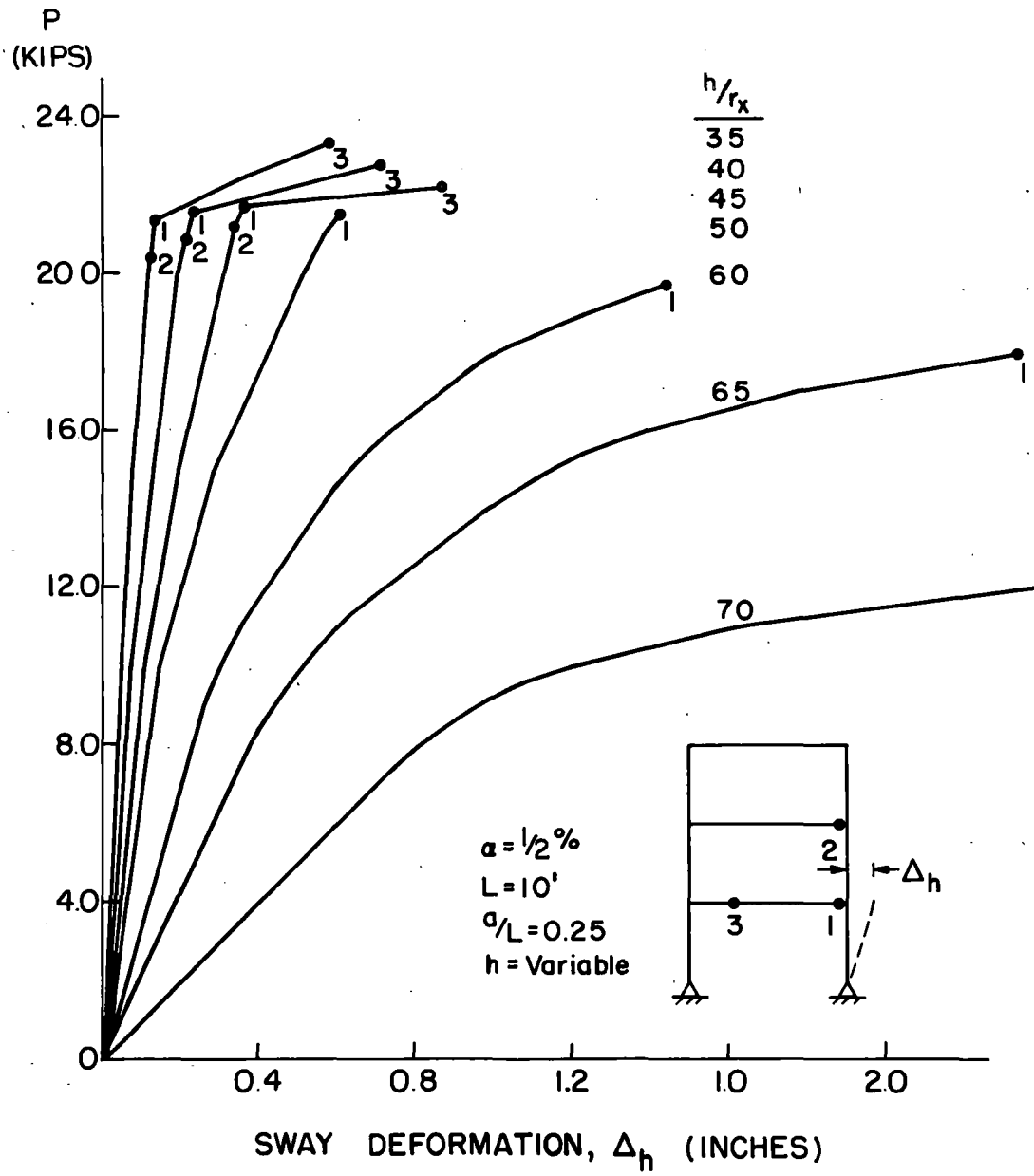


Fig. 6.2 Load-Response Curves, Column Slenderness Ratio

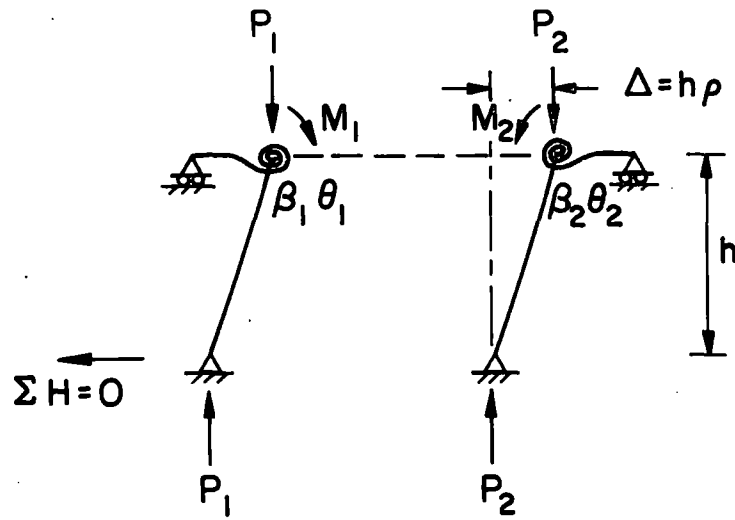


Fig. 6.3 Restrained Columns

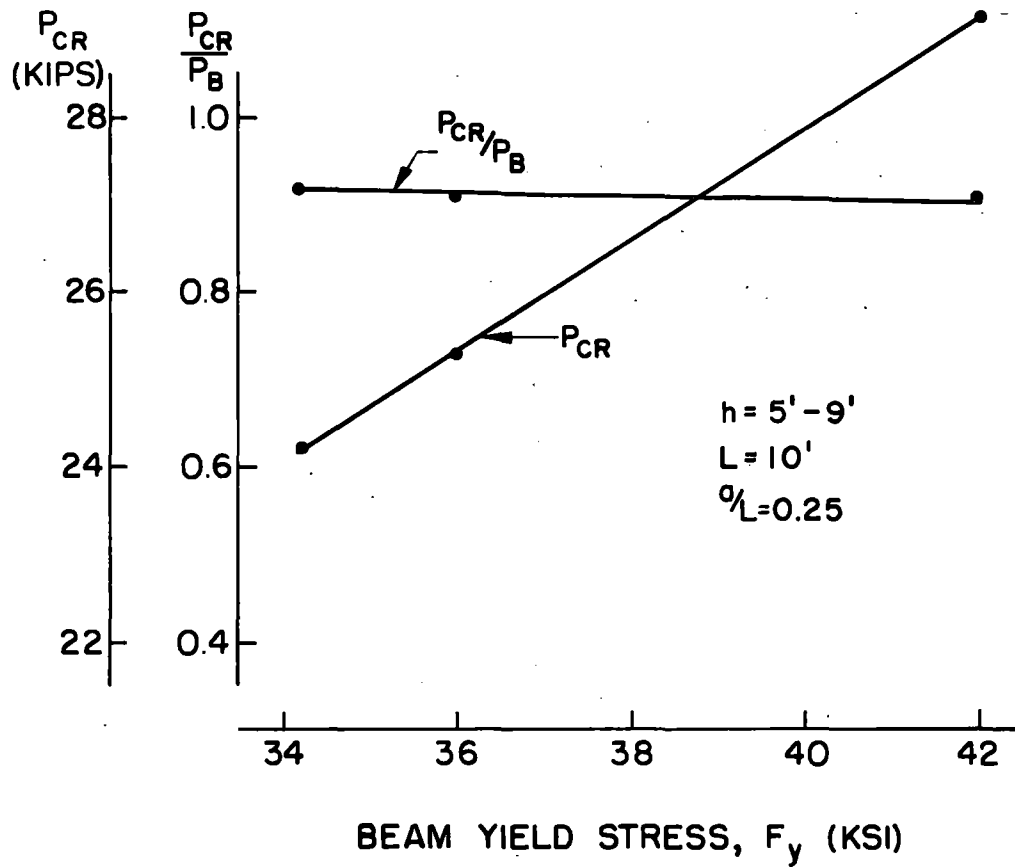


Fig. 6.4 Frame Buckling Loads, Beam Yield Stress

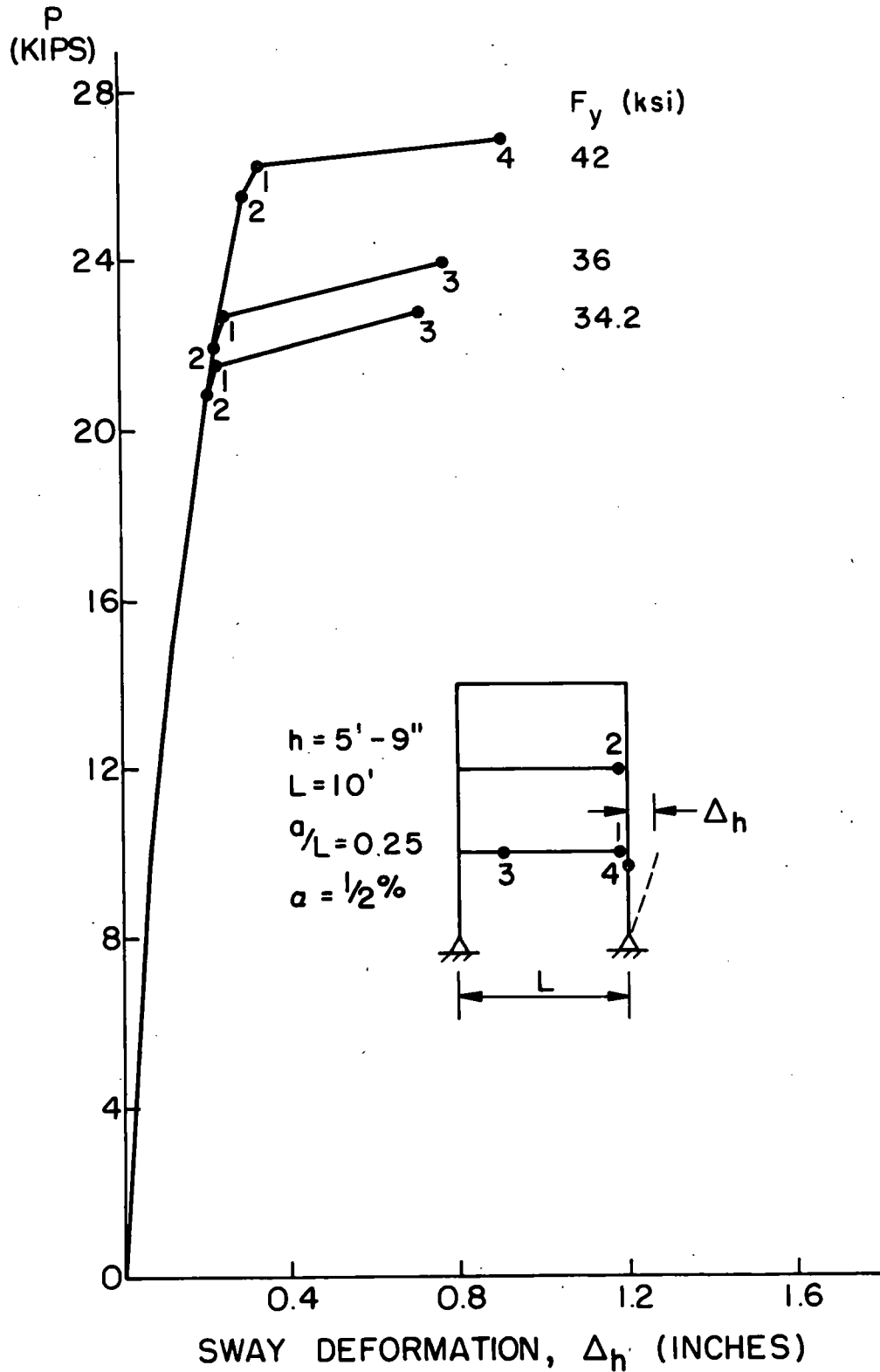
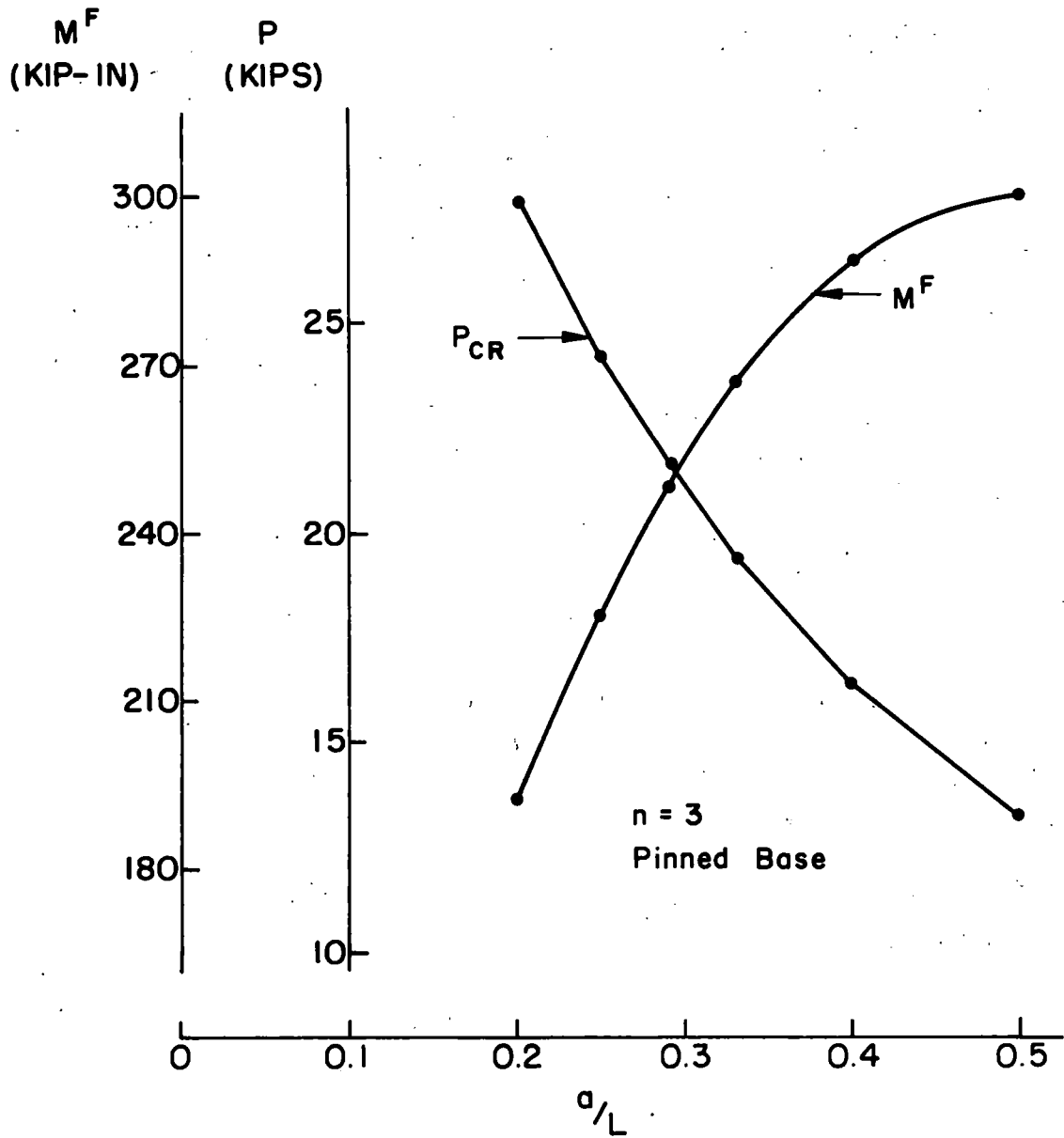


Fig. 6.5 Load-Response Curves, Beam Yield Stress

Fig. 7.1 Frame Buckling Loads, Primary Bending,  $n = 3$

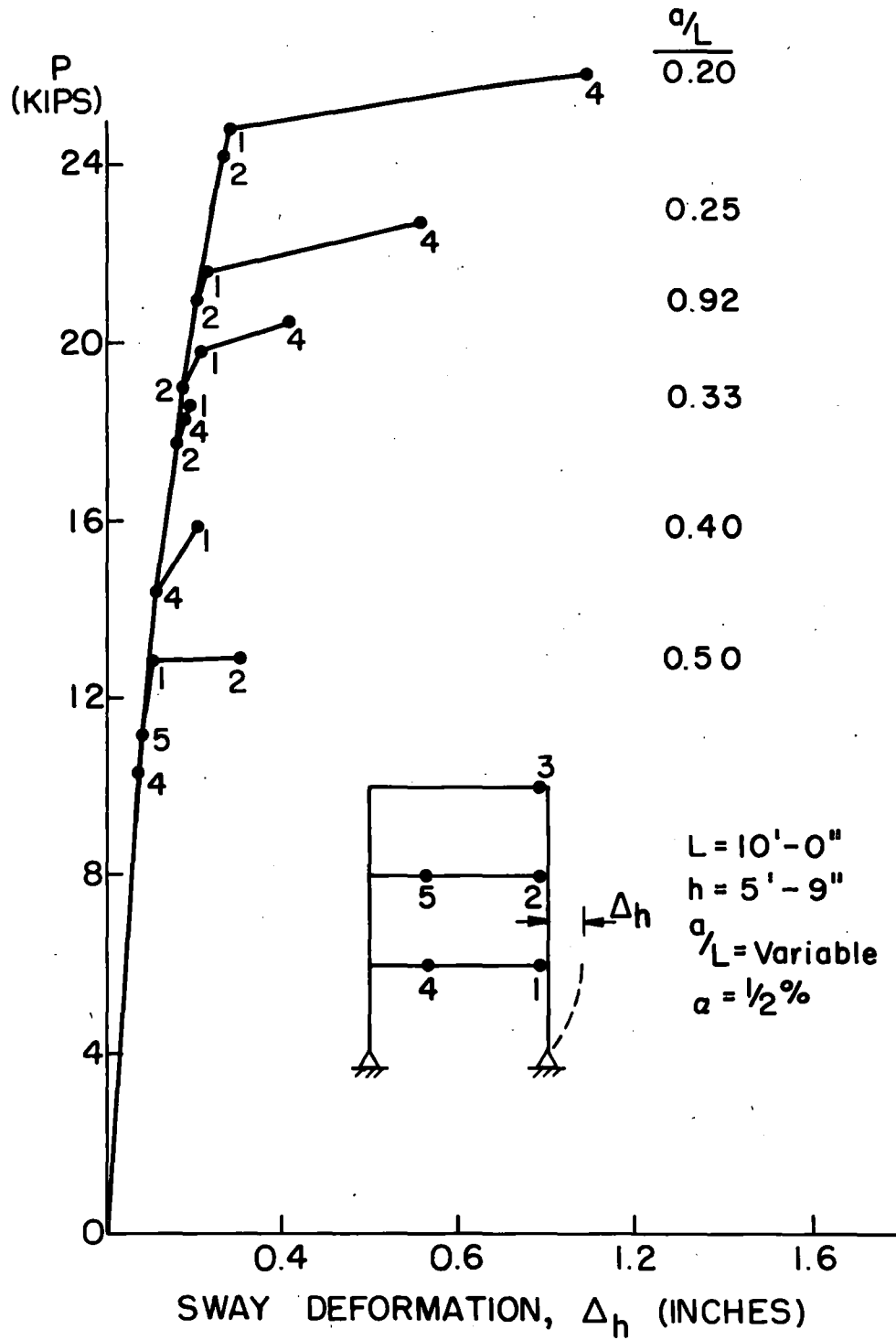


Fig. 7.2 Load-Response Curves, Primary Bending, n = 3

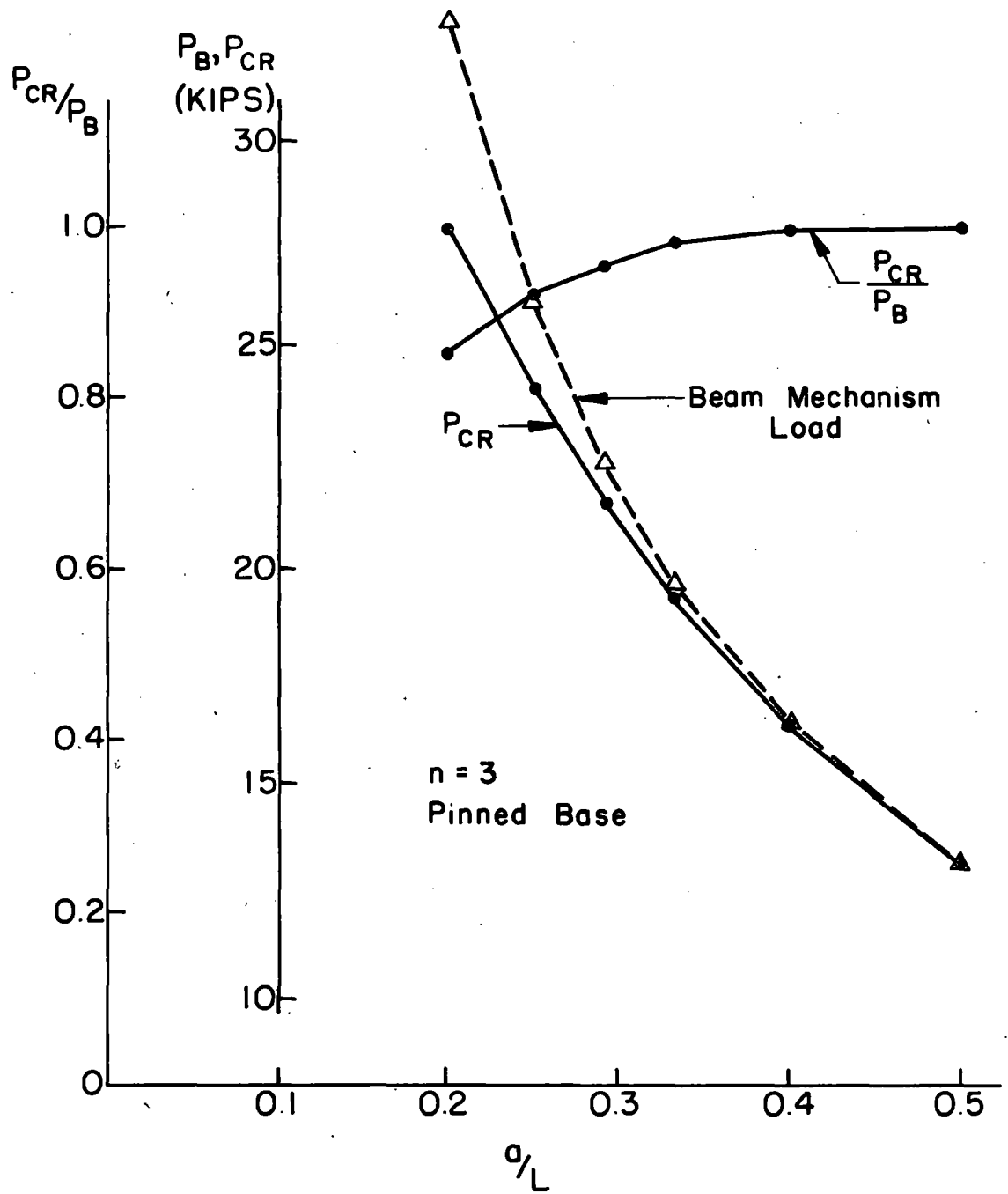


Fig. 7.3 Effect of Primary Bending,  $n = 3$

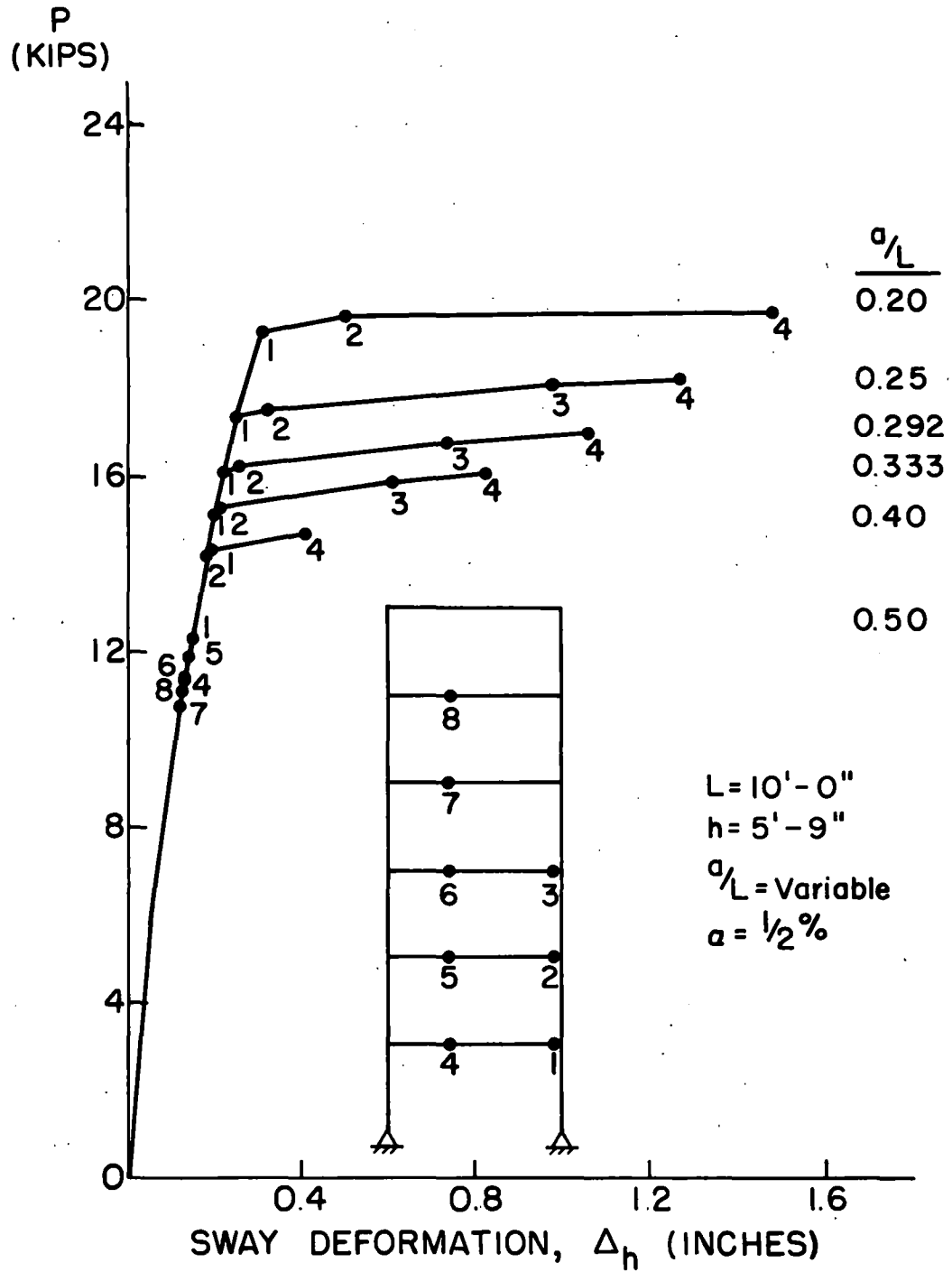


Fig. 7.4 Load-Response Curves, Primary Bending, n = 6

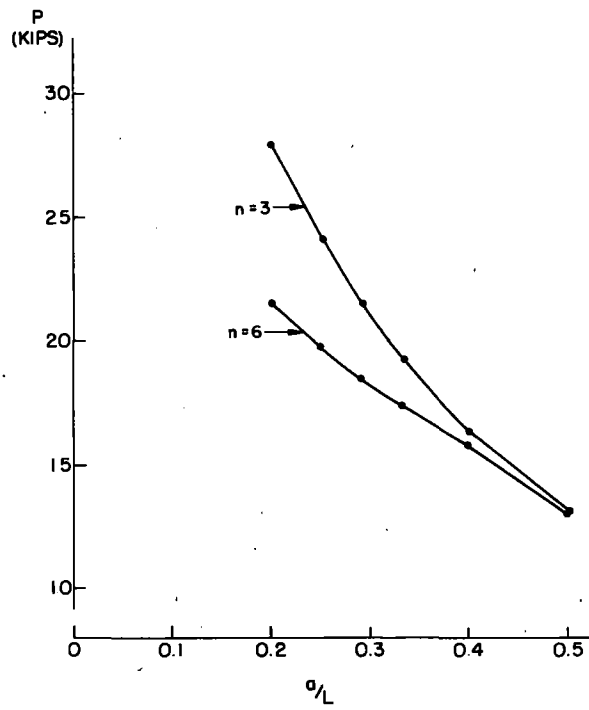


Fig. 7.5 Effect of Primary Bending,  $n = 3$  and  $n = 6$

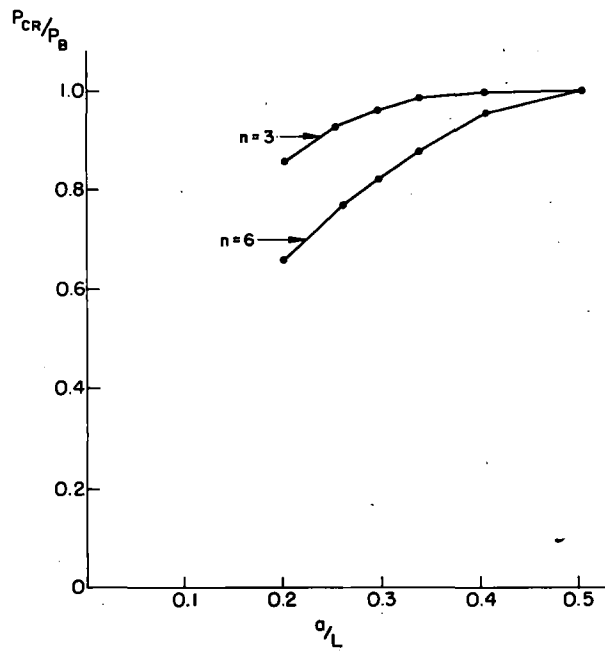


Fig. 7.6 Non-Dimensionalized Comparison,  $n = 6$

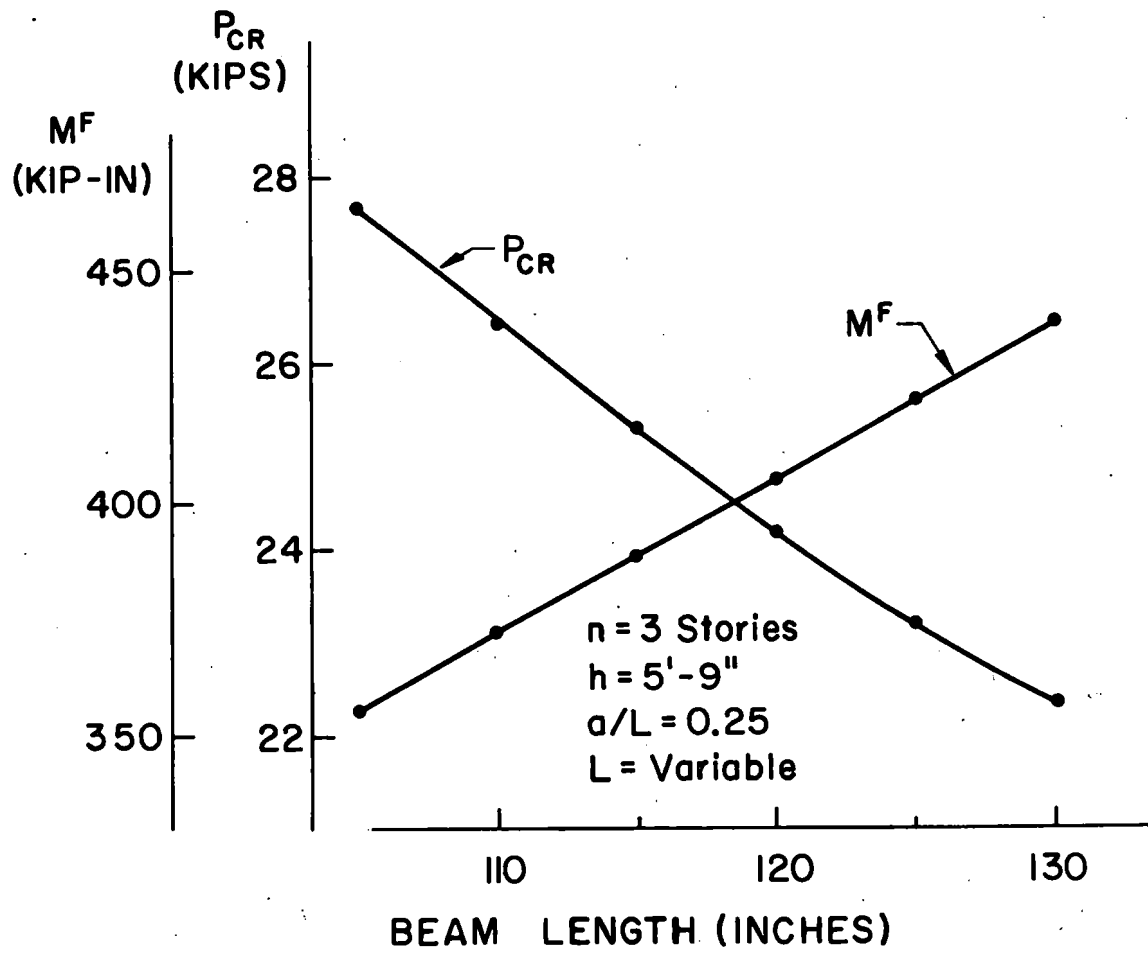


Fig. 7.7 Frame Buckling Loads, Beam Length

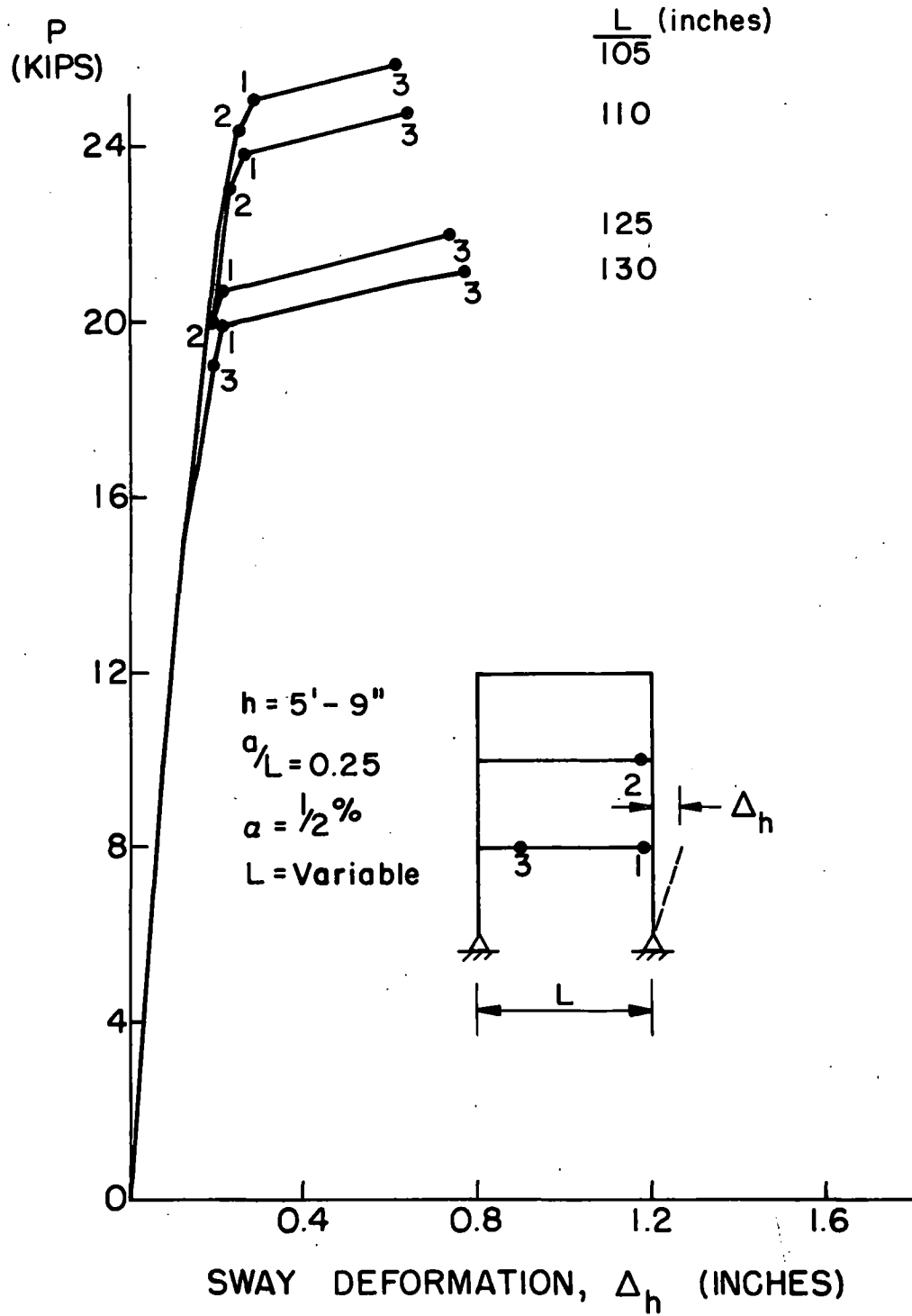


Fig. 7.8 Load-Response Curves, Beam Length

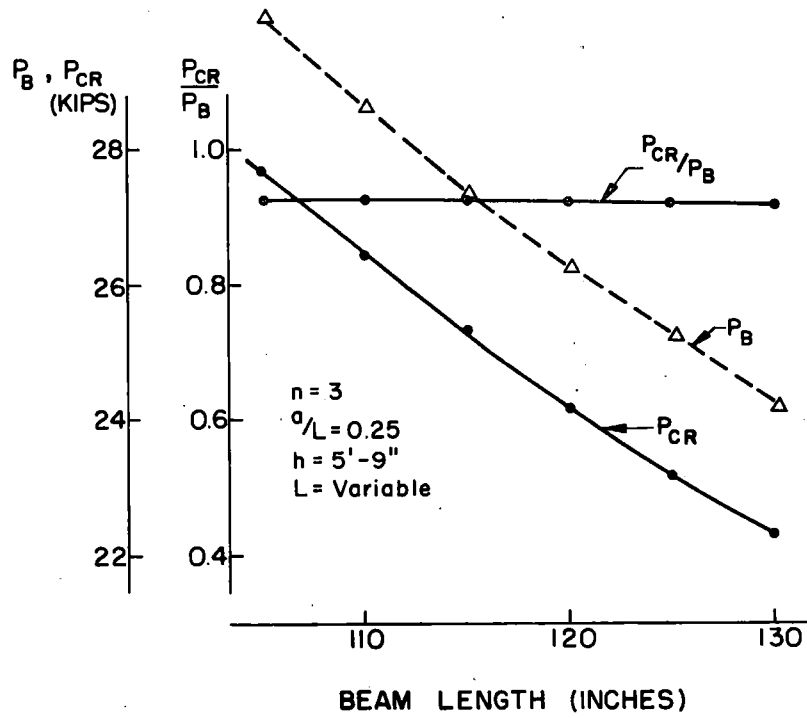


Fig. 7.9 Non-Dimensionalized Curve, Beam Length

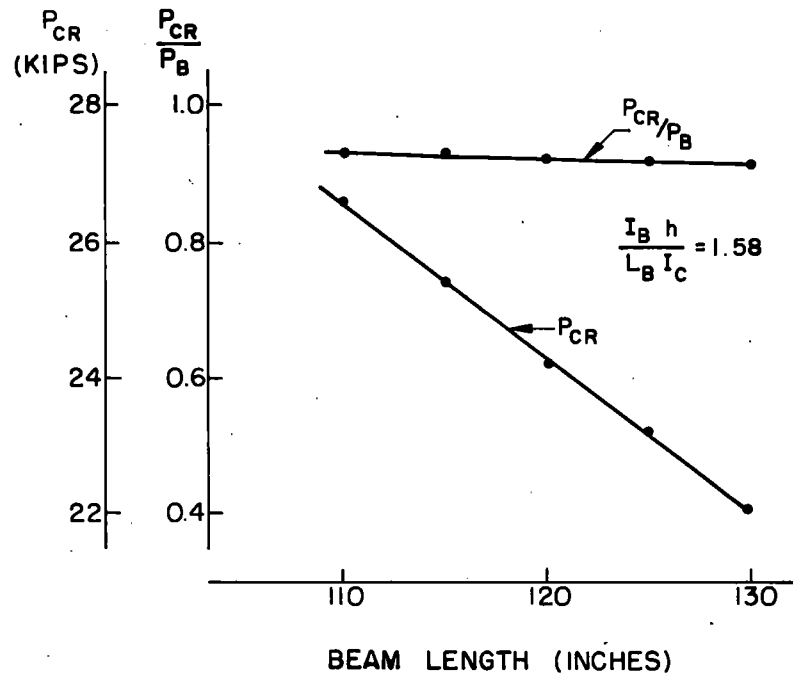


Fig. 7.10 Frame Buckling Loads, Constant Relative Stiffness

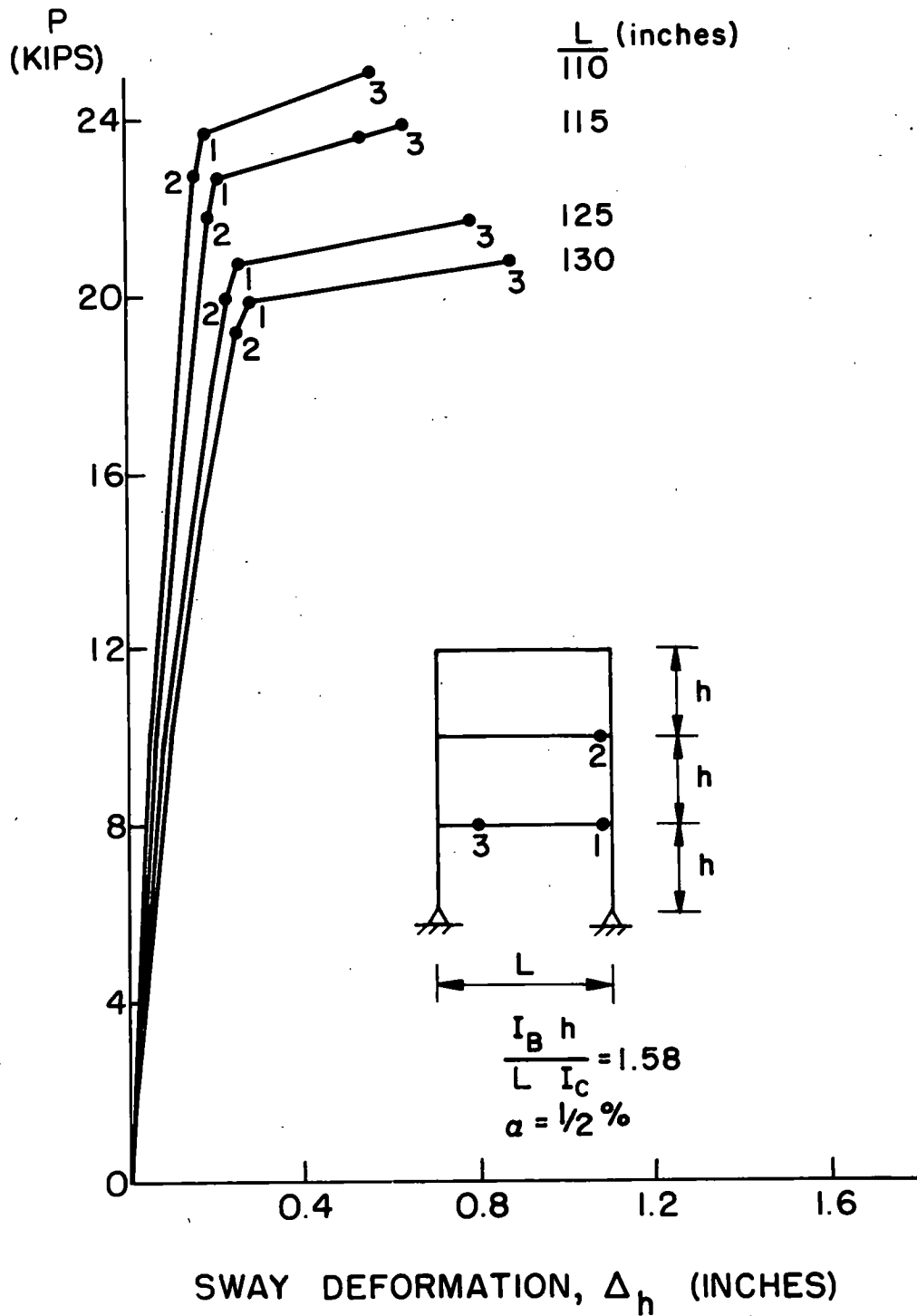


Fig. 7.11 Load-Response Curves, Constant Relative Stiffness

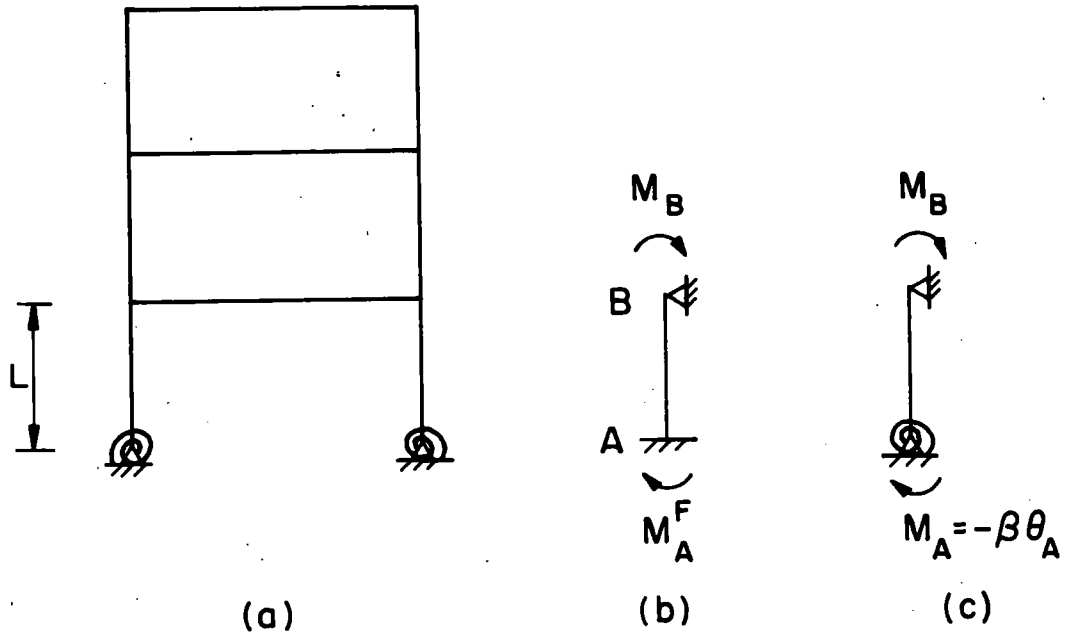


Fig. 8.1 Partial Base Fixity

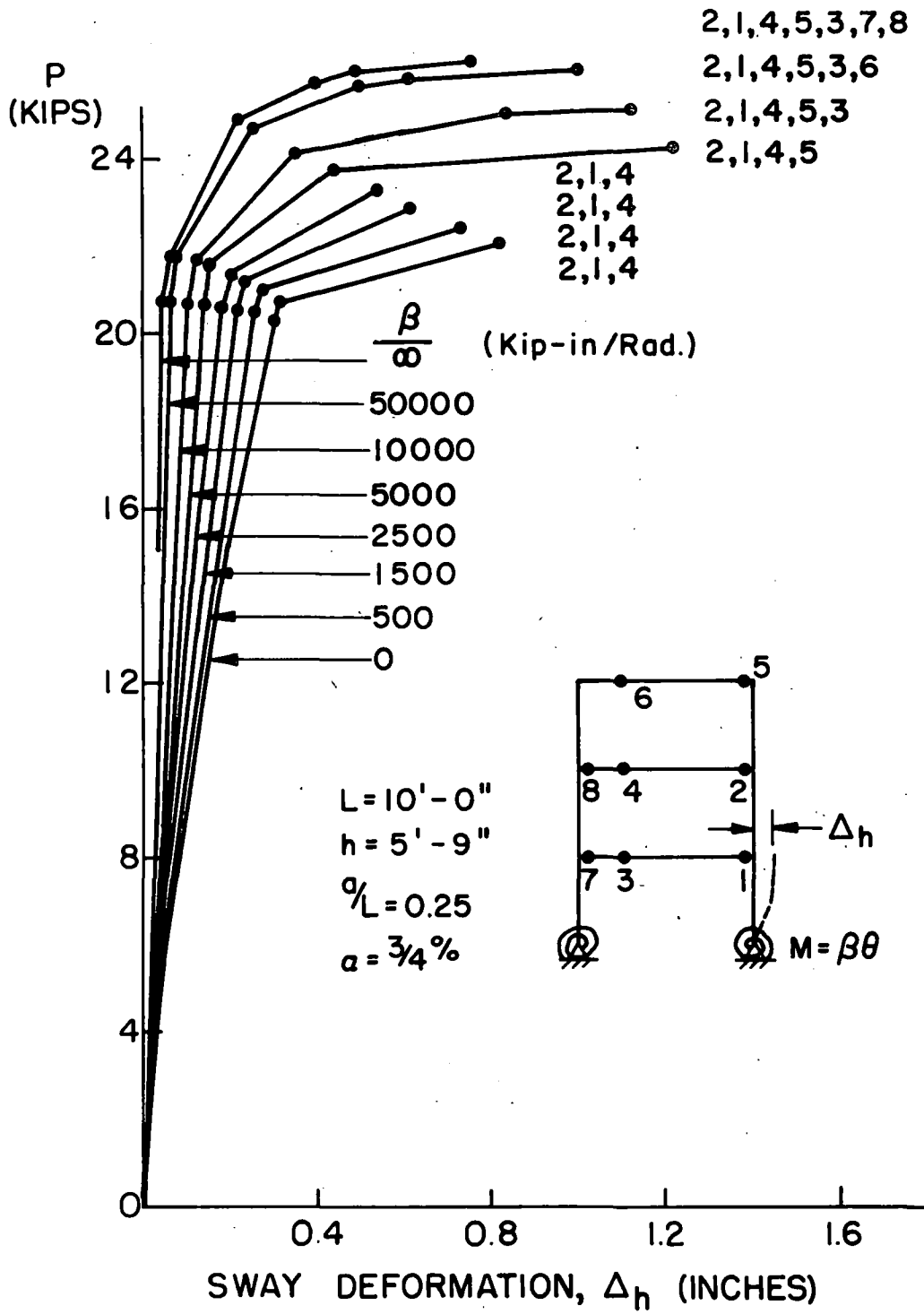


Fig. 8.2 Load-Response Curves, Partial Base Fixity,  $n = 3$

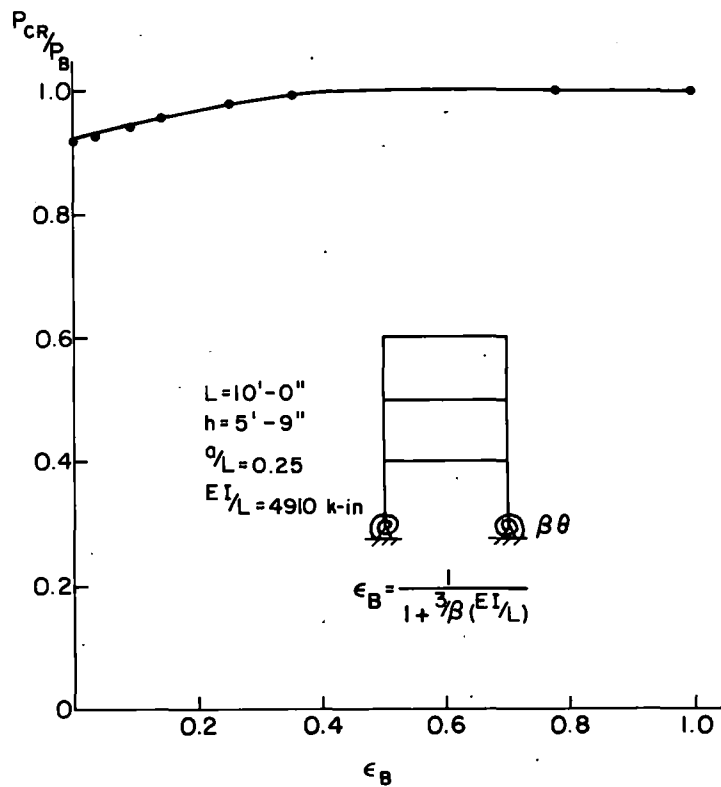


Fig. 8.3 Frame Buckling Loads, Partial Base Fixity,  $n = 3$

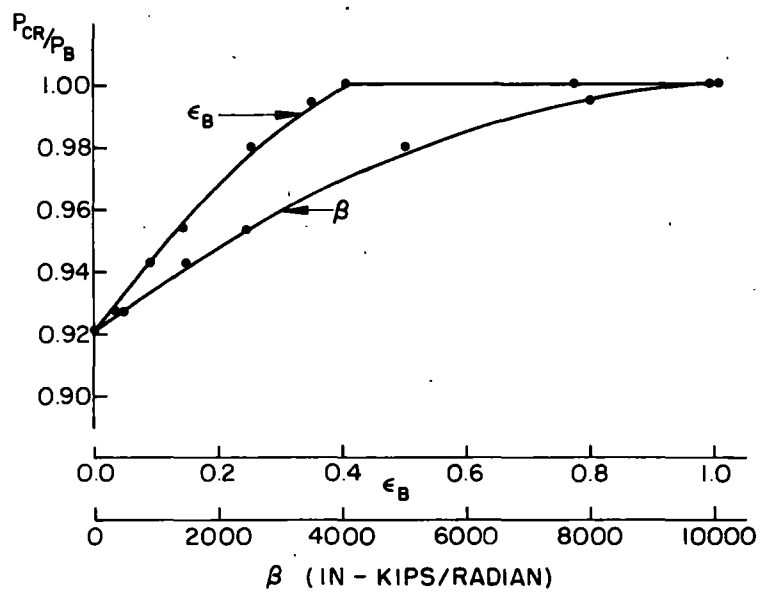


Fig. 8.4 Frame Buckling Loads, Foundation Modulus,  $n = 3$

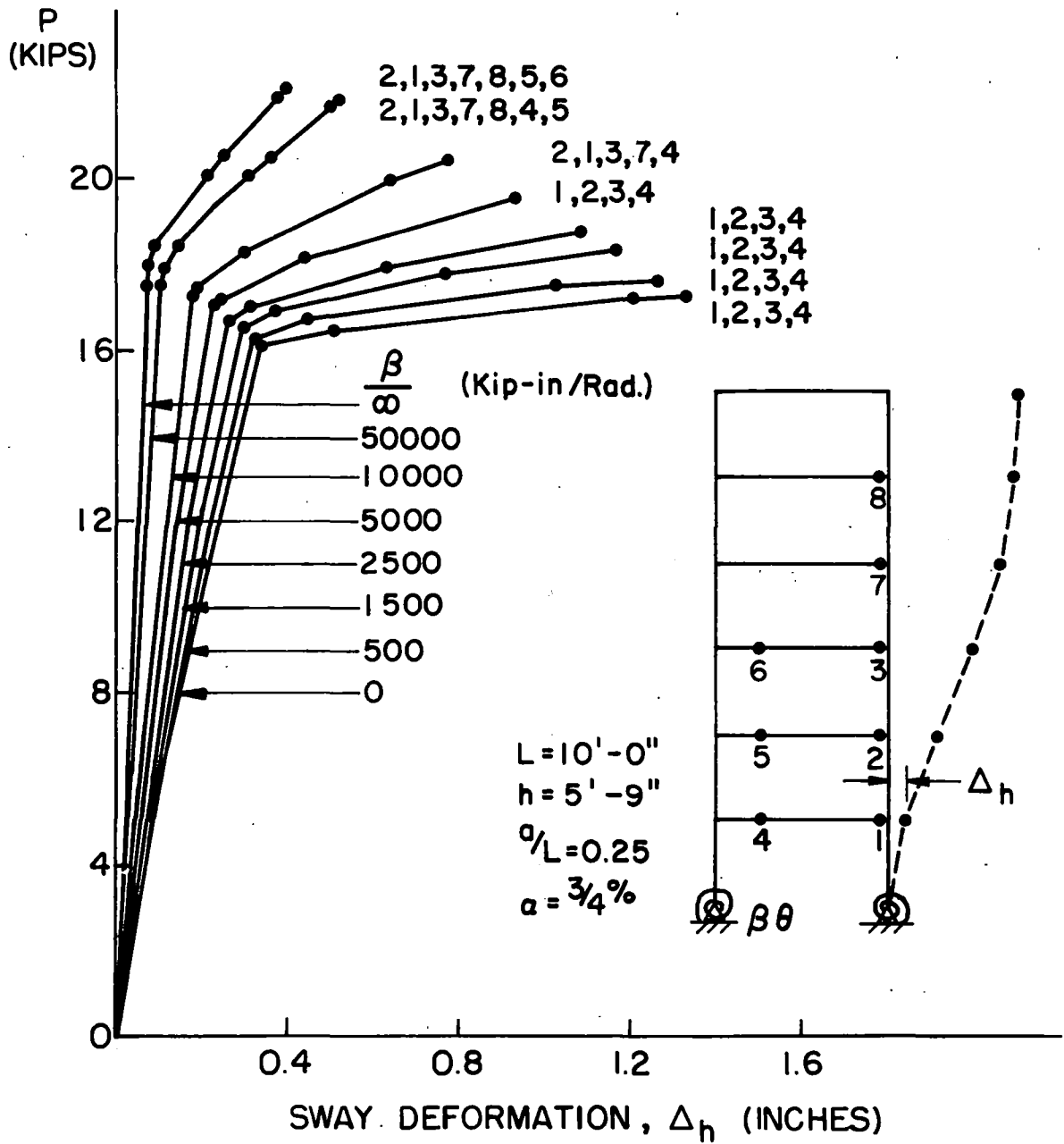


Fig. 8.5 Load-Response Curves, Partial Base Fixity,  $n = 6$

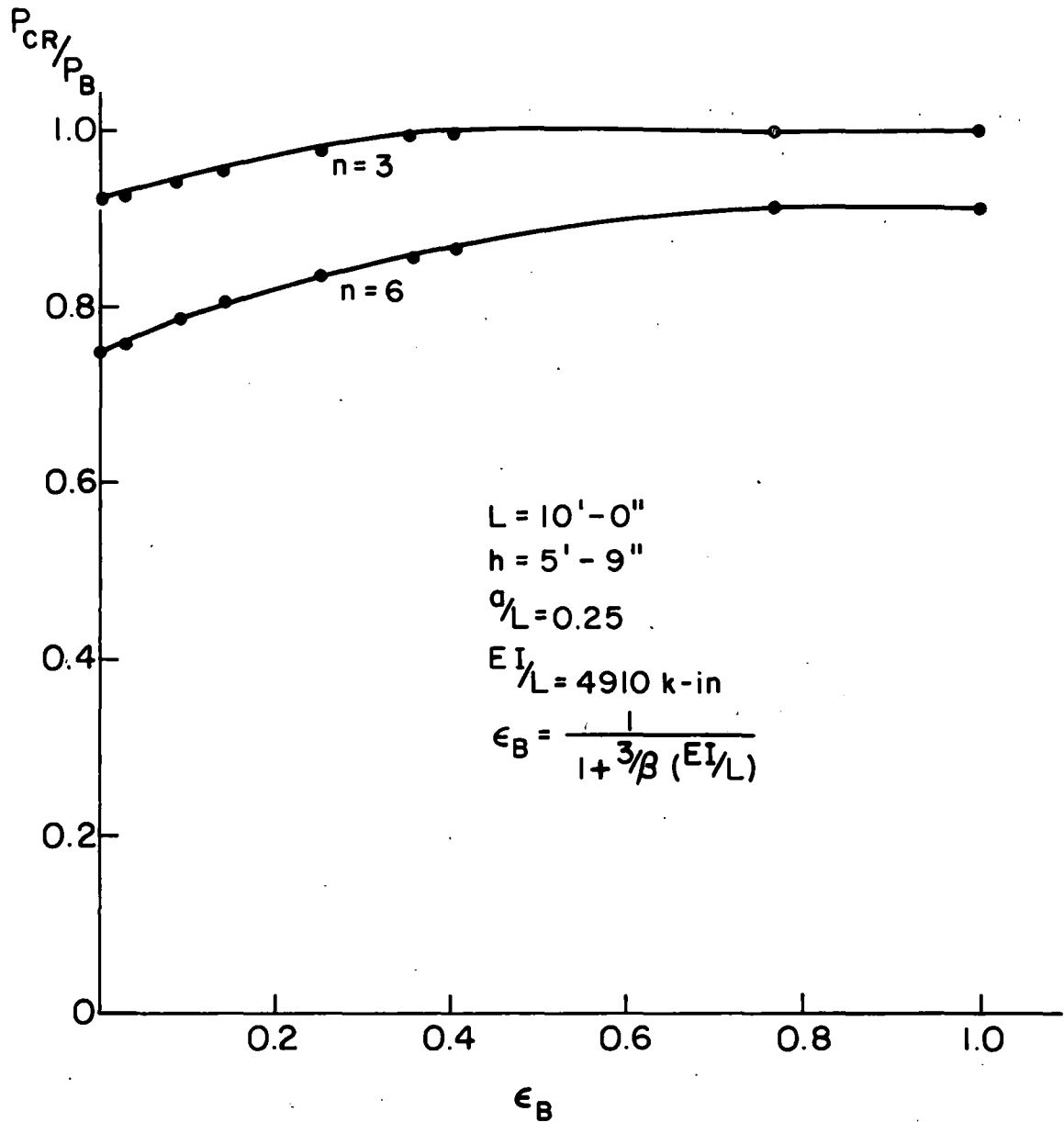


Fig. 8.6 Frame Buckling Loads, Partial Base Fixity,  $n = 6$

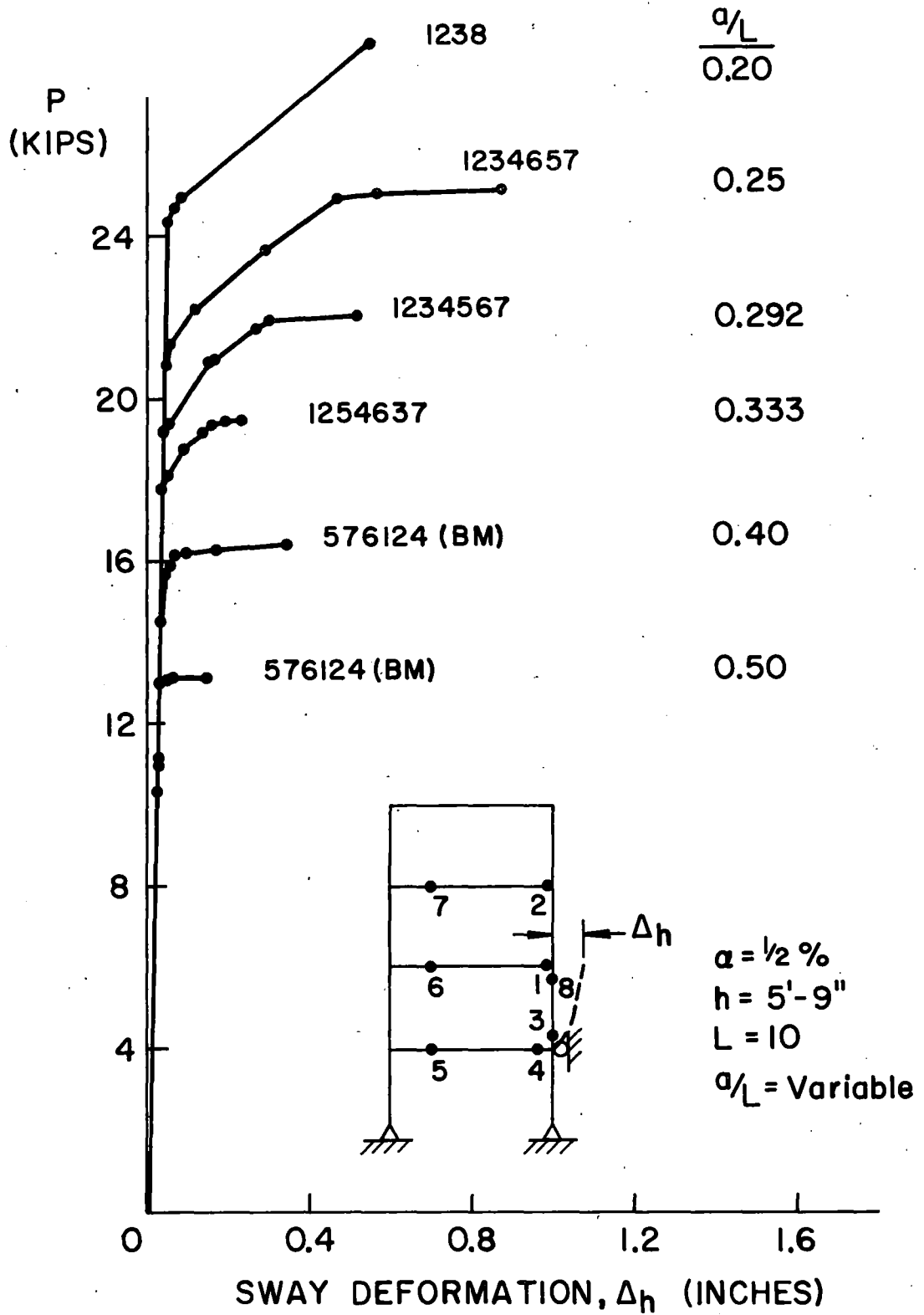


Fig. 9.1 Load-Response Curves, Variable Base Restraint,  $n = 3$

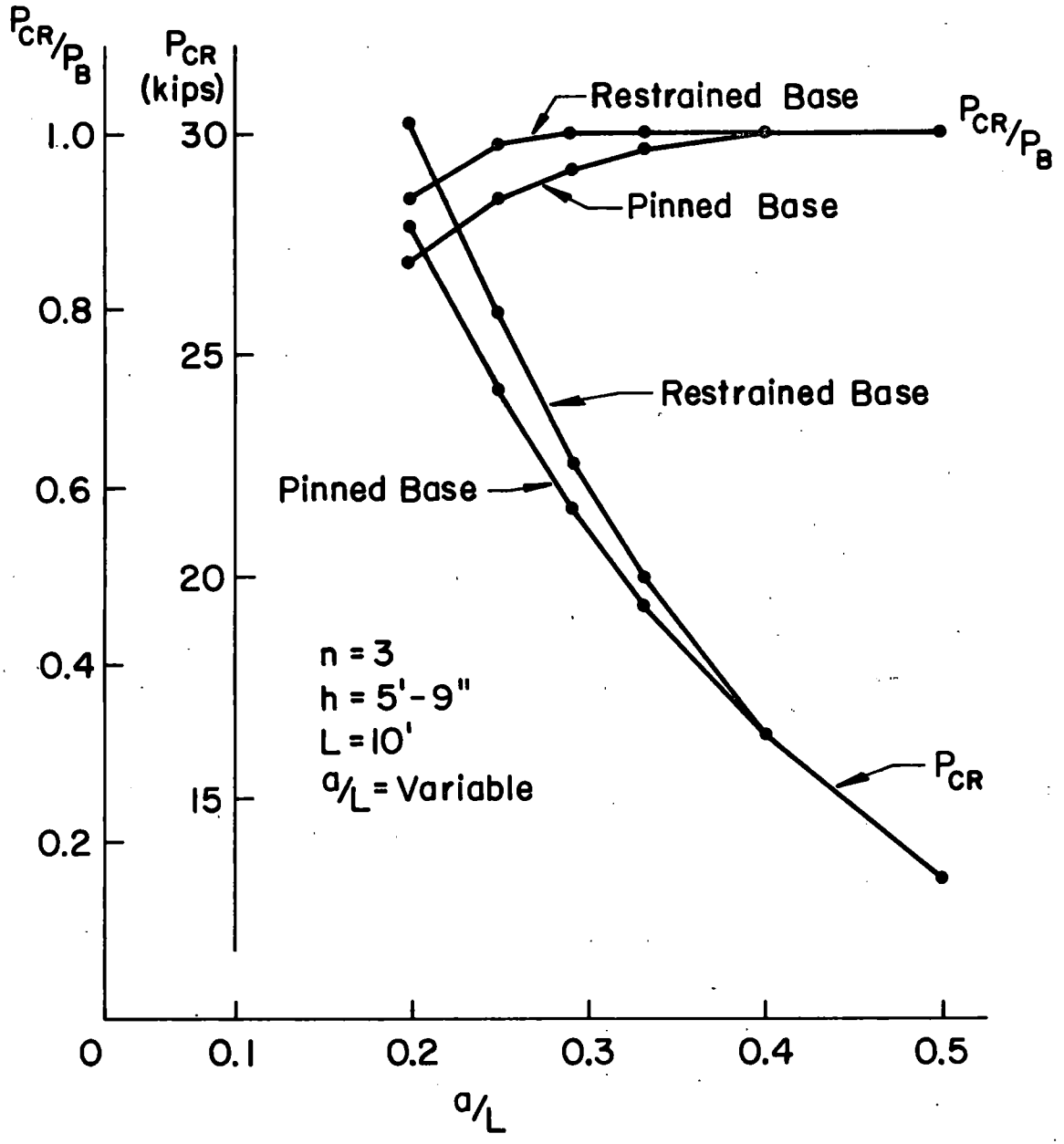


Fig. 9.2 Frame Buckling Curves, Variable Base Restraint,  $n = 3$

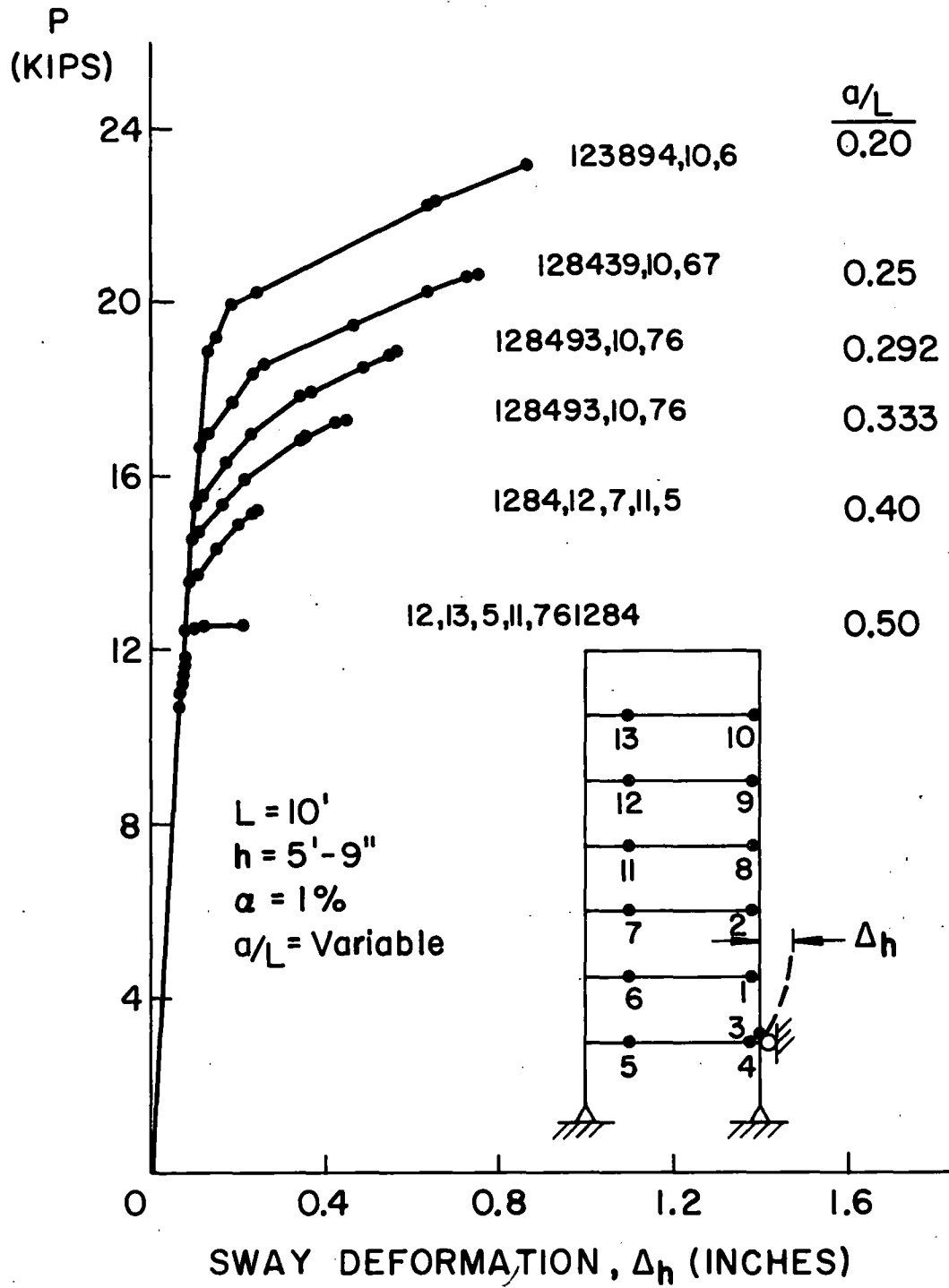


Fig. 9.3 Load-Response Curves, Variable Base Restraint,  $n = 6$

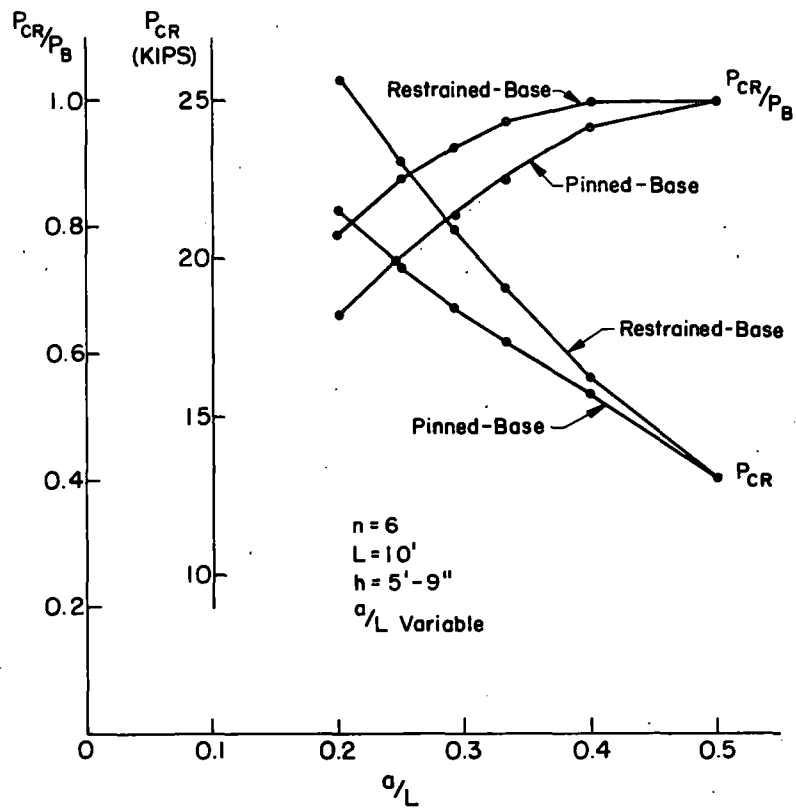


Fig. 9.4 Frame Buckling Curves, Variable Base Restraint,  $n = 6$

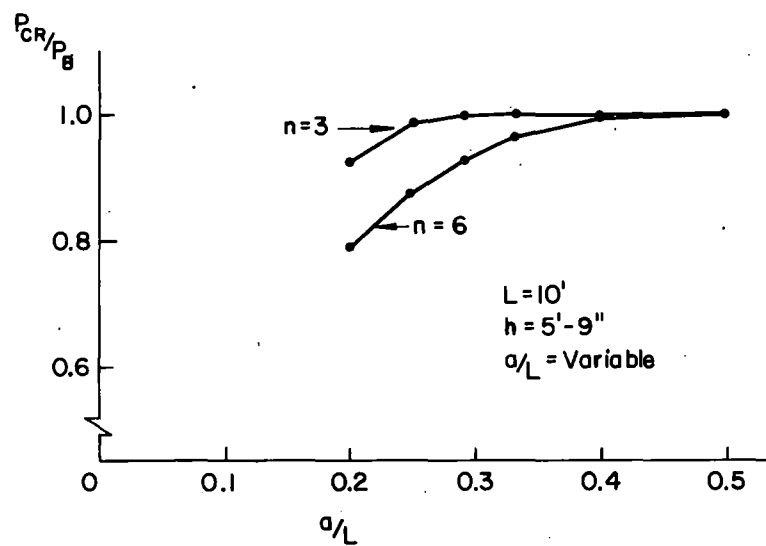


Fig. 9.5 Buckling Load Comparison, Variable Base Restraint

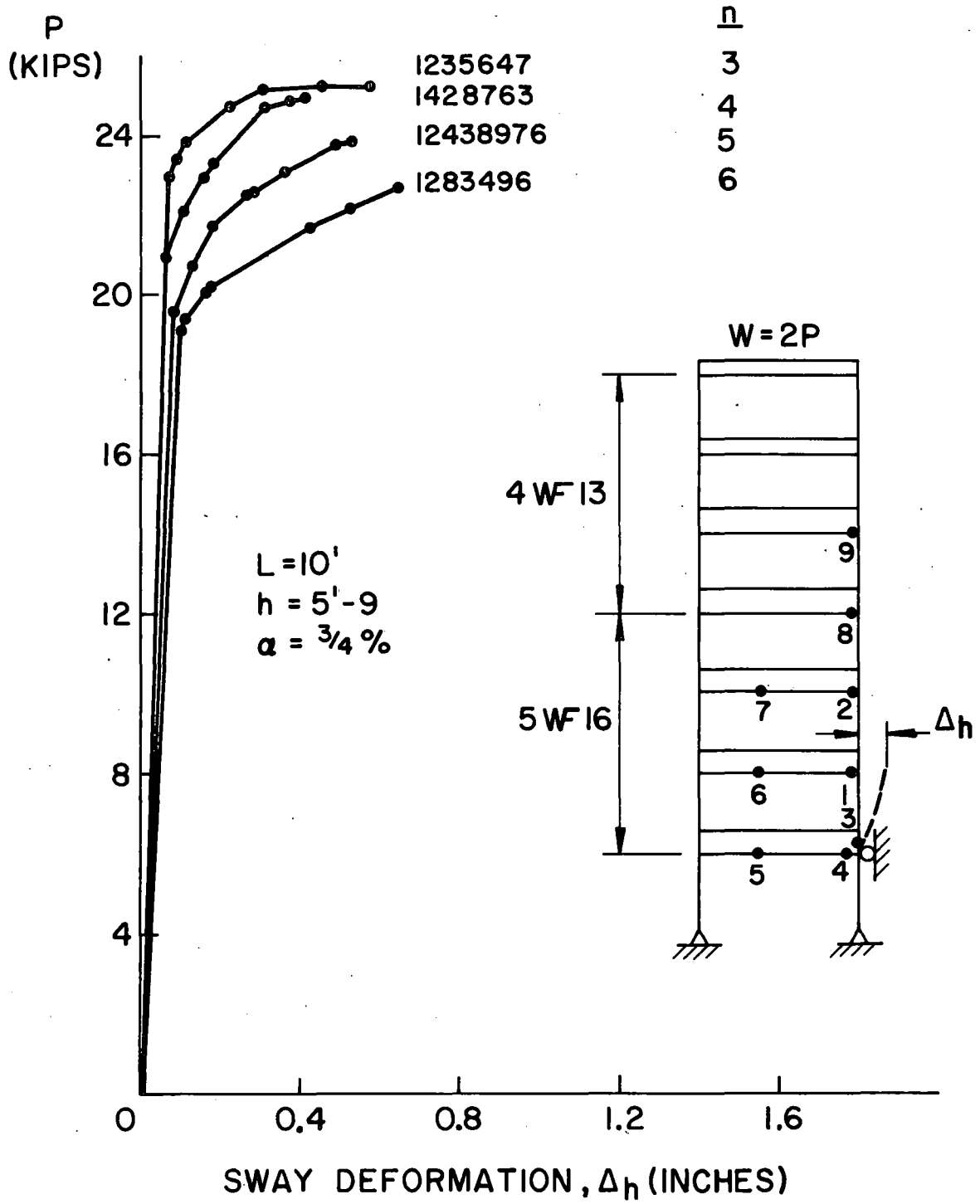


Fig. 9.6 Load-Response Curves, Distributed Load, Variable  $n$

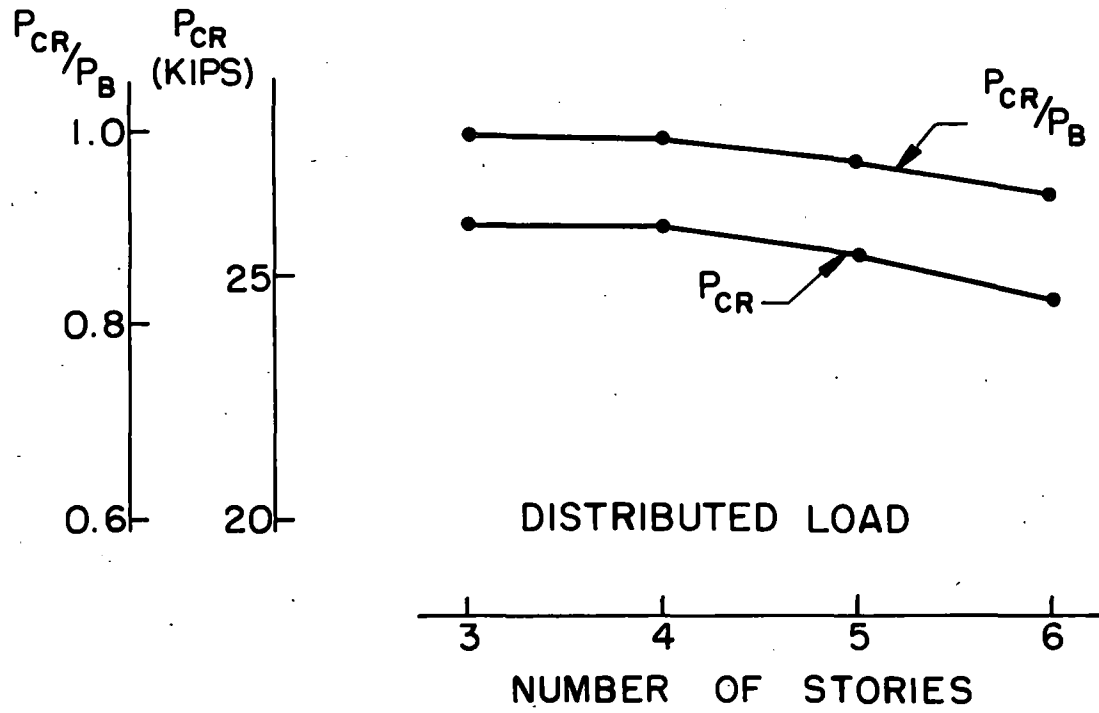


Fig. 9.7 Frame Buckling Loads, Distributed Load, Variable n

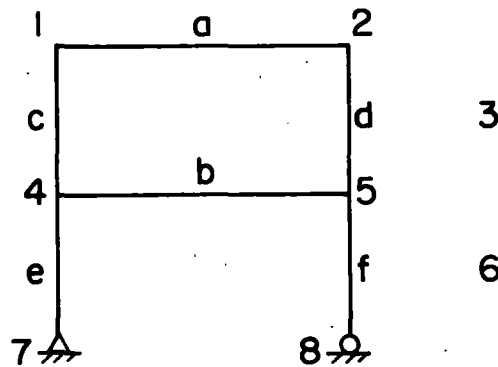


Fig. A-1 Joint and Member Designation, Example 2

15. REFERENCES

- 1.1 Baker, J. F.  
SYMPOSIUM ON THE DESIGN OF HIGH BUILDINGS, Chapter 1,  
University Press, Hong Kong, 1962
- 1.2 Cross, H.  
CONTINUITY AS A FACTOR IN REINFORCED CONCRETE DESIGN,  
Proc. ACI, 1929
- 1.3 Kazinczy, G.  
KISERLETEK BEFALAZOTT TARTOKKAL (EXPERIMENTS WITH CLAMPED  
GIRDERS), Betonszemle, Vol. 2, p. 68, 1914
- 1.4 Yarimci, E.  
INCREMENTAL INELASTIC ANALYSIS OF FRAMED STRUCTURES AND  
SOME EXPERIMENTAL VERIFICATIONS, Ph.D. Dissertation,  
Lehigh University, 1966, University Microfilms, Inc.,  
Ann Arbor, Michigan
- 1.5 AISC  
MANUAL OF STEEL CONSTRUCTION, 6th Ed., AISC, New York,  
1963
- 2.1 Parikh, B. P.  
ELASTIC-PLASTIC ANALYSIS AND DESIGN OF UNBRACED MULTI-  
STORY STEEL FRAMES, Ph.D. Dissertation, Lehigh University,  
1966, University Microfilms, Inc., Ann Arbor, Michigan
- 2.2 Lu, L. W.  
A SURVEY OF LITERATURE ON THE STABILITY OF FRAMES, Welding  
Research Council, Bulletin 81, September, 1962
- 2.3 Adams, P. F.  
LOAD-DEFORMATION RELATIONSHIPS FOR SIMPLE FRAMES, Fritz  
Engineering Laboratory Report No. 273.21, December, 1964
- 2.4 Lu, L. W.  
INELASTIC BUCKLING OF STEEL FRAMES, Proc. ASCE, Vol. 91  
(ST6), December, 1965
- 2.5 Moses, F.  
INELASTIC FRAME BUCKLING, Proc. ASCE, Vol. 90 (ST6),  
December, 1964
- 2.6 Sapp, D. H.  
INELASTIC STABILITY OF RECTANGULAR STEEL FRAMES, Ph.D.  
Dissertation, University of Illinois, 1964, University  
Microfilms, Inc., Ann Arbor, Michigan

- 2.7 Lu, L.W.  
STABILITY OF FRAMES UNDER PRIMARY BENDING MOMENTS, Proc. ASCE, Vol. 89 (ST3), June, 1963
- 2.8 Chu, K. H. and Pabacius, A.  
ELASTIC AND INELASTIC BUCKLING OF PORTAL FRAMES, Proc. ASCE, Vol. 90 (EM 5), October, 1964
- 2.9 Yen, Y. C.  
ELASTIC AND PARTIALLY PLASTIC INSTABILITY OF MULTI-STORY FRAMES, Ph.D. Dissertation, Lehigh University, 1966, University Microfilms, Inc., Ann Arbor, Michigan
- 2.10 Majid, K. J.  
ELASTIC-PLASTIC STRUCTURAL ANALYSIS, Ph.D. Dissertation, Manchester University, 1963
- 2.11 Wang, C. K.  
GENERAL COMPUTER PROGRAM FOR LIMIT LOAD ANALYSIS, Proc. ASCE, Vol. 89 (ST 6), December, 1961
- 2.12 Wood, R. H.  
THE STABILITY OF TALL BUILDINGS, Proc. Inst. of Civil Engrs., Vol. 11, September, 1958
- 2.13 Merchant, W.  
THE FAILURE LOAD OF RIGID JOINTED FRAMEWORKS AS INDUCED BY STABILITY, Structural Engineer, Vol. 32, No. 7, July, 1954
- 2.14 Johnston, B. G.  
BUCKLING BEHAVIOR ABOVE THE TANGENT MODULUS LOAD, Trans. ASCE, Part 1, Vol. 128, 1963
- 2.15 Timoshenko, S. P. and Gere, J. M.  
THEORY OF ELASTIC STABILITY, 2nd Ed., p. 31, McGraw Hill Co., New York, 1961
- 2.16 O'Connor, C.  
BUCKLING IN STEEL STRUCTURES (THE USE OF A CHARACTERISTIC IMPERFECT SHAPE IN THE DESIGN OF DETERMINATE PLANE TRUSSES AGAINST BUCKLING IN THEIR PLANE), University of Queensland, July, 1965
- 3.1 Bleich, F.  
BUCKLING STRENGTH OF METAL STRUCTURES, p. 211, McGraw Hill Co., New York, 1952
- 4.1 Fritz Laboratory Staff  
LECTURE NOTES ON PLASTIC DESIGN OF MULTI-STORY FRAMES, Fritz Laboratory Report No. 273.11, Lehigh University, Summer, 1965

- 4.2 Yarimci, E., Yura, J. A. and Lu, L. W.  
TECHNIQUES FOR TESTING STRUCTURES PERMITTED TO SWAY,  
Fritz Laboratory Report No. 273.40, Lehigh University,  
1966
- 8.1 Appeltauer, J. W. and Barta, T. A.  
Discussion of INFLUENCE OF PARTIAL BASE FIXITY ON FRAME  
STABILITY, Trans. ASCE, Vol. 126, p. 929, 1961
- 8.2 Galambos, T. V.  
INFLUENCE OF PARTIAL BASE FIXITY ON FRAME STABILITY,  
Trans. ASCE, Vol. 126, p. 929, 1961

16. VITA

The author was born in Philadelphia, Pennsylvania on September 13, 1930. He is the second of five children of Michael and Catherine McNamee. He received the degree of Bachelor of Science in Civil Engineering from Drexel Institute of Technology in 1953. After graduation, he was employed as a Civil Engineer in the Bridge Department of the Pennsylvania Railroad. In November of 1953, he was inducted into the United States Army. He spent two years as a Topographic Surveyor in the Army Map Service of the Corps of Engineers.

In 1955, the author was appointed as an Instructor in the Civil Engineering Department of Drexel Institute of Technology. In 1958, he was promoted to the rank of Assistant Professor. In 1959, he received the degree of Master of Business Administration from Drexel Institute. In 1963, he received the degree of Master of Science in Civil Engineering from the University of Pennsylvania. In 1964, he was appointed as an Associate Professor. He is currently on leave of absence from Drexel Institute.

While at Lehigh, the author has held the titles of Research Assistant and Research Instructor. The author is a member of Chi Epsilon, Tau Beta Pi, Phi Kappa Pi, and Sigma Xi.

In 1957, he married the former Nancy Kelly of Upper Darby, Pennsylvania. They have five children, Michael, John, Bernard, Robert, and Patricia.